Mechanisms of Ciliary Entry

by

Hooi Lynn Kee

A dissertation submitted in partial fulfillment
of the requirements for the degree of
Doctor of Philosophy
(Cell and Developmental Biology)
in The University of Michigan
2012

Doctoral Committee:

Associate Professor Kristen J. Verhey, Chair
Assistant Professor Benjamin Allen
Professor Benjamin L. Margolis
Associate Professor Jeffrey R. Martens

To my family

Acknowledgements

I would like to thank my Advisor and Committee Chair, Kristen Verhey for the invaluable support she provided during my time as a graduate student. Kristen taught me many important lessons in science and life, and I will forever be grateful for her mentorship, patience and friendship.

I would also like to thank my thesis committee members, Ben Margolis, Jeffrey Martens and Ben Allen for their guidance and advice regarding my thesis work. I am indebted to the members of the Verhey lab for their contributions to my thesis work. I am also grateful to Roland Kwok, my undergraduate research mentor, who first trained me and taught me to think critically as a scientist.

I would like to acknowledge individuals for technical help that enabled me to perform certain experiments: Steve Lentz, members of the MIL core, Shuling Fan, and Toby Hurd. Chapters 2 and 3 of this dissertation include experiments contributed by others and I would like to acknowledge them as co-authors.

Chapter 2 Co-Authors: John Dishinger, Lynne Blasius, Paul Jenkins, Jeffrey Martens, Ason Chiang, Qi Xiao, Kristen Verhey. Paul Jenkins, from Jeffrey Martens' laboratory performed the KIF17 experiments in Odora olfactory senseory neuronal cells, Figure 2.1 e, f, g, h, j, and in MDCK cells, Figure 2.1b and Figure 2.4a. John Dishinger, performed KIF17 experiments in Odora and NIH3T3 cells in Figure 2.1a, c. and Figure 2.4a-c. Additionally, John Dishinger conducted the immunoprecipitation experiments in Figure 2.5a, which contributed greatly to the understanding of KIF17 ciliary trafficking. Qi Xiao performed the mutagenesis screen in KIF17 and identified the H897R mutant. Ason Chiang carried out the molecular biology to create additional KIF17 single mutants.

Chapter 3 Co-Authors: John Dishinger, Lynne Blasius, Albert Liu, Ben Margolis, Kristen Verhey. John Dishinger performed the microinjection experiments of recombinant proteins, Figure 3.3. Lynne Blasius carried out the immunostaining experiments in NIH3T3 cells and tracheal cells, Figure 3.7a and 3.8c,d. Albert Liu in Ben Margolis' lab conducted the immunogold electron microscopy, Figure 3.7e-g and Figure 3.9.

Chapter 4 Co-Authors: Jeremy McIntyre, Jeffrey Martens. Jeffrey Martens proposed the lipid-anchor GFP experiments that I conducted in cultured cells. Jeremy McIntyre conducted similar experiments in mouse olfactory sensory neurons, which contributed to the overall understanding.

Lastly, I would like to show my appreciation to my parents, siblings Hou and Jean, and Jay for their continuous love and support.

Preface

Part of Chapter 2 (Figure 2.1, 2.4a-c and 2.5) is published as Dishinger, J.F., Kee, H.L., Jenkins, P.M., Fan, S., Hurd, T.W., Hammond, J.W., Truong, Y.N., Margolis, B., Martens, J.R., and Verhey, K.J. Ciliary entry of the kinesin-2 motor KIF17 is regulated by importin-β2 and Ran-GTP. Nature Cell Biology. 2010 Jul;12(7):703-10. PMID: 20526328

Chapter 3 is published as Kee, H .L., Dishinger, J.F., Blasius, T.L., Liu C.J., Margolis B. and Verhey, K.J. A Size-Exclusion Permeability Barrier and Nucleoporins Characterize a Ciliary Pore Complex that Regulates Transport into Cilia. Nature Cell Biology. 2012 Mar 4;14(4):431-7. PMID: 22388888

Table of Contents

List of Figures

Abstract

Cilia are microtubule-based projections that extend from the surface of all mammalian cells. These specialized organelles function in motility and in sensing extracellular signals during development and homeostasis. Mutations in proteins that localize to and function within cilia result in a range of human diseases, collectively termed ciliopathies. How ciliary proteins gain access to and are compartmentalized in the ciliary compartment is not well characterized.

I demonstrated for the first time that the cilium utilizes a permeability barrier to exclude soluble cytoplasmic molecules in a size-dependent manner, similar to the passive mechanisms that restrict entry into the nucleus. This demonstrates that the cilium is maintained as a privileged domain, accessible to specific components.

I investigated the molecular mechanisms regulating active trafficking of the kinesin-2 motor KIF17 to cilia in mammalian cells. KIF17 is essential for photoreceptor cell formation and regulates the ciliary trafficking of select membrane proteins including opsin and olfactory CNG channels (Insinna and Besharse, 2008; Jenkins et al., 2006). We determined that ciliary entry of KIF17 requires components that regulate active uptake into the nuclear compartment: a ciliary localization sequence similar to a nuclear localization sequence, the importin-β2 transport receptor, and the GTPase Ran (Dishinger et al., 2010).

Finally, I found that specific nucleoporins, key components of the nuclear pore complex (NPC) in the nuclear membrane, localize to the base of cilia and function to regulate ciliary entry of KIF17. I thus propose a model in which nuclei and cilia use similar active and passive mechanisms to regulate transport into the compartment. Further studies will be focused on determining mechanisms that distinguishes ciliary trafficking from nuclear transport.

This body of work provides the evidence that ciliary and nuclear import is regulated through similar mechanisms, suggesting important parallels between the function and relationship between nuclei and cilia. My study leads to a greater understanding of the cilia trafficking network and provides insight in the basis of human diseases associated with ciliary dysfunction.

Chapter 1
Introduction

A eukaryotic cell maintains proper function and morphology by compartmentalizing specific cellular activities in membrane-bound organelles, and coordinating intracellular trafficking between these organelles (Figure 1.1). The most notable example of a complex cellular organelle is the nucleus, which compartmentalizes the cell's genome within a bilayer membrane known as the nuclear envelope. Cytoplasmic components are restricted from passively entering into the nuclear compartment, while nuclear-destined components in the cytoplasm are actively transported through "gates" embedded within the nuclear membrane. Intracellular trafficking between organelles occurs via a network of actin filaments and microtubules that maintains cellular architecture but also acts as highways for molecular motors including kinesin, dynein and myosin (Figure 1.1c). For example, in polarized neuronal cells, the coordinated action of molecular motors brings vesicular cargoes from the cell body down the axon and dendrites for proper neuronal function (Hirokawa et al., 2010).

Cilia and Flagella

Most cells project a cilium or flagellum from their surface. Cilia and flagella are tiny, microtubule-based organelles that function in response to environmental cues and contribute to cellular motility. For example, motile cilia (or flagella) beat to move mucus up the trachea in respiratory cells, establish left-right asymmetry in the embryonic node, and propel sperm motility. Non-motile cilia, also called primary or sensory cilia, house many developmental signaling pathways that transduce external stimuli into intracellular signals. For a long time, these primary cilia were believed to be vestigial organelles without complex function, but they

are now believed to act as cellular “signaling antennas” responsible for a variety of functions including olfaction in olfactory neurons, photoreception in photoreceptor cells, mechanosensing of fluid flow in kidney epithelial cells, and responding to extracellular signals like Hedgehog (Hh), Wnt and PDGF ligands (Goetz and Anderson, 2010; Huangfu et al., 2003; Ross et al., 2005; Schneider et al., 2005).

Ciliopathies

The modern view of primary cilia as sensory antennae has been driven by recent findings that defects in ciliary formation, function, and/or signaling underlie a group of phenotypically diverse disorders now known as ciliopathies (Badano et al., 2006). Initially, disorders associated with in defects in ciliary function were primarily those of motile cilia dysfunction (El Zein et al., 2003; Ibanez-Tallon et al., 2003). Motile cilia are found on sperm, embryonic node, and epithelial cells including respiratory tract, brain ventricle and oviduct cells and function in cell motility, mucociliary clearance, nodal flow and ependymal flow. Thus, defects in ciliary beating and/or motility result in a plethora of phenotypes including randomization of left-right asymmetry, infertility, and respiratory defects.

More recently, defects in primary cilia have been associated with developmental disorders (Goetz and Anderson, 2010). Phenotypes include polydactyly, mental retardation, anosmia, hyperphagia, infertility, renal cysts, pancreatic cysts, hepatic cysts, long-bone malformation, neural tube abnormalities, crano-facial defects, brain stem malformation, retinal degeneration, aneurism, and genital malformation (Badano et al., 2006; Tobin and Beales, 2009). Ciliopathy patients can present with one or combinations of the above phenotypes in diseases such as Retinitis Pigmentosa, Polycystic Kidney Disease, Nephronophthisis, Meckel-Gruber Syndrome, Joubert Syndrome, Bardet-Biedl Syndrome, Senior-Loken Syndrome, Jeune Asphyxiating Thorasic Dystrophy, Oral-Facial-Digital

Syndrome and Sensenbrenner Syndrome (Badano et al., 2006; Tobin and Beales, 2009).

Cilium structure

Cilia are microtubule-based organelles with a core axoneme structure composed of nine outer doublet microtubules arranged symmetrically [(9+0 configuration) depicted in Figure 1.2b)]. Motile cilia also contain a central pair of single microtubules [(9+2 configuration) depicted in Figure 1.2e] and protein complexes responsible for ciliary beating including axonemal dynein and radial spokes. However, there are exceptions to this categorization; not all (9+0) and (9+2) cilia are immotile and motile, respectively. For example, embryonic node cilia are motile and beat to coordinate left-right asymmetry, but have a (9+0) axonemal structure. Furthermore, olfactory sensory neurons (OSNs) have a unique structural configuration. Electron microscopy studies show that olfactory cilia are composed of proximal and distal segments, with the proximal segment projecting 2-3 microns from the basal body in a (9+2) configuration, which then transitions into the distal segment of 50 microns in length with 1-4 singlet microtubule structure (Cuschieri and Bannister, 1975a; Cuschieri and Bannister, 1975b; Jenkins et al., 2009; Menco, 1984; Reese, 1965). Each OSN has a large number of cilia, typically 10-30, and although they possess a (9+2) structure, they are immotile as they lack the dynein arms required for movement. These numerous long cilia allow for the formation of a meshwork of cilia with increased surface area for odorant detection. Rod and cone photoreceptor cells also contain a specialized ciliary structure with an axoneme that extends from the inner segment within the cell body into the outer segment where phototransduction occurs within membrane folds (Greiner et al., 1981; Insinna and Besharse, 2008; Knabe and Kuhn, 1997). The photoreceptor's (9+0) axoneme begins as doublet microtubules and transitions into singlet microtubules. The significance of singlet microtubules in these specialized ciliary structures is not known.

Microtubules are cylindrical filaments that are assembled by the polymerization of α and β tubulin heterodimers (Figure 1.1c). The asymmetry of the α/β-tubulin subunit results in a polar microtubule filament with two different ends, a plus end where tubulin assembly takes place and a minus end, which is anchored in the centrosome or microtubule organizing center. The centrosome is composed of a pair of centrioles, small cylinders containing triplet microtubules in a 9+0 arrangement, and accessory proteins such as γ-tubulin. Cytoplasmic microtubules are nucleated from γ-tubulin complexes within the centrosome. Formation of a cilium requires maturation of the centrosome to form a basal body and nucleation of the axonemal microtubules from the triplet microtubules of the mother centriole (Figure 1.2 b, d). It is not known how the triplet microtubules of the basal body transition into the doublet microtubules of the axoneme. The basal body is anchored to the plasma membrane through distal (transition fiber) and subdistal (basal foot) appendages (Johnson and Rosenbaum, 1992). Once assembled, axonemal microtubules become marked by various post-translational modifications (PTMs) of their tubulin subunits including acetylation, polyglutamylation, detyrosination and glycylation (Gaertig and Wloga, 2008). Research suggests that the PTMs contribute to regulation of ciliary assembly, disassembly and stability (Gaertig and Wloga, 2008; Pan et al., 2004; Pathak et al., 2011; Pugacheva et al., 2007; Wloga et al., 2009) as well as regulation of axonemal dyneins (Ikegami et al., 2010; Kubo et al., 2010; Suryavanshi et al., 2010). Modified tubulin is frequently used as an immunostaining marker for cilia and basal bodies.

In cycling cells, the transition between basal body and centrosome needs to be carefully regulated (Nigg and Raff, 2009). Maturation of the centrosome into a basal body and formation of the cilium occur during the G0/1 phase of the cell cycle (Figure 1.3a). For a cell to move forward in cell division, the axoneme needs to be disassembled to release the basal body so that it can be replicated in S phase to form two pairs of centrioles. The centriole pairs coordinate to

organize the formation of a bipolar spindle during mitosis (Figure 1.3b) Each daughter cell receives a pair of centrioles, and post-division the mother centriole will form the basal body that anchors the cilium. In post-mitotic cells, maturation of the centrosome into a basal body is a final product of cellular differentiation. In multi-ciliated cell types such as OSNs, the centrioles are first duplicated into multiple copies in the cell body which then migrate along the developing dendrite and are anchored below the plasma membrane of the dendritic knob, thus priming ciliogenesis and enabling the axonemes to extend from the basal bodies to form multiple cilia (Figure 1.3c, (Jenkins et al., 2009). Interestingly, in contrast to OSNs, the basal bodies in sensory neurons in *C. elegans* degenerate after ciliogenesis (Reiter et al., 2012). It is not clear why and how the degeneration occurs, but the cilia structure and function remain unaffected.

Intraflagellar Transport

Cilia lack the machinery for protein synthesis and thus components must be synthesized in the cytoplasm, targeted to the ciliary compartment, and transported along the ciliary shaft. Transport within the ciliary compartment is carried out by Intraflagellar Transport (IFT), a bi-directional trafficking system along the axonemal microtubules (Rosenbaum and Witman, 2002). IFT was first discovered in the biflagellate alga *Chlamydomonas reinhardtii* when particles were observed moving up and down the flagellum by differential interference contract (DIC) microscopy (Kozminski et al., 1993). Further studies showed IFT particles as non-vesicular electron-dense complexes located between the microtubule axonemal core and the flagellar membranes (Kozminski et al., 1995). Detailed analyses in *Chlamydomonas* using genetics, biochemistry and cell biology have characterized the IFT complex as essential for ciliogenesis and maintenance (Cole et al., 1998; Iomini et al., 2001; Pan and Snell, 2005; Pazour et al., 1998; Piperno et al., 1998; Qin et al., 2004; Wloga et al., 2008). In parallel, studies in the nematode *C. elegans* demonstrated IFT builds and maintains neuronal sensory cilia (Orozco et al., 1999; Signor et al., 1999a; Signor et al.,

1999b). A large body of work has gone on to show that IFT is conserved throughout ciliated organisms from *Tetrahymena*, to zebrafish, mouse and humans (Rosenbaum and Witman, 2002).

IFT was put in the spotlight when it was discovered that Polaris, the mouse ortholog of the *Chlamydomonas* IFT particle protein IFT88, localizes to cilia in various cell types and is essential for the formation of primary cilia in kidneys (Pazour et al., 2000; Taulman et al., 2001). Tg737 mice with a hypomorphic mutation in Polaris/IFT88 had shorter cilia and developed polycystic kidney disease, situs inversus, hydrocephalus, pancreatic and liver defects. Tg737 mice lacking Polaris/IFT88 fail to form nodal cilia, and are embryonic lethal with more severe phenotypes including left-right asymmetry and neural tube defects (Murcia et al., 2000). The link between ciliary trafficking and human disease was advanced by studies demonstrating that kidney disease-associated gene products polycystin-1 and -2 localized to renal primary cilia and their homologs localize to the sensory neuronal cilia in *C. elegans* where they control male mating behavior (Barr and Sternberg, 1999; Pazour et al., 2002; Yoder et al., 2002). Collectively, these studies demonstrated a novel link between ciliary IFT, signaling, and genetic disease and pioneered investigations examining cilia as a complex signaling organelle.

Ciliary kinesin motors

Anterograde IFT movement to the tip of the cilium is powered by plus end-directed kinesin-2 family motors, and retrograde movement from the tip to the base is driven by the minus end-directed motor cytoplasmic dynein (Figure 1.2). Molecular motors walk on the surface of microtubules by utilizing ATP hydrolysis to convert chemical energy into mechanical energy and force. Kinesin motors involved in intracellular trafficking move processively to the plus (rapidly growing) ends of microtubules by taking many ATP-dependent steps along the microtubule before detaching (Hirokawa et al., 1989; Kikkawa et al., 2001; Nitta

et al., 2004). Kinesin motors are a superfamily of 14 different families that share a core kinesin motor domain containing microtubule- and ATP-binding sequences (Hirokawa et al., 2009). Outside of the core motor domain, kinesin families contain distinct sequences for oligomerization, cargo specificity, cellular localization and motor activity regulation (Miki et al., 2005). Kinesin motors typically form homodimers via coiled-coil segments, however some families form heterotetramers, heterotrimers or homotetramers. Kinesin motor activity must be tightly regulated in cells to prevent futile ATPase activity and microtubule binding. Kinesin motors have evolved to utilize autoinhibitory mechanisms to restrict enzymatic activity and prevent microtubule transport jams (Verhey and Hammond, 2009). In the absence of cargo association, kinesin motors fold into a compact structural conformation where the C terminal tail domain interacts with and inhibits the N terminal motor domain (Coy et al., 1999; Hammond et al., 2010; Hammond et al., 2009). It is thought that cargo binding releases this autoinhibition to allow microtubule binding and processive motion.

The kinesin-2 family is comprised of a heterotrimeric and homodimeric subfamilies. The heterotrimeric kinesin-2 complex is made up of two KIF3 motor domain-containing subunits, KIF3A and KIF3B, and a non-motor accessory protein KAP (Yamazaki et al., 1995; Yamazaki et al., 1996) (depicted in Figure 1.4a). KIF3A forms a heterodimer with KIF3B or KIF3C, and KAP associates with the dimer (Yamazaki et al., 1995; Yamazaki et al., 1996). KIF3A/KIF3B/KAP complex is the only identified heterotrimeric motor complex. It is not understood why this motor has evolved to function as a heterotrimeric motor.

Detailed analysis in sea urchins and *Chlamydomonas* first demonstrated that heterotrimeric kinesin-2 functions as an IFT motor protein of cilia and flagella (Orozco et al., 1999; Scholey, 2008; Signor et al., 1999b). However, the significance of kinesin-2 function in mammalian development was not fully appreciated until it was revealed that the disruption of heterotrimeric kinesin-2 abrogated ciliogenesis of nodal cilia in mouse embryos, resulting in left-right

asymmetry defects and embryonic lethality (Marszalek et al., 1999; Nonaka et al., 1998; Takeda et al., 1999). Transgenic kidney-specific knockout mice resulted in loss of renal cilia, formation of renal cysts, and ultimately renal failure (Lin et al., 2003). Together, these studies illustrated the importance of kinesin-2 in ciliary structure during development.

The second member of the kinesin-2 family is the homodimeric KIF17 (depicted in Figure 1.4b), which was cloned and characterized as a microtubule-based motor involved in dendritic trafficking in neurons (Setou et al., 2000). Genetic analysis in *C. elegans* discovered that the KIF17 homolog OSM-3 localizes to cilia, builds the distal segment of amphid channel cilia, and functions cooperatively with heterotrimeric kinesin-2 in the middle segments of channel cilia (Ou et al., 2005; Scholey, 2008; Signor et al., 1999b). In other neuronal cilia types, OSM-3 moves independently of kinesin-2 and is not required to build the distal segments of amphid wing "B" wing cilia (Mukhopadhyay et al., 2007). Detailed studies investigating mammalian KIF17 observed endogenous KIF17 localization in cilia in Madin–Darby canine kidney (MDCK) epithelial cells and olfactory epithelium (Jenkins et al., 2006). Expression of a dominant negative construct demonstrated that KIF17 regulates trafficking of cyclic nucleotide gated (CNG) channels to the ciliary compartment (Jenkins et al., 2006). Further studies in zebrafish showed that KIF17 is required to build the outer segment of photoreceptor cells and regulates opsin localization (Insinna et al., 2009). Collectively, it is believed that heterotrimeric Kinesin-2 is the core anterograde motor, and KIF17 functions are specific to cell type and cargo. Recent work suggests that KIF17/OSM-3 is not the only accessory kinesin motor in cilia as members of the kinesin-4 and kinesin-3 families have been found to localize to and/or function in cilia (Cheung et al., 2009; Endoh-Yamagami et al., 2009; Liem et al., 2009; Morsci and Barr, 2011; Verhey and Hammond, 2009).

Enrichment of specific proteins in the ciliary compartment

Proper motile and sensory function requires that many signaling factors are enriched in the ciliary compartment. In photoreceptor cells, the G protein coupled receptor (GPCR) rhodopsin and its associated signaling molecules transducin and arrestin concentrate in the outer segment in a light-dependent manner (Insinna and Besharse, 2008). Similarly, odorant receptors, G proteins Gαolf and Gγ13, Adenyl Cyclase III, and cyclic nucleotide gated (CNG) channels localize to the cilia in olfactory sensory neurons (McEwen et al., 2008). Other signaling factors that have been found to concentrate in the cilium in mammalian cells include: the polycystic kidney disease (PKD)-associated gene products fibrocystin, cystin, polycystin-1 and polycystin-2 (Follit et al., 2010; Tao et al., 2009; Yoder et al., 2002), the hedgehog signaling components Gli2, Gli3, Smoothened, Patched1 (Corbit et al., 2005; Haycraft et al., 2005; Rohatgi et al., 2007), the GPCRs somatostatin receptor 3 (Sstr3), serotonin receptor 6 (Htr6), melanin-concentrating hormone receptor1 (Mchr1) (Berbari et al., 2008a), and Dopamine receptor 1 (Domire et al., 2011), and the enzyme adenylyl cyclase II (ACII) (Bishop et al., 2007).

The ciliary membrane and intraciliary compartment are continuous with the plasma membrane and cytoplasm, respectively. How signaling factors are targeted to and concentrated in such a small region of the cell has been an active area of research. Entry into the cilium takes place in a region at the base of the cilium termed the transition zone where the basal body transitions into the axoneme (Figure 1.2c). The transition zone is characterized by transition fibers and Y-link structures that link the membrane to the basal body/axoneme, and bead-like membrane protrusions called the ciliary necklace (Figure 1.2c). The molecular components of the transition fibers, Y-link structures and ciliary necklace remain uncharacterized. It was hypothesized that the transition fibers and basal body act as a docking stage for ciliary entry and form a ciliary pore complex to exclude non-ciliary proteins from entering in a sieve-like manner,

analogous to the way that nuclear pore complexes prevent the entry of cytoplasmic components into the nucleus (Rosenbaum and Witman, 2002).

Movement of soluble proteins is thought to take place through 60nm gaps between the transition fiber pinwheel (Nachury et al., 2010). It is conceivable that soluble proteins could diffuse into and out of the ciliary compartment. Similarly, membrane proteins could passively slide laterally into and out of the ciliary membrane. However, specific proteins are enriched in the cilium when compared to the cytoplasm. Moreover, the entry and exit of ciliary proteins is both activity- and time-dependent. Thus, unique mechanisms must be in place to ensure proper trafficking of selected proteins into the cilium. The Hedgehog signaling pathway demonstrates the complexity of temporal and spatial ciliary trafficking of membrane and soluble proteins (Wong and Reiter, 2008). The transmembrane proteins Patched (Hedgehog receptor) and its downstream target Smoothened localize to the cilary membrane in a mutually exclusive manner depending on Hedgehog activation (Corbit et al., 2005; Rohatgi et al., 2009; Rohatgi et al., 2007). Additionally, soluble Gli transcription factors localize to the cilium but Gli2 is trafficked to the nucleus upon activation by Smoothened (Haycraft et al., 2005). The molecular mechanisms governing the movement into and out of the cilium are not well understood, and how movement into and out of the cilium modulates signaling activities is still not clear.

Ciliary targeting motifs

Proteins are directed to their destined compartment by organelle-specific targeting motifs. For example, proteins containing a signal sequence are targeted to the endoplasmic reticulum and then retained in this compartment by a Lysine-Aspartate-Glutamate-Leucine (KDEL) sequence (Rapoport, 2007). Ciliary targeting motifs have not been identified yet on soluble proteins. In contrast, several different ciliary targeting sequences (CTS) have been identified on ciliary membrane proteins. Rhodopsin contains a QVSPA motif on its C terminal tail that

is found mutated in patients with retinal degeneration. Localization studies in *Xenopus laevis* determined that the QVSPA motif is a CTS necessary for targeting into the outer segment of photoreceptor cells. Additionally, rhodopsin is lipid modified by dual palmitoylation and the fusion of rhodopsin's CTS to a lipid-anchored GFP was sufficient to confer outer segment localization (Deretic et al., 2005; Tam et al., 2000). Similar consensus CTS have been identified in other membrane proteins. The polycystic kidney disease-associated gene product polycystin-2 contains a RVxP motif in its CTS located within the N-terminal cytoplasmic tail (Geng et al., 2006). Furthermore, the olfactory CNG channel subunit CNG1b contains a RVSP in its C-terminus that is necessary but not sufficient for ciliary trafficking in MDCK cells (Jenkins et al., 2006). Another CTS identified is the Ax(S/A)xQ motif found on the third intracellular loop of GPCRs including somastatin receptor 3 (SSTR3) and serotonin receptor 6 (5HT6) (Berbari et al., 2008a).

Ciliary localization can be directed by lipid motifs as well as protein sequence motifs. The 18-residue CTS motif CLVCCWFKKSKTRKIPE in the C terminal tail of the single pass transmembrane protein fibrocystin, which is associated with human autosomal recessive PKD, is dually palmitoylated and shown to associate with lipid-raft type membranes (Follit et al., 2010). The PKD-associated gene product cystin is N-terminally lipidated by myristoylation and contains a unique CTS in AxEGG (Tao et al., 2009). Collectively, these studies demonstrate that a common theme amongst many ciliary transmembrane and membrane-associated proteins is the post-translational lipidation by myristoylation and palmitoylation. It appears that lipidation is necessary for ciliary localization of these proteins and suggest that it provides a signal to partition the membrane proteins with specific lipid microdomains that are preferentially targeted to the cilium.

Mechanisms of ciliary trafficking

What are the cellular pathways that regulate the specific localization of ciliary proteins to this compartment? Several pathways have been discovered yet the molecular and functional relationships between these pathways remain ill defined. One model proposes that active transport by IFT particles is responsible for delivering ciliary proteins to the compartment. This model is largely based on the role of IFT in powering transport along the ciliary axoneme. In addition, the finding that IFT particles have α-solenoids and β-propeller domains found in COPI, COPII and clathrin coat complexes suggests that they share conserved roles in protein trafficking. However, it is not well understood how IFT particles are trafficked from the cytoplasm to the cilium. Since ciliogenesis requires IFT proteins, studies to determine whether the IFT protein complex forms before, during or after ciliary entry are technically challenging.

The active transport model proposes that membrane proteins synthesized in the ER are trafficked into post-Golgi vesicles that are selectively targeted to and fuse with the periciliary membrane (Rosenbaum and Witman, 2002). The membrane proteins then associate with IFT particles and motors proteins at the ciliary base and move laterally into the ciliary membrane. Several lines of evidence support the idea that IFT is involved in ciliary protein entry. IFT regulates the ciliary import of large protein assemblies of outer dynein arms and radial spoke complexes that are formed in the cytoplasm (Hou et al., 2007; Qin et al., 2004). Also, IFT52 localizes to transition fibers in *Chlamydomonas* by immuno-electron microscopy, suggesting that the transition fibers act as a docking point for IFT particles (Deane et al., 2001). Additionally, IFT20 associates with the trans-Golgi network and post-Golgi vesicles (Follit et al., 2006), and to bridge IFT particle complexes with heterotrimeric Kinesin-2 (Baker et al., 2003). Therefore, it is believed that IFT20 directs ciliary proteins from the Golgi network to the ciliary base. It was proposed that IFT association facilitates Smoothened transport into the ciliary domain from intracellular pools (Wang et al., 2009) although another study has

suggested that Smoothened enters the ciliary compartment laterally from the plasma membrane in a process that may be IFT-independent (Milenkovic et al., 2009).

In addition to the IFT particle proteins, the multi-protein BBSome complex also shares structural homology to COPI and COPII coat proteins. The genes encoding subunits of the BBSome were identified in studies on Bardet–Biedl syndrome, a ciliopathy with phenotypes including obesity, mental retardation, polydactylyl and hyperphasia. The BBSome forms planar, polymerized, coat-like complexes on liposomes *in vitro* and regulates ciliary trafficking of GPCRs including SSTR3 (Berbari et al., 2008b; Jin et al., 2010). The model suggests that the BBSome associates with membrane proteins to transport them into the ciliary membrane (Jin et al., 2010).

Transport to the ciliary base is also likely to involved members of the small GTPase family. In photoreceptor cells, the GTPase Arf4 was identified as binding to rhodopsin's CTS and assembling into a trafficking complex with Arf GTPase-activating protein ASAP1 (Deretic et al., 2005; Mazelova et al., 2009) and Rab8 mediates ciliary trafficking of rhodoposin-containing Golgi-derived vesicles (Deretic et al., 2005; Moritz et al., 2001). Rab8 localizes to primary cilia and is also involved in ciliary formation and maintenance in cultured cells (Follit et al., 2010; Westlake et al., 2011; Yoshimura et al., 2007). There are a growing number of Rab and Arf proteins involved in the directed trafficking from the Golgi complex to cilia (Nachury et al., 2010).

A second model for ciliary trafficking proposes that a large complex of proteins associated with various ciliopathies function as gatekeepers (Omran, 2010). A growing body of work has shown that these gatekeeper proteins localize to the base of the cilium at the basal body and transition zone (Garcia-Gonzalo and Reiter, 2012; Hildebrandt et al., 2009). Knockdown experiments and FRAP assays demonstrated that the Nephronophthisis, Meckel and Joubert syndrome-

associated NPHP-MKS-JBTS protein complex regulates localization of membrane proteins in mammalian cells (Chih et al., 2011; Garcia-Gonzalo et al., 2011; Sang et al., 2011). In complementary studies, genetic disruption of both MKS and NPHP proteins in *C. elegans* results in transition zone structural defects visualized through electron microscopy, and allows spurious entry of non-ciliary membrane proteins into the cilium (Williams et al., 2011; Williams et al., 2010). In *Chlamydonomas*, immuno-gold electron microscopy showed that NPHP6/CEP290 localizes to the transition zone Y-link structures. Furthermore, disruption of NPHP6/CEP290 results in abnormal ciliary protein content with increased IFT B and BBS4 protein levels and decreased polycystin-2 and IFT A protein levels (Craige et al., 2010). This is in agreement with a previous study in which a hypomorphic NPHP6/CEP290 mutation in mice results in loss of the peripheral membrane G proteins Golf and Gγ13 from olfactory cilia but does not affect enrichment of transmembrane olfactory ACIII and CNG channels (McEwen et al., 2007). Further studies uncovering the role of these disease gene products will help to elucidate the underlying molecular mechanisms in which this complex functions to regulate protein entry.

In the case of membrane proteins, a third model has been put forth indicating a membrane diffusion barrier that restricts proteins in the ciliary membrane. In fluorescence recovery after photobleaching (FRAP) experiments, little fluorescence recovery was observed when the ciliary-localized fluorescently-tagged membrane proteins were bleached. However, knockdown of the filament-forming GTPase septin resulted in increased recovery, suggesting that septin forms a membrane diffusion barrier that retains membrane proteins within the ciliary membrane (Hu et al., 2010). Another study showed that ciliary entry of membrane proteins can be prevented by a selective exclusion mechanism that retains membrane proteins within the plasma membrane. Francis et al. demonstrated that association with the apical actin cytoskeleton network prevents ciliary entry of cytoplasmic membrane proteins such as podocalyxin. Disrupting this association allowed for podocalyxin entry into the ciliary

membrane (Francis et al., 2011). Whether selective exclusion is a universal mechanism for preventing ciliary entry of cellular membrane proteins is not known.

A question that remains unanswered is: how are soluble proteins transported to, and retained in the ciliary compartment? For example, the most prevalent protein within the cilium is soluble tubulin subunits that form the structural axonemal core. As tubulin is ubiquitously found throughout the whole cell, how axonemal precursors are loaded into the cilium is unclear. It has been suggested that IFT transports tubulin subunits into *Chlamydomonas* flagella (Hou et al., 2007; Qin et al., 2004). The IFT particles are large protein complexes unique to the cilium, but how their entry and exit is regulated is not known. In contrast to membrane proteins, IFT particle movement between the ciliary and cytoplasmic compartments is dynamic as fluorescently-tagged IFT88 showed rapid fluorescence recovery when the ciliary pool was bleached in a FRAP assay (Hu et al., 2010).

In Chapter 2, I set out to answer how the soluble Kinesin-2 homodimeric KIF17 motor traffics to cilia in mammalian cells. We determined that ciliary trafficking of KIF17 is regulated by nuclear import machinery (Dishinger et al., 2010). In Chapter 3, I examine whether the cilium forms a diffusion barrier to cytoplasmic molecules in mammalian cells, and determine that the base of the cilium forms a permeability barrier that allows passive entry of small molecules but restricts large molecules. In Chapter 3, I investigate whether components of the nuclear pore complex (NPC) localize to the ciliary base in cells. In the section below, I will describe the mechanisms of nuclear entry.

Mechanisms of Nuclear Entry

The nucleus houses the eukaryotic cell's genetic material and transcriptional machinery. To ensure proper functioning of nuclear activity, the entry into and out

of the nucleus is tightly regulated. The nucleus is bounded by a limiting double membrane called the nuclear envelope (Watson, 1955). The compartmentalization within the nucleus functions to first, protect and condense the genome with a subcellular space from the cytoplasm, and second, provide a platform for controlled access and regulation of chromatin to transcriptional machinery.

Embedded in the nuclear envelope are protein gateways called nuclear pore complexes (NPCs) that control the exchange of molecules between the cytoplasm and nucleus. Two modes of passage through the NPC have been characterized. First, a passive diffusion mechanism allows the NPC to accommodate diffusion of small molecules. Studies have determined that the NPC forms a permeability barrier where molecules up to 30kDa can rapidly enter the nuclear compartment (Lang et al., 1986; Mohr et al., 2009; Peters et al., 1986). However the movement of molecules that are 30-40kDa is significantly hindered in comparison (Lang et al., 1986; Mohr et al., 2009; Peters et al., 1986).

Second, an active signal-mediated mechanism is utilized by NPC to control the passage of molecules into the nucleus from the cytoplasm (Figure 1.5). The first piece of evidence for a signal-mediated transport system came from a study where nucleoplasmin was injected into the cytosol and rapidly entered the nucleus (Dingwall et al., 1982). However, when the tail domain was removed, the remaining nucleoplasmin did not traffic into the nucleus, suggesting that the tail domain was necessary for nuclear entry. Furthermore, the tail domain alone was sufficient to accumulate in the nucleus, suggesting that a nuclear entry signal is contained within the tail domain. Consequently, studies determined that proteins that are actively transported into the nucleus contain an import signal called a nuclear localization sequence (NLS). The first NLS was discovered in the simian virus 40 (SV40) large T-antigen (Kalderon et al., 1984; Lanford and Butel, 1984). Nucleoplasmin and SV40 contain a classical NLS that are characterized by a stretch of basic residues Lysines and Arginines (Kalderon et al., 1984; Lanford

and Butel, 1984; Robbins et al., 1991). There are other forms of NLSs, such as the acidic M9 NLS found on an RNA binding protein, heterogeneous nuclear ribonucleoprotein A1.

In addition to NLSs, active signal-mediated nuclear import requires nuclear transport receptors that recognize NLS-containing proteins in the cytoplasm. These receptors come in two forms: importin α and importin β (Adam and Adam, 1994; Adam and Gerace, 1991; Chi et al., 1995; Gorlich et al., 1994; Gorlich et al., 1995). Importin αs bind to classical NLS, and subsequently Importin βs associate with Importin α. Importin βs then mediates the shuttling of the complex through the NPCs. In some cases Importin βs can directly bind to specific non-basic NLS such as the M9 NLS (Bonifaci et al., 1997; Fridell et al., 1997).

NPCs are big cylindrical protein complexes embedded in the nuclear envelope (Brohawn et al., 2009; D'Angelo and Hetzer, 2008; Davis and Blobel, 1986). Each NPC is composed of multiple copies of 30 different nucleoporins. Nucleoporins assemble into distinct subcomplexes that function to carry out specific roles within the NPC. Cytoplasmic nucleoporin filaments extend from the NPC into the cytoplasm (Kraemer et al., 1994). The FG-nucleoporin subcomplex is characterized by natively unfolded Phenylalanine-Glycine (FG) repeats (Starr et al., 1990; Strawn et al., 2004). FG-nucleoporins are largely unstructured and line the surface of the central channel of the NPC to form the transport barrier (Denning et al., 2003). It is believed that the FG repeats provide docking sites for the cargo-Importin complex to translocate through into the nucleus (Isgro and Schulten, 2007). The exact nature of how the FG-nucleoporins provide a path for cargo-Importin complexes remains controversial. Linker nucleoporins facilitate in anchoring the FG nucleoporins (Schrader et al., 2008). The core scaffold that makes up the central ring of the NPC is composed of the inner and outer ring nucleoporins (Alber et al., 2007). The transmembrane nucleoporins span the outer and inner nuclear membrane and function to anchor the NPC within the nuclear envelope (Hallberg et al., 1993). Finally the nuclear nucleoporins

emanate into the nucleoplasm, forming a platform for nuclear specific activities (Krull et al., 2004).

The directionality of nuclear import is governed by a Ran-GTPase system. Ran is a GTP-binding protein that is found highly concentrated in its GTP-bound form in the nucleus (Bischoff and Ponstingl, 1991). Conversely, GDP-bound Ran is high in the cytoplasm. The high Ran-GTP concentration in the nucleus dissociates the Importin-cargo complex. The Ran-GTP gradient across the nuclear envelope is regulated by the guanine nucleotide exchange factor RCC1 (Bischoff and Ponstingl, 1991), Ran-GTPase activating protein RanGAP1 (Bischoff et al., 1994), and Ran-binding protein RanBP1 (Bischoff et al., 1995).

In summary, the permeability barrier formed by the NPC serves to protect and maintain the nucleus as a privileged domain with unique composition that is accessible to specific molecules. Moreover, the receptor-mediated active transport mechanism allows for the spatial and temporal control of trafficking of content from the cytoplasm into the nucleus.

Conclusion

In conclusion, the cilium is a unique organelle with diverse sensory and motility functions specified by its protein composition. The cell controls which proteins reach the ciliary base and utilizes multiple mechanisms to facilitate entry, retention and exclusion. Given their critical and wide-ranging roles, ciliary dysfunction results in a wide range of human diseases with pathological phenotypes. Thus, understanding how the cilium compartmentalizes signaling molecules has broad implications in cell biology and will lead to a greater understanding of the molecular mechanisms in human diseases.

Figures

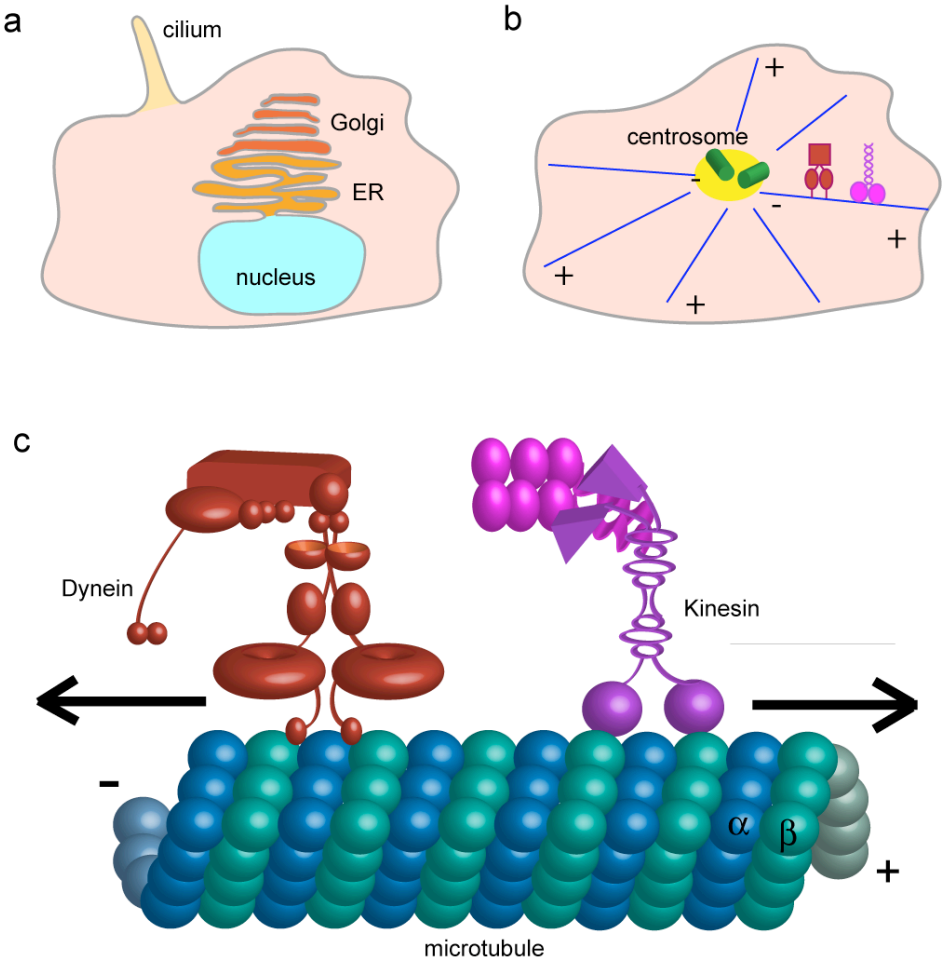

Figure 1.1 Cellular compartmentalization and intracellular trafficking in mammalian cells

(a) Cells compartmentalize subcellular activities into organelles that are bounded by lipid membranes (grey lines). Examples include the nucleus (blue), endoplasmic reticulum (ER, orange) and Golgi (red). The primary cilium (yellow) protrudes from the surface of the cell and does not have a limiting membrane as the ciliary membrane is continuous with the plasma membrane. (b-c) Intracellular trafficking is powered by motor proteins that walk on microtubule highways to carry cargoes including vesicles, protein complexes and organelles. Microtubules are filamentous structures composed of polymerized heterodimeric α/β-tubulin subunits. In cells, microtubules are usually oriented with the growing (plus) ends at the cell periphery and their anchored (minus) ends anchored in the centrosome or microtubule organizing center. Plus end-directed transport is driven by kinesin motor proteins and minus end-directed transport is driven by dynein motor proteins.

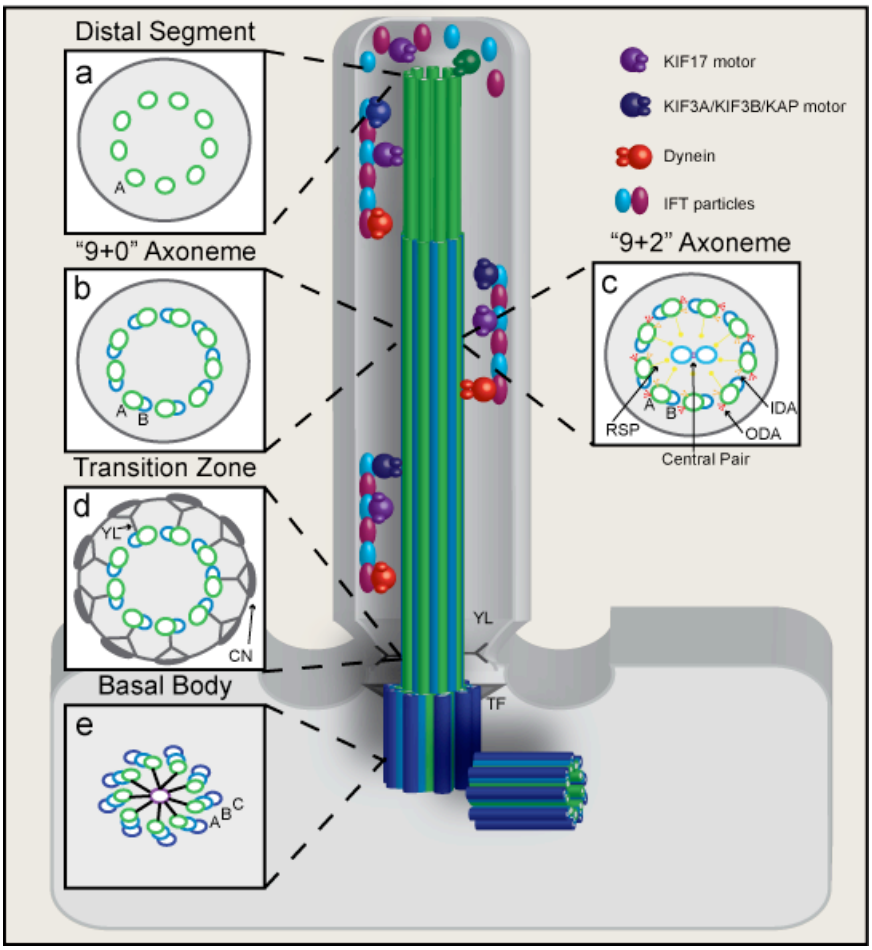

Figure 1.2 Structure of cilium

The basal body anchors the microtubule axoneme that forms the structural core of the primary cilium. Kinesin motor proteins Kinesin-2 (dark blue) and KIF17 (purple) power anterograde IFT from the base of the cilium to the tip (left side of the axoneme). IFT particles form trains that associate with kinesin motors. IFT particles are reorganized at the distal tip and cytoplasmic dynein motors (red) power retrograde transport back to the base of the cilium. Insets depict cross-sections of the microtubule structure: (a) Microtubule singlets of the distal segment. (b) 9+0 microtubule doublets of the axoneme. (c) 9+2 microtubule doublets and central pair of the axoneme with associated radial spokes (RSP), outer and inner dynein arms (ODA and IDA). (d) The transition between the axoneme and the basal body is called the transition zone (TZ), which is characterized by Y-link structures (YL) and ciliary necklace (CN). (e) Microtubule triplets of the basal body barrel.

This figure was adapted and modified from Pieczynski JN and Yoder BK. Seldin and Giebisch's The Kidney, 5th Edition. Volume 2, Chapter 11. *Renal Cilia Structure, Function, and Physiology.* Elsevier Publishing. 1 Oct 2012. Edited by Robert Alpern, Orson Moe, and Michael Caplan.

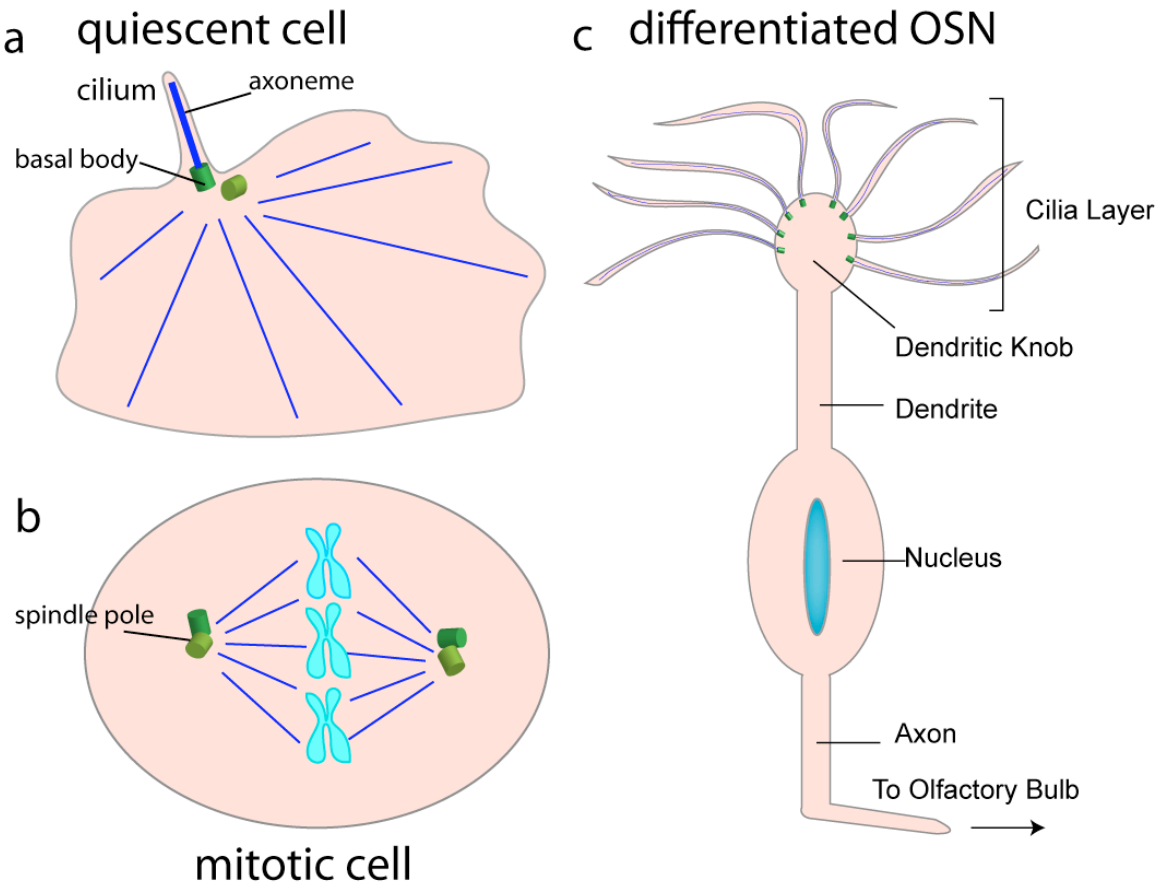

Figure 1.3 Coordination of cell cyle, ciliogenesis and differentiation

(a) In a non-proliferating cell, the mother centriole (dark green) forms the basal body that anchors the ciliary axoneme. (b) During mitosis, two centriole pairs function to form the poles of the mitotic spindle. (c) In post-mitotic differentiated cells such as the olfactory sensory neuron (OSN), multiple centrioles are assembled and migrate to the surface of the dendritic knob, forming basal bodies that extend cilia.

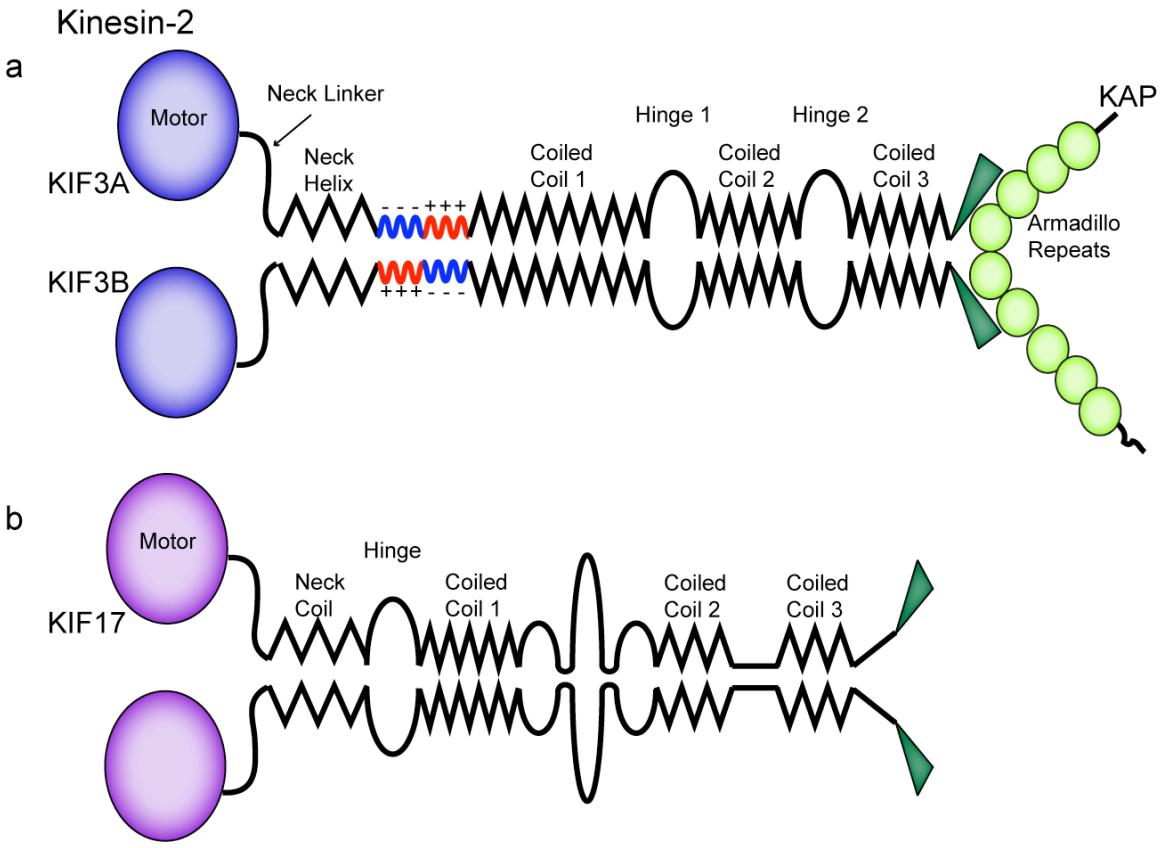

Figure 1.4 Subunit composition of Kinesin-2 motors

All kinesin motors contain an N-terminal kinesin motor domain (purple) responsible for microtubule plus end-directed ATP-dependent processive motion. Other domains include the neck domain and coiled-coil stalk domains for oligmerization. (a) Kinesin-2 is a heterotrimeric motor composed of two motor domain-containing heterodimerizing subunits KIF3A and KIF3B. Charged regions in red and blue also contribute to heterodimerization. Kinesin-associated protein (KAP) associates with the C terminus of KIF3A/KIF3B. (b) KIF17 forms a homodimer.

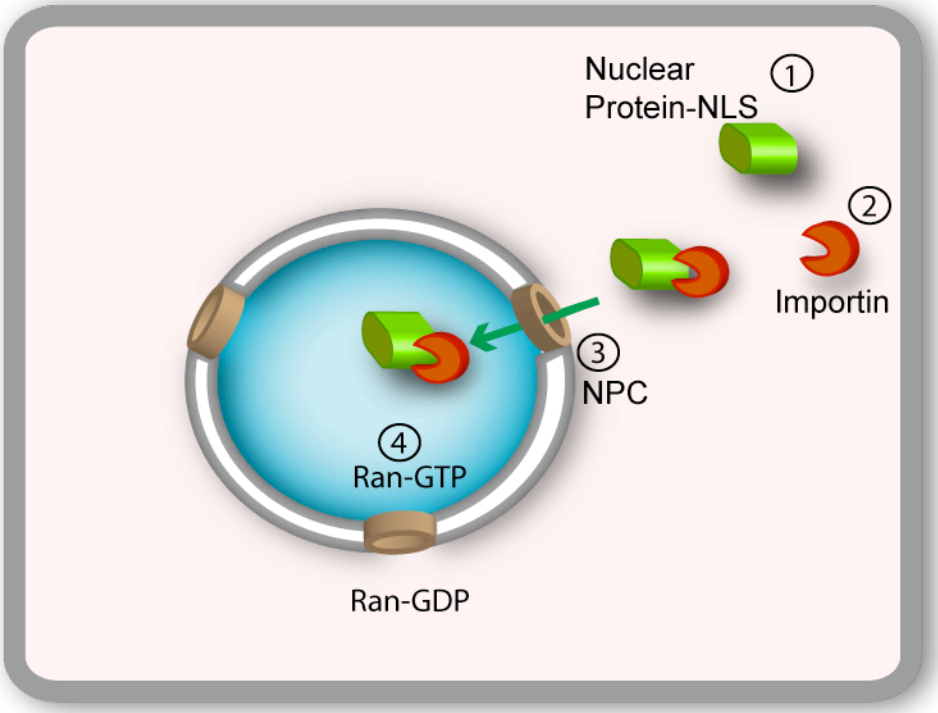

Figure 1.5 Schematic of nuclear import cycle

During nuclear import, (1) a protein containing a nuclear localization sequence (NLS) is (2) recognized by a nuclear transport receptor known as importin. (3) The cargo-importin complex is translocated through a nuclear pore complex (NPC) into the nucleus, where a high Ran-GTP concentration facilitates disassembly of the complex.

Chapter 2
Mechanisms of KIF17 trafficking into Cilia

Introduction

A large body of work in the last decade has characterized the role of the kinesin-2 family of motors in ciliogenesis and ciliary trafficking. Pioneering work carried out in the nematode *C. elegans*, including detailed genetic studies and imaging of fluorescently tagged motors, have investigated the role of homodimeric OSM-3, the KIF17 homologue, and heterotrimeric kinesin-2 (KLP-11, KLP-20 and KAP-1) complexes in the "channel" cilia projecting from the dendritic endings of sensory neurons (Cole, 2005; Orozco et al., 1999; Ou et al., 2005; Pan et al., 2006; Signor et al., 1999b; Snow et al., 2004). The axonemes of these channel cilia contain two specific domains, the middle segment of nine doublet microtubules and the distal segment of nine singlet microtubules. *osm-3* mutants that lack functional OSM-3 do not have distal segments, suggesting that OSM-3 is required to build the distal segments of cilia (Cole, 2005; Snow et al., 2004). Interestingly, *klp-11* or *kap-1* single mutants lacking functional heterotrimeric kinesin-2 have full-length cilia (Cole, 2005; Snow et al., 2004). In contrast, *klp-11;osm-3* or *kap-1;osm-3* double mutants lacking both hetero- and homodimeric kinesin-2 motor functions fail to form the ciliary axoneme (Cole, 2005; Snow et al., 2004). From this genetic analysis, a model was proposed where OSM-3 and heterotrimeric kinesin-2 function redundantly to build the middle segment, but OSM-3 alone builds the distal segments. Further work using *in vitro* motility assays and *in vivo* transport assays demonstrated that both OSM-3 and kinesin-2 mechanically compete with each other in the middle segment resulting in an intermediate IFT velocity, although the mechanism of how two motors can cooperate yet compete in such a manner is not clear (Cole, 2005; Ou et al.,

2005; Snow et al., 2004). Subsequently, this model has proven to be not universal to all *C. elegans* neuronal cilia, as in-depth studies investigating different a neuronal type, AWB wing cilia, showed that OSM-3 is not required to build AWB distal segments, and that OSM-3 moves independently of kinesin-2 in the middle segment (Mukhopadhyay et al., 2007). Therefore, OSM-3 and kinesin-2 may function in a cell-type specific manner in *C. elegans* cilia.

Using zebrafish as a model system to study the role of the homodimeric motor KIF17, Insinna et al. observed KIF17 expression in photoreceptors and other ciliated tissues (Insinna and Besharse, 2008). They found that KIF17 co-localized with IFT proteins in the outer segments of the photoreceptor cells. Additionally, KIF17 interacted with IFT proteins in co-immunoprecipitation studies from retina extracts. Interestingly, knockdown of KIF17 did not cause lethality or developmental defects, but did result in mistargeting of opsin to the outer segment and disruption of proper outer segment formation. This suggests that KIF17 has retina-specific functions in protein targeting and photoreceptor development in zebrafish. However, other motors may be able to functionally replace KIF17 as a recent study in zebrafish showed that a chemically-induced *kif17*^{sa0119} truncation mutant did not have any obvious cilia-associated morphological defects, with the exception of the olfactory cilia that were slightly shorter in length (Zhao et al., 2012). Intriguingly, this *kif17*^{sa0119} mutant zebrafish did not have any opsin mislocalization in the photoreceptors.

The role of KIF17 in mammalian cilia has also been examined. Endogenous KIF17 localizes within the ciliary layer of olfactory sensory neurons (OSNs) in the olfactory epithelium and in the cilia of cultured MDCK cells (Jenkins et al., 2006). Expressing a dominant negative KIF17 construct in MDCK cells abolished ciliary trafficking of the olfactory CNG channel CNGB1b. Furthermore, co-immunoprecipitation assays from rat olfactory epithelium lysates showed that KIF17 interacts with the CNG channel. Overexpression of the dominant negative KIF17 construct did not affect cell polarity or ciliogenesis, whereas expression of

dominant negative KIF3a, part of the heterotrimeric kinesin-2 motor, did abolish ciliogenesis. This was the first study to show that mammalian KIF17 regulates trafficking of a ciliary cargo,

The fact that only a subset of kinesin motors localize to and function within the cilium indicates that entry into the cilium from the cytoplasm is a selective and specific process. An important question that remains is what are the molecular mechanisms by which KIF17 gains access to the ciliary compartment? Entry into the ciliary compartment takes place at the base of the cilium distal to the basal body. This region has been termed the transition zone (TZ) and is characterized by the ciliary necklace and Y-shaped structures (Y-links) seen by scanning and transmission electron microscopy (Figure 1.2c) (Anderson, 1972; Gilula and Satir, 1972; Reiter et al., 2012). Ciliary localization sequences have been identified on membrane proteins and several small GTPases and protein complexes are involved in membrane protein trafficking (reviewed (Nachury et al., 2010)). However, whether ciliary motors also utilize specific localization sequences to confer ciliary targeting is not known.

I set out to determine how KIF17 motors are selectively transported into the ciliary compartment in mammalian cells. In this study, I demonstrate that KIF17's tail domain is both necessary and sufficient to enter into primary cilia of cultured cells. I determined that the KIF17 tail domain contains a ciliary localization signal (CLS) necessary for ciliary targeting of the motor. The CLS is similar in nature to nuclear localization signals (NLS) that facilitate nuclear import, suggesting parallels between nuclear and ciliary trafficking. Furthermore, KIF17 binding to a specific nuclear import receptor was found to be CLS-dependent. Finally, I generated preliminary data to suggest a potential secondary signal that could regulate KIF17 ciliary trafficking.

Results

To study mechanisms of ciliary trafficking of KIF17, fluorescently-tagged KIF17 was expressed in various cultured ciliated cells. Cells were fixed and immunostained with antibodies to acetylated tubulin to mark the ciliary axoneme. Human KIF17 fused to monomeric Citrine (mCitrine, a variant of yellow fluorescent protein), was localized in a diffuse manner within the cytoplasm of all cells tested. The diffuse localization of KIF17-mCit is consistent with previous reports that full length KIF17 is inactive for microtubule-based motility due to the autoinhibited state of the motor (Hammond et al., 2010). KIF17-mCitrine also localized to the distal tips of the primary cilia in all cell types, including NIH3T3 (mouse embryo fibroblast), Odora (rat olfactory sensory neuronal), hTERT-RPE (mouse retinal pigment epithelial) and MDCK (canine kidney epithelial) cells (Figure 2.1a-d, (Dishinger et al., 2010)). This localization is presumably due to activation of KIF17 by its ciliary cargo and ATP-dependent motility to the plus ends of the microtubules in the cilium distal tip.

Tail domain of KIF17 is necessary and sufficient for ciliary localization

How KIF17 traffics specifically to the ciliary compartment is not understood. To determine the domains necessary for ciliary localization, truncated forms of the KIF17 motor were constructed and expressed in Odora cells. KIF17 is composed of an N-terminal motor domain, a neck coiled-coil (NC) domain, three coiled-coil segments (CC1, CC2, CC3), and a C-terminal tail domain (schematic in Figure 2.1i). Removing the tail domain to create KIF17(aa1-846)-mCitrine resulted in the abolishment of ciliary localization in Odora cells (Figure 2.1e, j (Dishinger et al., 2010)). Additional C terminal truncations, KIF17(1-795)-mCitrine, KIF17(1-738)-mCitrine and KIF17(aa1-490)-mCitrine, also showed reduced ciliary localization (Figure 2.1 f, g, h, j (Dishinger et al., 2010)). KIF17(aa1-490)-mCitrine and KIF17(1-738)-mCitrine are active motors due to deletion of autoinhibitory sequences and accumulated at the plus ends of the microtubules in the cell periphery (Figure 2.1 g,h), similar to previous work in

hippocampal neurons (Hammond et al., 2010). Collectively, these results suggest that the C-terminal tail domain is essential for ciliary entry. This may be mediated by the tail domain's interaction with cargo or IFT machinery, as the tail domain of KIF17 is a believed to associate with cargo.

To test whether the KIF17 tail domain is sufficient for ciliary targeting, two constructs were generated, one containing the coiled-coil stalk region and the tail domain [mCitrine-KIF17(aa488-1029), Figure 2.2f] and one containing only the tail domain [mCitrine-KIF17(aa801-1029), Figure 2.2n]. When the stalk+tail domain construct was expressed in NIH 3T3 cells together with the ciliary marker Arl13b-mCherry, mCitrine-KIF17(aa488-1029) localized to the distal tips of cilia in the majority of the cells (n=19 of 25) (Figure 2.2a, b, g). In some of these cells (n=8 of 25), mCitrine-KIF17(aa488-1029) was also localized at the base of the cilium (Figure 2.2c, g). In a few cells, mCitrine-KIF17(aa488-1029) was observed along the ciliary axoneme (Figure 2.2d, g). These localization studies suggest that the combined stalk+tail domains of KIF17 are sufficient to enter the ciliary compartment.

When the tail domain construct was expressed in NIH 3T3 cells, mCitrine-KIF17(aa801-1029) localized to the cilium in the majority of expressing cells [(n=18 of 23) Figure 2.2h, o]. In half of these cells (n=8 of 18), mCitrine-KIF17(aa801-1029) localized along the cilium (Figure 2.2k, m, o). In the other half of these cells (n=8 of 18), mCitrine-KIF17(aa801-1029) localized to the distal tip similar to full-length KIF17-mCitrine (Figure 2.2h, i, o). mCitrine-KIF17(aa801-1029) was also found at both the cilia tip and base in a few cells (Figure 2.2j, l, o).

Taken together, the localization of the stalk+tail [mCitrine-KIF17(aa488-1029)] and tail [mCitrine-KIF17(aa801-1029)] constructs indicates that the tail domain is sufficient for ciliary entry. That ciliary entry of KIF17 does not require its motor activity was initially surprising as motor activity was previously thought to be

required for localization along the cilium and at the distal tip. Localization of truncated KIF17 motors at the distal tip or along the cilium may be a result of the tail domain's association with endogenous full-length motors, IFT particles and/or associated cargo proteins. This can be examined by conducting experiments testing association of the KIF17 tail domain with IFT particles.

Basic sequence is necessary for ciliary and nuclear localization of KIF17 tail domain

Surprisingly, in addition to ciliary localization, both the KIF17 stalk+tail and tail constructs localized predominantly to the nuclei as shown by co-localization of mCitrine-KIF17(aa488-1029) and mCitrine-KIF17(aa801-1029) with Hoescht in NIH 3T3 cells (Figure 2.2a, h). Nuclear localization of these constructs was observed regardless of the epitope tag (myc or mCherry) (Dishinger et al., 2010). The nuclear localization of the tail domain constructs suggests that there are similarities in the trafficking between nuclear and ciliary compartments. To investigate whether ciliary entry of KIF17 utilizes similar mechanisms of nuclear import, the primary sequence of KIF17 was scanned for residues that resemble a nuclear localization sequence (NLS), which are import sequences found on proteins that are transported into the nucleus.

In looking for a sequence within the KIF17 motor that resembles a NLS, a basic sequence Lysine-Arginine-Lysine-Lysine (KRKK) was found within the KIF17 tail domain at residues 1016-1019. A construct mutating these basic residues to Alanines (AAAA) within the tail domain construct was created and expressed in NIH 3T3 cells (schematic, Figure 2.3g). mCitrine-KIF17(aa801-1029,1016-1019Ala) was no longer localized exclusively in the nucleus like wild-type mCitrine-KIF17(aa801-1029), but was found in both nuclear and cytoplasmic compartments with similar fluorescence intensities (Figure 2.3a, b, f). These results indicate that the stretch of basic residues in the KIF17 tail domain can function as an NLS.

To determine whether mutation of the basic residues at aa1016-1019 in the KIF17 tail domain also affects the ciliary localization, mCitrine-KIF17(aa801-1029,1016-1019Ala) localization in cilia was tested. mCitrine-KIF17(aa801-1029,1016-1019Ala) showed reduced localization to the cilium, being localized along the cilium in only 5 of 18 cells (Figure 2.3f). Interestingly, mCitrine-KIF17(801-1029,1016-1019A) was localized below the Arl13b-mCherry ciliary marker in all the cells (Figure 2.3 a,b, f). To test whether this localization corresponds to the centrosome/basal body, expressing cells were counter-stained with gamma-tubulin. Colabeling mCitrine-KIF17(aa801-102,1016-1019A) with gamma-tubulin clearly demonstrated colocalization at the basal bodies (Figure 2.3e). To confirm that the basal body localization was not an artifact of fixation, this construct was expressed and imaged under live conditions. In live conditions, mCitrine-KIF17(801-1029,1016-1019A) was clearly at the basal body region in all 18 cells (Figure 2.3 c, d). Collectively, these experiments suggest that the basic residues at aa1016-1019 can act as a NLS but can also function to regulate ciliary localization in the context of the KIF17 tail domain.

Ciliary localization signal is necessary for ciliary localization of full length KIF17

To test whether the KRKK sequence at aa1016-1019 is necessary for ciliary targeting of the full-length motor, these residues were mutated to Alanines in full length KIF17 and this construct was expressed in ciliated cells. KIF17(aa1016-1019Ala)-mCitrine showed reduced ciliary localization in Odora, MDCK, NIH 3T3 and hTERT-RPE cells (Figure 2.4a-d, (Dishinger et al., 2010)). This suggests that the basic residues at aa1016-1019 function as a ciliary localization signal (CLS) in the context of a full length KIF17 motor.

To test the contribution of individual Lysine residues within the CLS to ciliary trafficking of KIF17-mCitrine, constructs containing single Lysine to Alanine substitutions (Figure 2.4e) were expressed in NIH 3T3 cells. KIF17(1016A)-mCitrine and KIF17(1019A)-mCitrine both had reduced ciliary localization, similar

to KIF17(1016-1019A)-mCitrine (Figure 2.4f). Flanking the KRKK sequence are additional Lysine residues at positions 1014 and 1021 (Figure 2.4e). To determine whether these Lysine residues also regulate ciliary trafficking of KIF17, constructs containing single Alanine substitutions at these positions were expressed in NIH 3T3 cells. KIF17(1014A)-mCitrine and KIF17(1021A)-mCitrine showed reduced ciliary localization (Figure 2.4f). These results indicate that multiple basic residues are required for a functional CLS.

Previous work demonstrated that the last three residues Glutamic acid-Proline-Leucine of KIF17's tail are important for the binding of KIF17 to the dendritic cargo protein mLin-10 (also known as Mint1/X11). mLin-10 is thought to act as a scaffold protein for KIF17 to associate with NMDA-receptor subunit NR2B (Setou et al., 2000). To investigate whether the mLin10-binding region of KI17 regulates ciliary trafficking of the motor, the Proline residue at position 1028 was substituted to Alanine and expressed in NIH 3T3 cells. The ciliary localization of KIF17(P1028A)-mCitrine was similar to that observed for wild-type KIF17-mCitrine (Figure 2.4f) suggesting that KIF17 binding to mLin-10 is not required for cilary entry. Whether KIF17 requires binding to different cargo (such as the IFT particle) prior to ciliary entry requires further analysis.

Interaction of KIF17 with Importinβ2 is dependent on residues 1016-9

During nuclear import, the NLS of cargo proteins are recognized by nuclear import receptors including importin αs and βs, and the complex is shuttled across nuclear membrane through nuclear pore complexes (reviewed in (Gorlich and Kutay, 1999)). Since we previously determined that KIF17 ciliary entry had similarities to that of nuclear entry, we sought to examine whether KIF17 interacts with nuclear import receptors. FLAG-tagged KIF17 was expressed in HEK293T cells and immunoprecipitated with an anti-FLAG antibody (Figure 2.5a, (Dishinger et al., 2010)). Importin-β2 was co-precipitated with FLAG-KIF17 demonstrating an interaction between FLAG-KIF17 and importin β2. This interaction was shown to be dependent on the CLS sequence in the KIF17 tail

domain as importin-β2 was not co-immunoprecipitated from lysates expressing mutant FLAG-KIF17(1016-1019Ala).

The interaction of KIF17 with importin-β2 was surprising because KIF17's CLS (KRKK) more closely resembles the classic NLS which has been demonstrated to associate importin- α and importin-β1 (Stewart, 2007). However, importin β1 was not co-precipitated from lysates expressing FLAG-KIF17, suggesting that FLAG-KIF17 does not form an interaction with importin β1 in a classical binding pattern (Figure 2.6a, (Dishinger et al., 2010)).

To further examine the role of importins in regulating KIF17 entry into cilia, the CLS of KIF17 at residues 1016-1019 was replaced with known NLSs that interact with importin-β1 or importin-β2. When the basic NLS of SV40 Large T Antigen, which interacts with importin-α and -β1, was inserted in place of the KIF17 CLS, KIF17(SV40-NLS)-mCitrine localized to the nucleus in Odora cells (Figure 2.5b, c (Dishinger et al., 2010)). However, when the M9 NLS from a ribonucleoprotein hRNP A1, which interacts with importin-β2, was inserted in place of the KIF17 CLS, KIF17(M9 NLS)-mCitrine localized to the distal tips of cilia (Figure 2.5b, c (Dishinger et al., 2010)). This data suggests the interaction of KIF17 with importin-β2 is specific and critical for ciliary entry of KIF17.

KIF17 tail domain is sufficient to drive non-ciliary motor KHC into the cilium

In our analysis of the KIF17 CLS and its role in targeting KIF17 to the cilium, we next asked the question as to whether KIF17 CLS targeting is a conserved process. To determine whether the KIF17 tail domain containing the CLS is sufficient to drive a non-ciliary motor to the cilium, the entire tail domain of KIF17 was fused to the C-terminus of the kinesin heavy chain (KHC) subunit of the cytoplasmic motor kinesin-1. When expressed in NIH 3T3 cells, mCitrine-KHC-KIF17(801-1029) localized to the distal tips of cilia in all expressing cells (n=21 cells, Figure 2.6a,d), whereas the mCitrine-KHC control protein localized to the

cytoplasmic compartment (Figure 2.6a,c). This suggests that the tail domain of KIF17 is sufficient to target a non-ciliary motor protein to the cilium.

To test whether the CLS sequence within the KIF17 tail domain is necessary and sufficient for ciliary targeting of kinesin-1, we performed two experiments. First, the KIF17 tail domain in which the CLS was mutated to Alanines (aa801-1029, 1016-1019Ala) was fused to the C-terminus of KHC. Mutation of the CLS within the KIF17 tail domain resulted in significantly reduced ciliary localization of mCitrine-KHC-KIF17(aa801-1029,1016-1019Ala). In cells where mutant mCit-KHC-KIF17(aa801-1029,1016-9Ala) still localized to cilia, the fluorescence intensity at the distal tips was much lower than with the wild-type KIF17 tail domain (Figure 2.6a, e, f). Second, the KIF17 CLS (residues 1001-1029 or 997-1025) of KIF17 rather than the entire tail domain were fused to the C-terminus of KHC (mCitrine-KHC-KIF17CLS) (schematic in Fig2.6b). A slight increase in ciliary localization was observed for mCitrine-KHC-KIF17CLS as compared to the cytoplasmic localization of mCitrine-KHC alone, but the CLS sequences were not sufficient to target every motor to the cilium in NIH3T3 cells (Figure 2.6a). These results indicate that the KIF17 CLS is necessary but not sufficient for targeting a non-ciliary kinesin motor to the ciliary compartment.

Screen for secondary ciliary targeting signal

The observation that the KIF17 CLS was not sufficient to target KHC to the cilium suggests that the tail domain could potentially contain a secondary signal that facilitates ciliary entry of KIF17. To identify potential sequences within KIF17 that function as a secondary signal for ciliary targeting, a mutagenesis screen was conducted utilizing error prone polymerase chain reaction (PCR) to generate random mutations within coding sequence of KIF17 aa690-1029. Mutants were screened for abnormal KIF17 ciliary localization in NIH 3T3 cells. One mutant, A1(16) showed a predominant nuclear localization. Sequencing of this mutant identified five point mutations in the KIF17 coding sequence: H897R, L905P, S980C, S987P, and Q999R. To investigate the contribution of these residues to

ciliary targeting of KIF17, single point mutations were constructed within the full-length KIF17-mCitrine molecule. A single mutation, KIF17(H897R)-mCitrine, showed a pronounced phenotype (Figure 2.7d,b). KIF17(H897)-mCitrine localized to the tip of the cilium in only 6 out of 21 cells and in these cells, the intensity of the mCitrine signal at the tip of the cilium was variable and in many cases reduced when compared to wild type KIF17-mCitrine. Furthermore, KIF17(H897R)-mCitrine localized exclusively to the nucleus (n=16 of 21), in contrast to cytoplasmic/ciliary localization of wild type KIF17-mCitrine. Even in cells where cytoplasmic fluorescence could be detected for KIF17(H897R)-mCitrine, the KIF17(H897R)-mCitrine signal was still predominantly compartmentalized within the nucleus(n=4 of 21). Interestingly, it was mainly these cells that had low cytoplasmic fluorescence where we observed ciliary localization of KIF17(H897R)-mCitrine.

To test whether H897 plays a role in regulating ciliary entry in the context of the isolated KIF17 tail domain, we expressed mCit-KIF17(801-1029,H897R) in NIH 3T3 cells and found that ciliary localization was abolished in the majority of cells (n=1 of 20). The H897R substitution had no effect on localization to the nucleus (Figure 2.7b, h). These results indicate that H897 plays a role in regulating the ciliary/nuclear localization of KIF17.

The finding that a Histidine to Arginine mutation dramatically altered the localization of full-length KIF17 was surprising as both residues contain large bulky side chains. To further investigate the role of H897, this residue was replaced with Alanine (Figure 2.7b, e). KIF17(H897A)-mCitrine reduced ciliary localization (n=13 of 21) but not to the extent of KIF17(H897R)-mCitrine (n=6 of 21). However, in cells where KIF17(H897A)-mCitrine localized to the ciliary tip, the fluorescence at the tip was lower than in wild-type KIF17-mCitrine. In addition, KIF17(H897A)-mCitrine did not localize exclusively to the nuclear compartment as KIF17(H897R)-mCitrine did. Rather, similar fluorescence intensities were observed in both nuclei and cytoplasm for the H897A mutant

(n=12 of 21). The fact that alteration of Histidine to Arginine has a stronger effect on the cellular localization of KIF17 than the Histidine to Alanine mutation indicates that addition of a positively charged residue is more deleterious than removal of a large bulky side chain.

We next sought to analyze whether residues near H897 may also influence the ability of KIF17 to localize correctly to the ciliary compartment. Interestingly, H897 is flanked by Proline residues (schematic shown in Figure 2.7a). To investigate whether the two Proline resides regulate ciliary and/or nuclear trafficking, constructs containing Proline to Alanine substitutions were expressed in cells. P898A substitution abolished ciliary localization (n=2 of 21) and resulted in an increase in cells showing similar fluorescence in both the nuclei and cytoplasm, and also cells with higher fluorescence in the nuclei than cytoplasm (Figure 2.7b,g). Similarly, P896A substitution reduced ciliary localization of KIF17-mCitrine (n=7 of 23) and resulted in similar localization between the nuclear and cytoplasmic compartments (Figure 2.7b,f). In summary, the PHP sequence at residues 896-898 regulates ciliary trafficking, but through molecular mechanisms that require further detailed analysis.

Discussion

In this work, we set out to determine how KIF17 is targeted to the cilium in mammalian cells. One of our initial observations, that the KIF17 tail domain [mCitrine-KIF17(801-1029)] is compartmentalized within the nuclei of expressing cells, suggested parallels between nuclear and ciliary trafficking mechanisms. In addition to the nucleus, the KIF17 tail domain [mCitrine-KIF17(801-1029)] is sufficient to enter the ciliary compartment. Interestingly, the localization within the cilium varies between accumulation at the distal tip, along the cilium axoneme, and accumulation at both the tip and the base of the cilium. The pool of mCitrine-KIF17(801-1029) at the base of the axoneme just distal to the basal body may represent a pool of KIF17 tail that has yet to traverse the length of the cilium.

Given that the tail domain lacks motor activity, the pool that accumulates at the distal tip likely represents KIF17 tail domains that interact with active, endogenous full-length motor or associated cargo such as IFT particles or ciliary proteins. To determine if the tail domain is sufficient to target a non-ciliary motor motor to the cilium, the tail domain was fused to a non-ciliary motor KHC [mCitrine-KHC-KIF17(801-1029)] and resulted in ciliary entry and distal tip accumulation. The distal tip accumulation is likely due to the motor activity of the KHC that walks along microtubules indiscriminately, regardless of context.

In our studies, we examined whether the tail domain contains any sequences essential for ciliary targeting. We identified a ciliary localization sequence (CLS) on KIF17 necessary for ciliary localization that is basic in nature and similar to the characterized NLS for nuclear trafficking. Mutation of the CLS in the context of the isolated KIF17 tail domain resulted in the loss of its nuclear compartmentalization as well as displacement to the basal bodies. Why mutant mCitrine-KIF17(801-1029,1016-1019A) accumulates at the basal bodies is unclear. The basal body is believed to be part of the docking machinery for ciliary-targeted components (Rosenbaum and Witman, 2002). It is conceivable that the wild-type tail domain is targeted to basal bodies and then imported into the ciliary compartment whereas the mutant tail domain localizes to the basal bodies but is unable to be selectively shuttled into the cilium. Our results indicate that depending on its protein context, the basic sequence in the KIF17 tail domain acts as a NLS, a CLS, or both.

To test whether the CLS was sufficient to target a non-ciliary KHC motor, cytoplasmic KHC was tagged with KIF17's CLS. In contrast to the KHC-KIF17tail fusion, the KHC-KIF17CLS construct was not sufficient to drive ciliary targeting. This suggests that additional signals in the KIF17 tail domain are required for ciliary entry. For example, there could be cargo binding sequences that facilitate ciliary entry. It is not known whether KIF17 is imported independently of its cargo,

or if KIF17 bind to its ciliary cargo in the cytoplasm to form a motor-cargo complex that is imported into the ciliary compartment.

To begin to address the above question, we investigated whether the tail domain contains additional signals for ciliary entry. By conducting a mutagenesis screen of the tail domain in KIF17, we discovered additional mutants [KIF17(H897R)-mCitrine, KIF17(P896A)-mCitrine and KIF17(P898A)-mCitrine] that displayed reduced cilia targeting and increased nuclear localization. How do these mutants reduce ciliary localization and increase nuclear localization? It is possible that these mutants regulate KIF17's conformational structure in such a way that promotes nuclear over ciliary trafficking. Alternatively, these mutants may affect cargo binding if cargo association facilitates ciliary entry. These two possibilities are not mutually exclusive and it may be that the mutants affect cargo association, which in turn affects the conformation of the motor. Previous studies have demonstrated that KIF17 forms an autoinhibited conformation through interaction between the CC2 and motor domains (Hammond et al., 2010). Whether cargo binding relieves KIF17's autoinhibited state and allows microtubule binding and processivity is not known.

Importins and Ran are required for shuttling of NLS-containing proteins between the nuclear and cytoplasmic compartments and have also been found in the ciliary proteome (Gherman et al., 2006; Liu et al., 2007). Thus, we investigated whether nuclear import receptors play a role in recognition of the KIF17 CLS and import into the ciliary compartment. Using co-immunoprecipitation, we demonstrated an interaction between KIF17 and importin-β2 that was dependent on KIF17's CLS sequence. Ran is a small GTPase and a high nuclear Ran-GTP concentration, driven by the guanine exchange factor (GEF) RCC1, promotes the dissociation of importin-cargo complexes in nuclear trafficking (reviewed in (Stewart, 2007)). To investigate the role of Ran in ciliary trafficking of KIF17 motors, a system was created to upregulate protein expression of Ran in a fast and controlled manner (Dishinger et al., 2010). GTP-locked Ran(G19V)

expression was quickly upregulated in the cytoplasm and ciliary entry of KIF17-mCitrine was determined with a fluorescence recovery after photobleaching (FRAP) assay. Expression of GTP-locked Ran resulted in significantly reduced recovery of KIF17-mCitrine in the cilium. This suggests that increasing the cytoplasmic Ran-GTP concentration disrupts ciliary entry of KIF17-mCitrine. How Ran-GTP is maintained in the ciliary compartment is not known and whether there is ciliary-specific GEF remains to be determined.

Studies in the Margolis and Martens lab have complemented our studies investigating the role of nuclear machinery in ciliary trafficking. The apical polarity protein Crumbs3b localizes to the cilium in MDCK cells and was shown to interact with importin-β1 (Fan et al., 2007). Knockdown studies suggest that importin-β1 targets Crumbs3b to the centrosomal region (Fan et al., 2007). The X-linked retinal pigmentosa 2 gene product RP2 interacts with importin-β2 and knockdown of importin-β2 resulted in decreased RP2 ciliary trafficking (Hurd et al., 2011). Furthermore, RP2 contains an M9 NLS-like sequence that binds to importin-β2 and is required for ciliary trafficking (Hurd et al., 2011). The Martens lab detected Ran in cilia of rat olfactory epithelium by immunostaining and immunoblotting (Dishinger et al., 2010). Using an antibody specific to Ran-GTP, the Margolis lab has shown that there is endogenous Ran-GTP within the cilium and at basal bodies of cultured cells. Furthermore, they demonstrated that Ran-GTP regulates ciliogenesis (Fan et al., 2011). This adds to the list of cellular functions of Ran, and leaves me wondering how Ran evolved to coordinate multiple functions throughout the cell cycle.

Further studies will tease out whether other ciliary proteins utilize the Ran-importin system for ciliary import. The heterotrimeric kinesin-2 complex KIF3A/KIF3B/KAP3 subunits contain NLS-like protein sequences. The KAP3 subunit was shown to shuttle from cilia to nuclei before nuclear envelope breakdown during mitosis in sea urchin cells (Morris et al., 2004). Difficulties in localizing fluorescently tagged versions of kinesin-2 to primary cilia have limited

studies examining how kinesin-2 motors localize to cilia in mammalian cells. I have attempted to transiently transfect fluorescently-tagged versions of KIF3A, KIF3B and KAP3 in ciliated cell lines, and observed diffuse cytoplasmic localization but not ciliary localization. It is possible that the expression of endogenous kinesin-2 or the presence of the fluorescent tag on the expressed subunit affects heterotrimeric complex assembly, which prevents us from visualizing the ciliary pool. The generation of stable cell lines with lower expression levels may allow for ciliary localization. Alternatively, expressing fluorescent KIF3A or KIF3B in KIF3A/B null MEFS may rescue ciliogenesis defects and allow visualization of ciliary-localized KIF3A and KIF3B subunits. This would allow us to address the question of whether heterotrimer kinesin-2 utilizes similar mechanisms as KIF17 to enter into the cilium.

Components of developmental signaling pathways translocate between nuclei and cilia. For example, in the Hedgehog signaling pathway activated Gli transcription factors shuttle from the cilium into the nucleus for transcriptional activation (reviewed in (Goetz and Anderson, 2010)). The molecular mechanisms that regulate the ciliary and nuclear trafficking of Hedgehog pathway remain elusive. Whether KIF17 motors, importins and Ran play a role in regulating this pathway would be intriguing to investigate.

Materials and Methods

Plasmids and antibodies

Full-length KIF17 constructs tagged with mCitrine or Flag were generated by PCR amplification from the Sport6-HsKIF17 cDNA (NP_065867) vector using HiFi-Expand PCR kit (Hammond). Truncated forms of KIF17 were constructed by PCR and cloned into the mCitrine-N1 or C1 vectors (modified from Clontech's EYFP-N1/C1 vectors by replacing EYFP with sequence for monomeric Citrine) or the pcDNA3-Flag vector using convenient restriction sites. KIF17 mutants were made using the Quickchange kit (Stratagene). All plasmids were verified by DNA sequencing. mCitrine-KHC has been described previously. The following antibodies were used: Flag (Sigma), and acetylated α-tubulin 6-11B-1 (Sigma).

Cell culture

Odora, NIH3T3 and HEK293T cells were grown in DMEM (Gibco) supplemented with 10% fetal clone II (Hyclone) and 1% GlutaMax (Gibco). Odora cells were maintained at 33 degrees C, in 5% CO2. Cells were transfected with Trans-IT (Mirus) or Expressfect (Denville) according to manufacturer's protocol. NIH3T3 cells were serum-starved for 24 hours to induce ciliogenesis before transfection, and then used for experiments 24 hours after transfection. MDCK II cells were grown in DMEM supplemented with fetal bovine serum and 1% GlutaMAX, and transfected with Lipofectamine (Invitrogen). hTERT-RPE cells were grown in DMEM/F12 media (Gibco) supplemented with 10% FBS and 0.01mg/ml hygromycin B, and transfected with Trans-IT. hTERT-RPE cells were serum starved for 47 hours to induce ciliogenesis.

Immunofluorescence

Cells were fixed and processed for immunofluorescence as described previously. Briefly, cells were fixed in 3.7% paraformaldehyde, permeabilized with 0.2% TX-100 for 5 min, and block in 0.2% fish skin gelatin (Sigma) in PBS buffer. Primary

and secondary antibodies were diluted in blocking solution and incubated for 1 hour at room temp. Samples were incubated with DAPI for 1min before mounting. Samples were mounted with Prolong gold (Invitrogen). Cells that were co-transfected with Arl13b-mCherry as a cilia marker did not need to be immunostained, and instead were incubated with Hoescht and mounted.

Images were collected with an inverted Nikon TE2000 microscope using a Plan-APO 60X/NA 1.4 objective and Photometrics CS ES2 camera.

Co-immunoprecipitation: HEK293T cells were first resuspended in lysis buffer (25mM HEPES, 115mM potassium acetate, 5mM sodium acetate, 5mM MgCl, 0.5mM EGTA and 1%TX-100) and 1mM protease inhibitors. Lysates were inubcated with antibody at 4C. Immunoprecipitates were recovered with protein A agarose beads (Invitrogen), washed with lysis buffer and analysed by SDS-PAGE and western blotting.

Figures

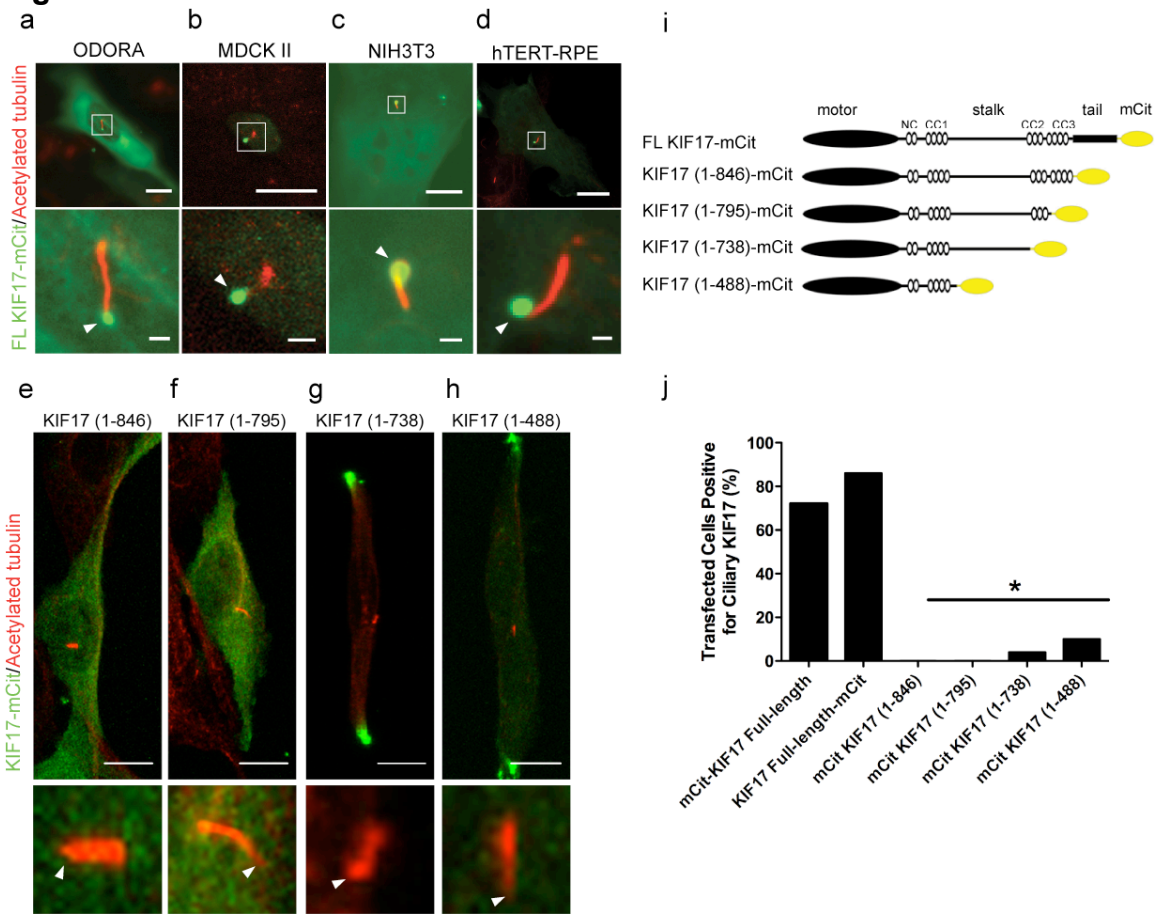

Figure 2.1 KIF17-mCitrine localizes to the distal tip of cilia and requires its tail domain for ciliary localization

(a-d) Odora, MDCKII, NIH 3T3 and hTERT-RPE cells expressing full-length KIF17-mCitrine (green) and stained with acetylated tubulin to mark the primary cilium (red). The top row are representative images of whole cells, and the bottom row are magnified images of the cilia indicated by white boxed regions in whole cell images. Scale bars, 10μm for cell, 1μm for ciliary region. White arrowhead points to KIF17-mCitrine localized to the distal tip of cilia.
(e-h) Odora cells expressing truncated forms of KIF17-mCitrine (green) and stained with acetylated tubulin to mark the primary cilium (red). C-terminal truncations abrogate ciliary targeting of KIF17-mCitrine.
(i) Schematic of full-length and truncated KIF17 motors. NC, neck coil; CC, coiled coil domains.
(i) Quantification of the results in (e-h). *N* = 50 cells for each KIF17 construct. P<0.0002 vs. full length KIF17 (Fisher's Exact test).

John Dishinger in the Verhey lab conducted experiments in Figures 2.1a, c. Paul Jenkins in the Martens lab conducted experiments in Figure 2.1b, e-j. Figure 2.1 was published in (Dishinger et al., 2010).

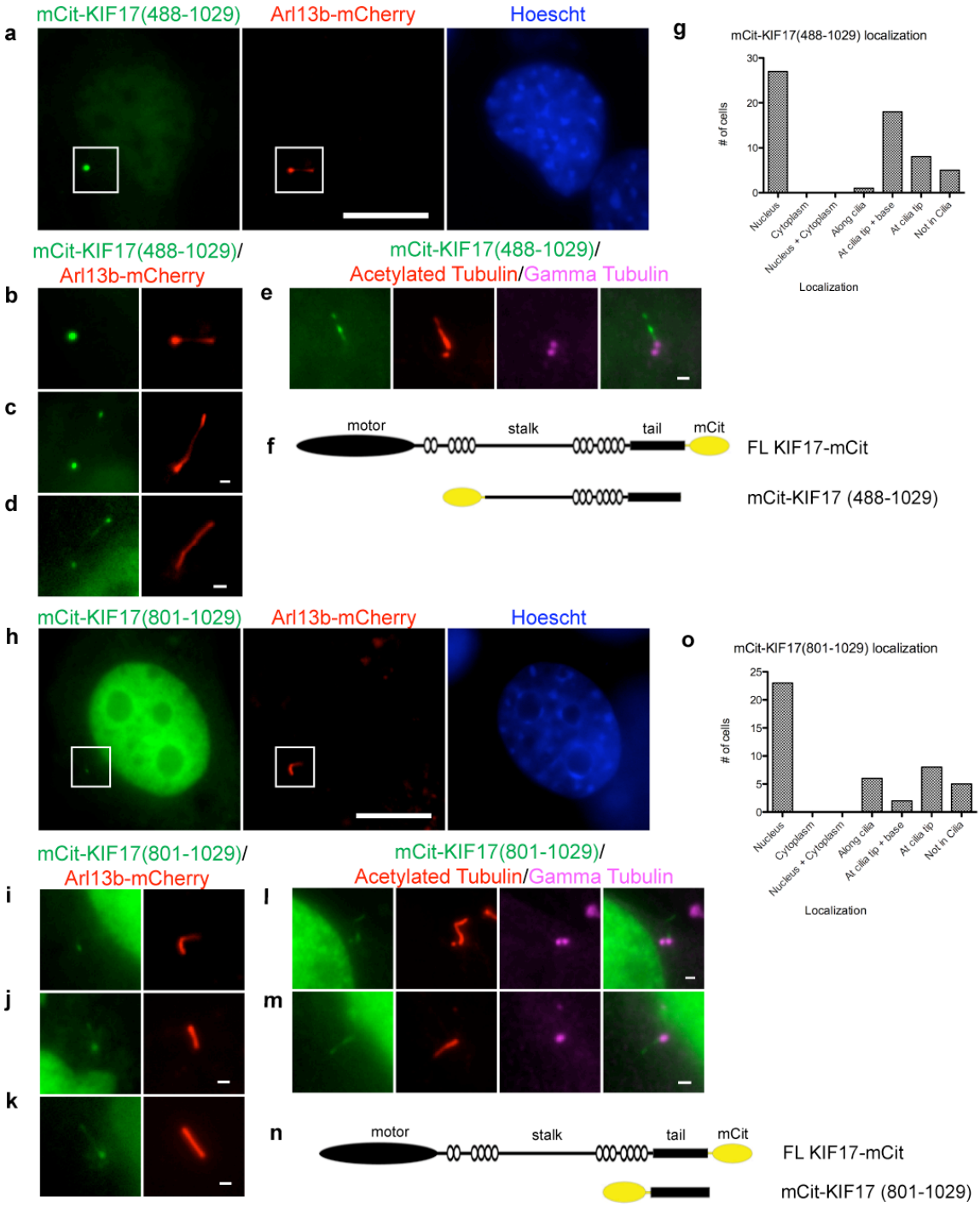

Figure 2.2 The KIF17 tail domain is sufficient for localization to the ciliary and nuclear compartments

(a) NIH3T3 cells co-expressing mCitrine-tagged KIF17 stalk+tail (aa488-1029) with Arl13b-mCherry (ciliary maker). Hoescht label nuclei. KIF17(aa488-1029) localized to the nucleus and the distal tip of the cilium.

(b-d) Representation images displaying the ciliary localization phenotypes of KIF17(aa488-1029)-mCitrine localized at (b) the tip of the cilium, (c)to the ciliary tip and base, and (d) along the cilium.
(e) NIH3T3 cells expressing KIF17(aa488-1029)-mCitrine were co-stained with antibodies to acetylated tubulin (red) and gamma-tubulin (magenta) to label the cilia and basal body, respectively. Scale bars, 10μm for whole cell images, 1μm for magnified ciliary image. (f) Schematic of truncated KIF17(aa488-1029) in comparison to full-length KIF17.
(g) Quantification of KIF17(aa488-1029) localization. *N* = 27 cells for the KIF17 construct
(h) NIH3T3 cells co-expressing truncated mCitrine-tagged KIF17 tail domain (aa801-1029) with Arl13b-mCherry as a ciliary maker. Hoescht labels the nuclei. KIF17(aa801-1029) co-localized with the nucleus.
(i-k) Representation images displaying the ciliary localization phenotypes of KIF17(aa801-1029)-mCitrine localized (i) at the tip of the cilium, (j) to the ciliary tip and base, and (k) along the cilium.
(l-m) NIH3T3 cells expressing KIF17(aa801-1029)-mCitrine were fixed and immunostained with antibodies to acetylated tubulin (red) and gamma-tubulin (magenta) to label the cilia and basal body, respectively. Scale bars, 10μm for whole cell images, 1μm for magnified ciliary image.
(n) Schematic of truncated KIF17(aa801-1029) in comparison to full length KIF17.
(o) Quantification of KIF17(aa488-1029) localization. *N*= 23 cells for the KIF17 construct

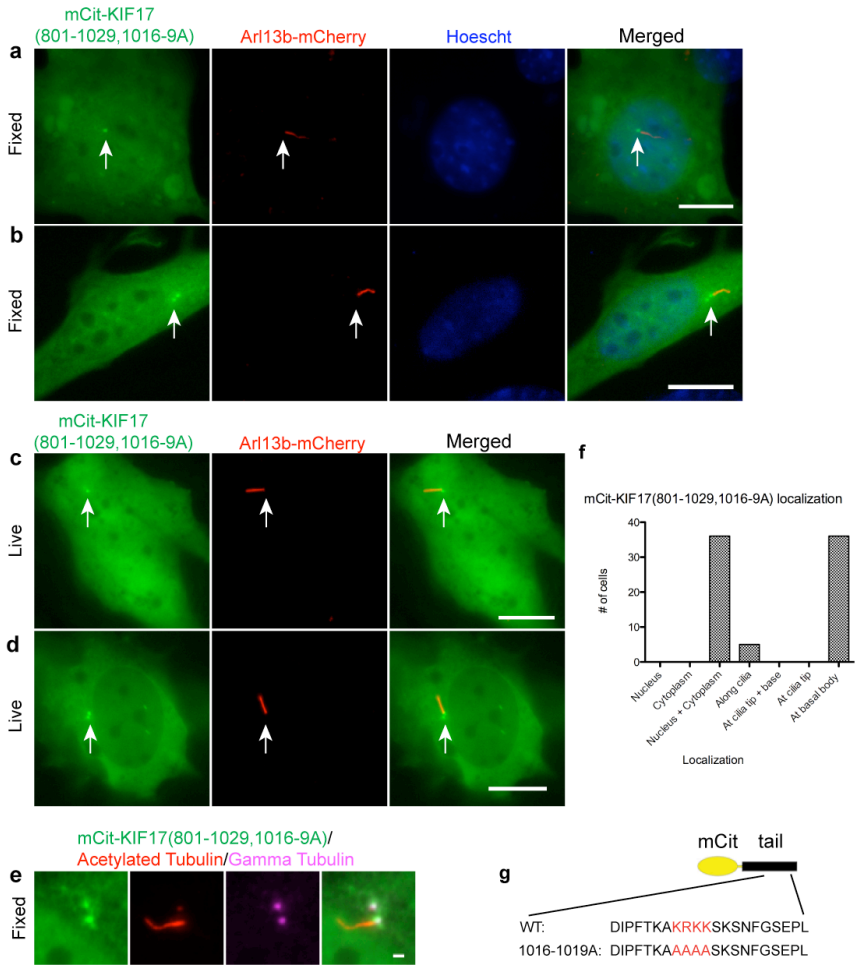

Figure 2.3 The KIF17 CLS is required for ciliary and nuclear targeting of the KIF17 tail domain

(a-b) NIH 3T3 cells expressing mCitrine-tagged KIF17(aa801-1029,1016-1019A) (green) and Arl13b-mCherry (red) as a ciliary maker were fixed and treated with Hoescht to label nuclei. KIF17(aa801-1029,1016-1019A)-mCitrine localized to both the nuclei and cytoplasm, and to puncta adjacent to the ciliary Arl13b-mCherry signal. In some cells, there are two puncta (b).
(c-d) NIH 3T3 cells expressing KIF17(aa801-1029,1016-1019A)-mCitrine were imaged live and similar puncta can be seen. Scale bars, 10 μm.
(e) NIH 3T3 cells expressing KIF17(aa801-1029,1016-1019A)-mCitrine co-stained with antibodies to gamma-tubulin and acetylated tubulin to mark the basal bodies and cilia, respectively. The KIF17(aa801-1029,1016-1019A)-mCitrine puncta co-localized with gamma-tubulin of the basal bodies. Scale bar, 1 μm. (f) Quantification of the localization of KIF17(aa801-1029,1016-1019A)-mCitrine. *N*= 36 cells for the construct.
(g) Schematic of the wild-type and mutant CLS sequences within the context of the KIF17 tail domain.

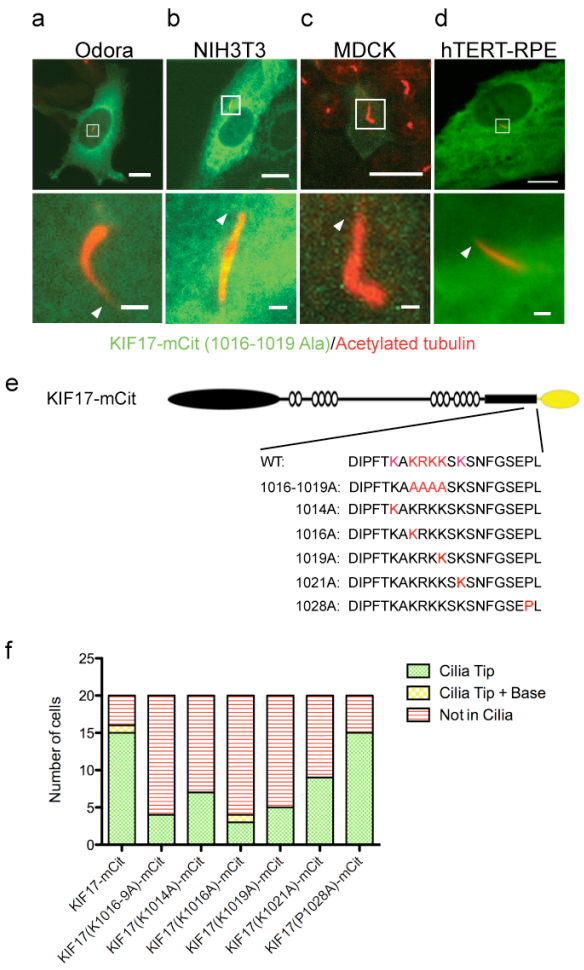

Figure 2.4 The KIF17 CLS is required for ciliary localization of the full-length motor

(a) Odora (b) MDCKII (c) NIH 3T3 and (d) hTERT-RPE cells expressing full-length KIF17(1016-1019A)-mCitrine (green) were fixed and stained with antibodies to acetylated tubulin to mark the primary cilium (red). Top row are representative images of whole cells, and bottom row are magnified images of the cilia indicated by white boxed regions in whole cell images. Scale bars, 10μm for cell, 1μm for ciliary region.
(e) Schematic of wild-type and CLS mutations in the context of the full-length KIF17-mCitrine construct.
(f) Quantification of ciliary localization of different KIF17-mCitrine mutant constructs in NIH 3T3 cells. *N* =20 cells for each construct.

John Dishinger in the Verhey lab conducted experiments in Figures 2.4a, b. Paul Jenkins in the Martens lab conducted experiments in Figure 2.4c. Figure 2.4a-c was published in (Dishinger et al., 2010).

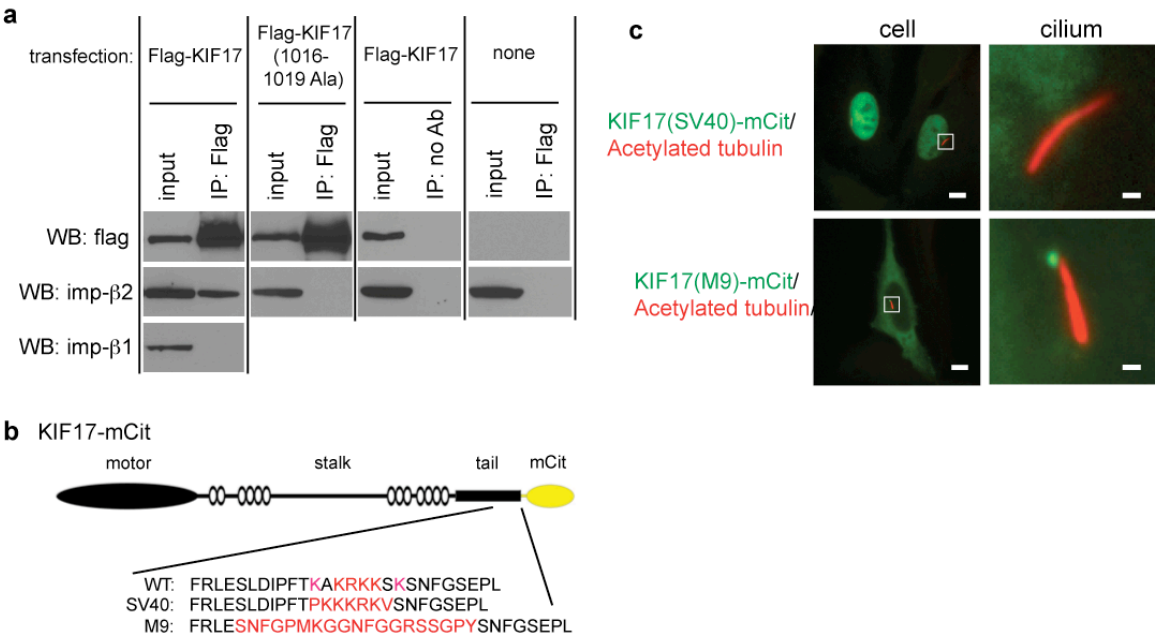

Figure 2.5 KIF17's interaction with importin-beta2 is CLS-dependent

(a) 293T cell lysates expressing Flag-tagged KIF17 were immunoprecipitated with antibodies to Flag. Immunoprecipitates were blotted with antibodies to Flag, importin-β1 or importin-β2. Importin-β2 but not importin-β1 was co-precipitated from the lysates.
(b) Schematic of KIF17-mCitrine constructs where the CLS is substituted with the NLS from SV40 Large T-antigen or the M9 NLS from hnRNP A1. (c) Odora cells expressing KIF17(SV40 NLS)-mCitrine and KIF17(M9 NLS)-mCitrine were fixed and stained with antibodies to acetylated tubulin to mark the cilium. Scale bars, 10μm for whole cell image, 1μm for ciliary image.

John Dishinger in the Verhey lab conducted experiments in Figures 2.5a. Figure 2.5 was published in (Dishinger et al., 2010).

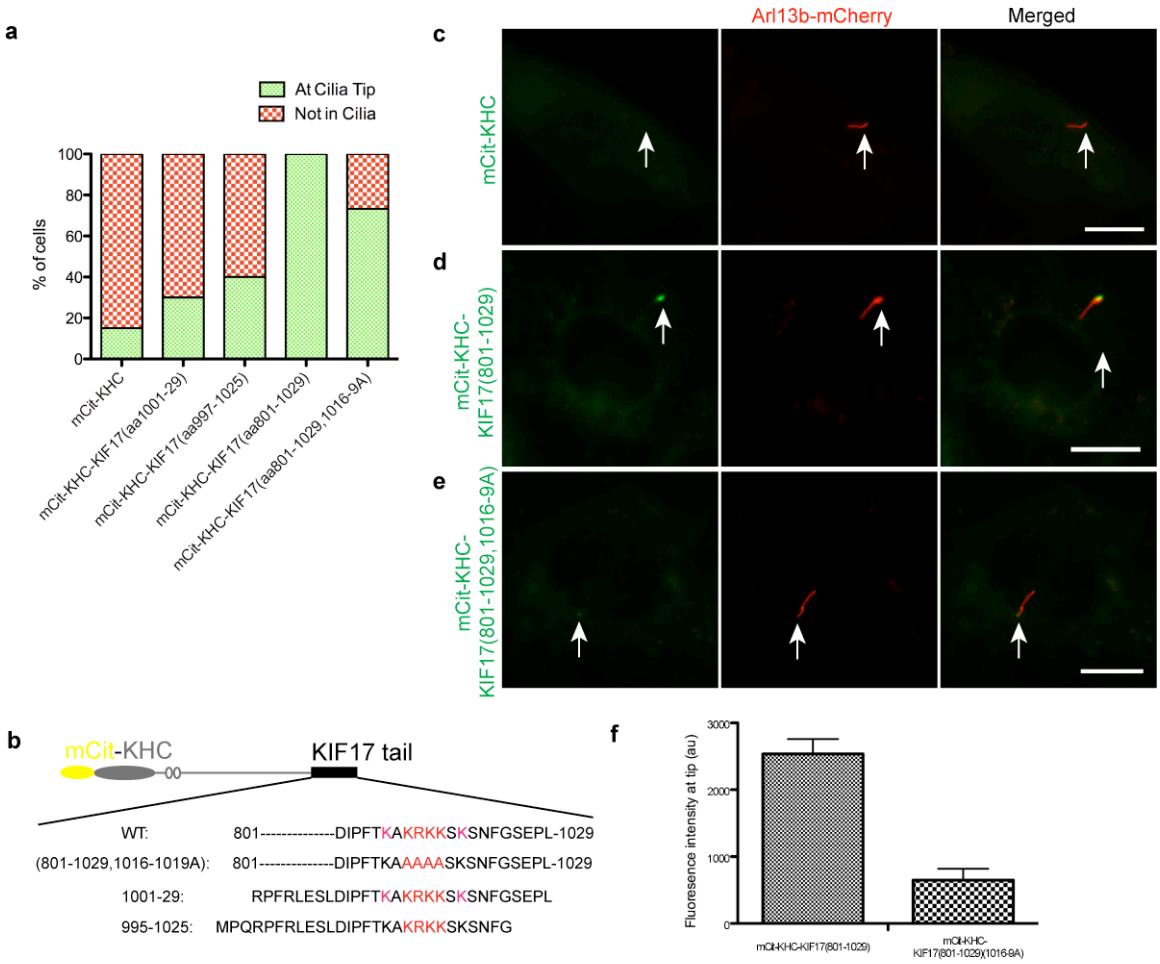

Figure 2.6 The KIF17 tail domain is sufficient to target a cytoplasmic motor to cilia

(a) Quantification of the ciliary localization of mCitrine-KHC, mCitrine-KHC-KIF17(aa1001-1029), mCitrine-KHC-KIF17(aa997-1025), and mCitrine-KHC-KIF17(aa801-1029) in NIH 3T3 cells. *N* =20 cells per construct.
(b) Schematic of different mCitrine-KHC-KIF17 domain constructs.
(c-e) NIH3T3 cells expressing Arl13b-mCherry as a ciliary marker and mCitrine-KHC (c), mCitrine-KHC-KIF17(aa801-1029) (d), or mCitrine-KHC-KIF17(aa801-1029,1016-1019A) (e) were fixed and imaged. White arrows point to distal tip of cilia. Scale bars, 10μm.
(f) Quantification of the average fluorescence intensity of mCitrine-KHC(801-1029) and mCitrine-KHC-KIF17(aa801-1029,1016-1019A) localized at the ciliary tip.

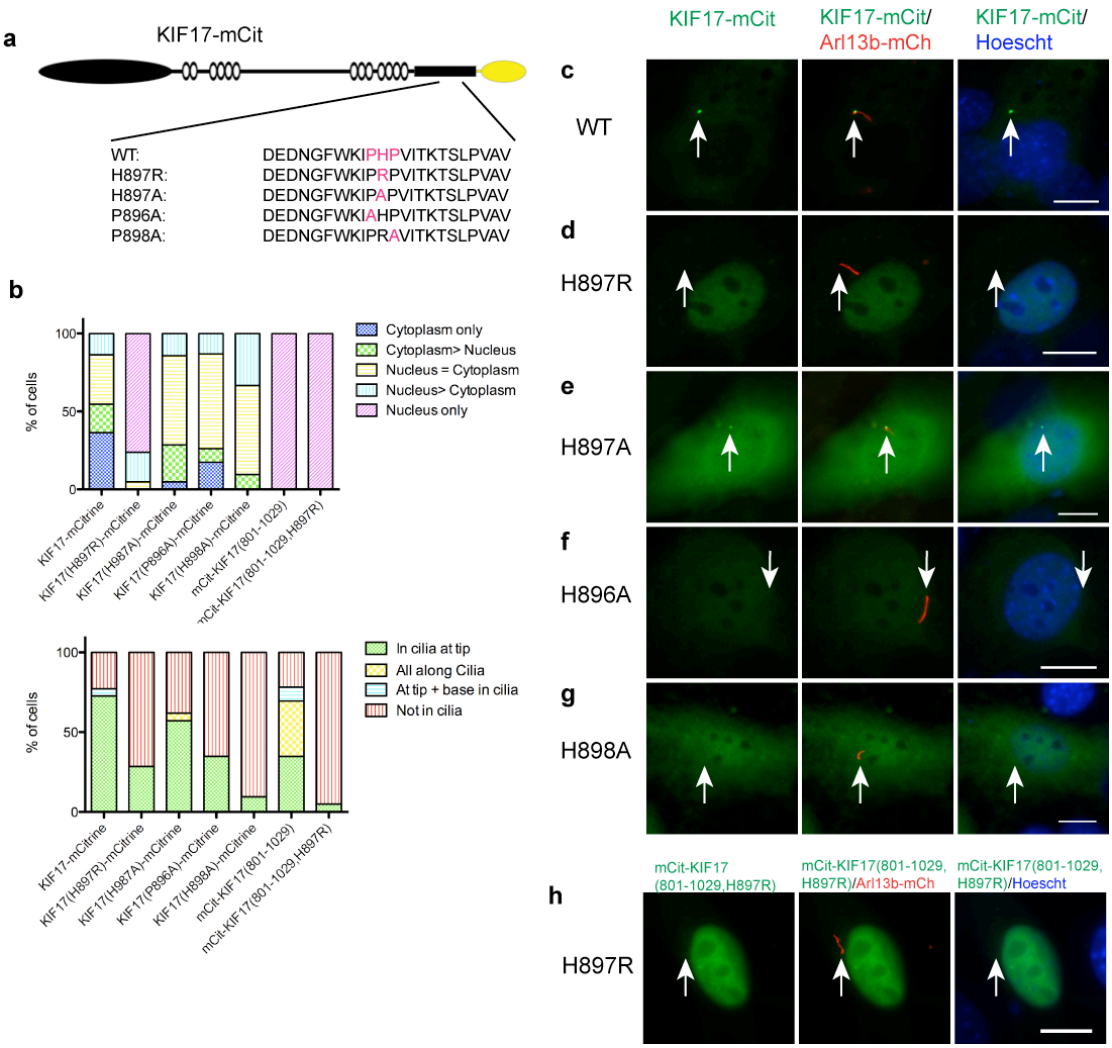

Figure 2.7 The KIF17 tail domain has a potential secondary sequence that contributes to ciliary localization

(a) Schematic of mutant KIF17 constructs.
(b-h) NIH 3T3 cells expressing different KIF17 mutants and Arl13b-mCherry as ciliary marker were fixed and labeled with Hoescht to stain the nuclei. Shown are representative images of cells with the most frequent phenotype for the expressed KIF17-mCitrine construct. White arrows point to distal tip of cilia. (b) Quantification of the observed (top graph) cellular and (bottom graph) ciliary localizations of the wild-type and mutant KIF17-mCitrine constructs. *N*=≥20 cells per construct. Scale bars, 10 μm.

Chapter 3
A Size-Exclusion Permeability Barrier and Nucleoporins Characterize a Ciliary Pore Complex that Regulates Transport into Cilia

Introduction

As an organelle with a unique protein and lipid composition, cilia must utilize specific mechanisms to ensure the accurate targeting to and retention of proteins within this compartment (Nachury et al., 2010). The mechanisms regulating entry into the ciliary compartment are unclear at first glance as the cilium lacks a limiting membrane separating it from the cytoplasm. The restriction point is believed to be a specialized region at the base of the cilium called the transition zone where Y-shaped structures and transition fibers can be seen by electron microscopy to link the microtubule core (the axoneme) and basal body structures to the ciliary membrane (Anderson, 1972; Deane et al., 2001; Gilula and Satir, 1972). Recent work has uncovered a network of protein components that localize to the transition zone and basal body region, and whose defects lead to various ciliopathies (Chih et al., 2011; Craige et al., 2010; Garcia-Gonzalo et al., 2011; Sang et al., 2011; Williams et al., 2011).

We recently demonstrated that ciliary entry of a cytoplasmic protein, the kinesin-2 motor KIF17, requires an import signal similar to a nuclear localization signal (NLS), the nuclear transport factor importin-β2 (transportin-1), and a RanGTP/GDP gradient between ciliary and cytoplasmic compartments (Dishinger et al., 2010). Thus, we hypothesized that the mechanisms that regulate ciliary entry of soluble proteins may be mechanistically similar to those that regulate nuclear entry. Consistent with this hypothesis, ciliary import of X-

linked Retina Pigmentosa protein RP2 utilizes importin-β2 and NLS-like sequences (Hurd et al., 2011). In addition, the transition zone region has been compared to the NPC and proposed to serve as a flagellar/ciliary pore complex (CPC) (Nachury et al., 2010; Rosenbaum and Witman, 2002). Thus, we set out to determine whether primary cilia utilize mechanisms similar to nuclei to regulate the entry of cytoplasmic components.

Nuclear-cytoplasmic shuttling is controlled by the NPC, a large multi-protein complex embedded in the double membrane of the nuclear envelope to form a pore-like structure (Fahrenkrog and Aebi, 2003). Transport of cytoplasmic components through NPCs is regulated in two ways (Gorlich and Kutay, 1999; Stewart, 2007). First, a size exclusion mechanism limits molecules >30 kDa from freely diffusing between compartments. Second, proteins above this size limit utilize NLS import signals, nuclear transport receptors and the small GTPase Ran to cross the physical barrier formed by the NPC.

In this chapter, I address the question of whether, like nuclei, cilia utilize a size exclusion mechanism to limit the diffuse entry of cytoplasmic proteins. I then examine whether nucleoporins of the NPC localize to the ciliary compartment and function to regulate active import of ciliary proteins.

Results

To test whether there is a size-dependent barrier that restricts ciliary entry of cytoplasmic molecules, I microinjected ciliated mammalian cells with fluorescently-labeled dextrans of various sizes, analogous to previous work defining a diffusion barrier for the NPC (Lang et al., 1986; Paine et al., 1975). hTERT-RPE cells were transfected with mCherry-tagged Arl13b as a live-cell marker of primary cilia (Figure 3.1) and observed 48 hours later by wide field fluorescence microscopy. Only cells with Arl13b-mCherry-labeled cilia that projected off the cell body were microinjected with fluorescent dextrans to clearly distinguish ciliary from cytoplasmic fluorescence. Dextran localization to the

nuclear and ciliary compartments was assessed 20 minutes after microinjection. Small dextrans (3 kDa and 10 kDa) freely diffused into both ciliary and nuclear compartments (Figure 3.2a,b). In contrast, larger dextrans (40 kDa and 70 kDa) were excluded from both ciliary and nuclear compartments (Figure 3.2c,d). Quantification of the fluorescence intensities in primary cilia demonstrates that the 40 kDa and 70 kDa dextrans were significantly restricted from entering the cilium (Figure 3.2e). Ciliary entry of 3 kDa and 10 kDa dextrans was rapid and could be detected within 5 minutes post-injection (Figure 3.1c), consistent with the rapid diffusion of small molecules into and within sea urchin spermatozoa (Takao and Kamimura, 2010).

To further investigate the size-dependent diffusion barrier for ciliary entry, we microinjected fluorescently-labeled soluble proteins of nearly spherical shape that act as inert probes (Mohr et al., 2009). Again, only cells with Arl13b-mCherry-labeled cilia projecting off the cell body were selected for microinjection and analysis. We found that α-lactalbumin (14 kDa), recombinant green fluorescent protein (rGFP, 27 kDa) and protein A (41 kDa) could enter both ciliary and nuclear compartments (Figure 3.3. a,b,d,f). Analysis in live cells is a critical component of these experiments as ciliary localization of expressed GFP could be reproducibly seen in live cells that were transfected (Figure 3.3c) but was difficult to determine after fixation and/or permeabilization (data not shown), consistent with recent reports (Calvert et al., 2010; Francis et al., 2011). In contrast to the ciliary localization of these smaller proteins, bovine serum albumin (BSA, 67 kDa) was restricted from both ciliary and nuclear compartments (Figure 3.3 e,f). Collectively, these experiments characterize a barrier for diffusion of cytoplasmic molecules into the ciliary compartment. Thus, like nuclei, cilia restrict the diffusional entry of cytoplasmic molecules based on size and utilize active transport mechanisms to facilitate entry of large proteins.

What are the molecular mechanisms by which ciliary entry of cytoplasmic molecules is restricted? One possibility is that ciliary-specific proteins create a

diffusional barrier resembling that of the nuclear pore. Alternatively, NPC components could localize to the ciliary base and create a permeability barrier. To test this latter possibility, we tested whether NPC components localize to primary cilia in mammalian cells. The NPC is a large proteinaceous structure composed of multiple copies of 30 different nucleoporin proteins that assemble into subcomplexes (Figure 3.4a) (Brohawn et al., 2009; D'Angelo and Hetzer, 2008). EGFP-nucleoporins have been used to study the kinetics and organizational dynamics of the NPC in live cells (Dultz and Ellenberg, 2010; Rabut et al., 2004). We expressed a fluorescently-tagged nucleoporin from each subclass in Odora cells, an immortalized cell line derived from rat olfactory sensory neurons that generates primary cilia (Murrell and Hunter, 1999). Localization at the ciliary base was observed for EGFP-NUP37 (outer ring nucleoporin, 12/15 cells, Figure 3.4e), EGFP-NUP35 (inner ring nucleoporin, 18/18 cells, Fig. 3.4f), NUP93-EGFP3 (linker nucleoporin, 19/19 cells, Figure 3.4g), and NUP62-EGFP3 (central FG nucleoporin, 16/17 cells, Figure 3h). Ciliary base localization was also observed when fluorescently-tagged nucleoporins were expressed in hTERT-RPE cells (Figure 3.6). In addition, EGFP-NUP214, a member of the cytoplasmic phenylalanine-glycine (FG)-containing nucleoporin and filament subcomplex, localized in distinct puncta near the γ-tubulin-labeled basal body (Figure 3.4c).

Interestingly, not all nucleoporins could be localized at the ciliary base. POM121-3GFP, GFP-GP210 and NDC1-GFP, transmembrane nucleoporins that anchor the NPC to the nuclear envelope, did not localize to the base of the primary cilium (Figure 3.4d, Figure 3.5h, i). Ciliary localization was also not observed for EGFP-NUP153, a nucleoporin that projects into the nucleoplasm (Figure 3.4i). These EGFP-nucleoporins localized correctly to the nuclear envelope (Figure 3.5), suggesting that the GFP tag does not hinder their ability to assemble into nucleoporin complexes. Collectively, these experiments demonstrate that specific nucleoporins localize to the ciliary base where they could regulate passive and active transport into the ciliary compartment.

To determine if endogenous nucleoporins localize to the base of the cilium, we immunostained cells with a monoclonal antibody, mAb414, that recognizes several FG-containing nucleoporins (NUP358, NUP214, NUP62 and NUP153) (Davis and Blobel, 1986). The FG repeats on these nucleoporins function to allow cargo-importin complexes to associate with and shuttle through the NPC meshwork. In NIH 3T3 cells, mAb414 staining showed discrete puncta present at the base of the cilium, in addition to the nuclear envelope (Figure 3.7a). To more clearly visualize mAb414 staining at the base of cilia, we extracted and performed immunofluorescence on trachea epithelial cells that project multiple motile cilia from their apical surface. In these cells, mAb414 stained not only the nuclear envelope but also the cilia-basal body border as shown by co-localization with γ-tubulin (Figure 3.7b). mAb414 staining also co-localized with basal body-associated SDCCAG8/NPHP10 protein, whose mutation causes the ciliopathy nephronophthisis (Otto et al., 2010) (Figure 3.7c). In a confocal section along the edge of epithelial cells, punctate mAb414 staining could be observed on the nuclear envelope and at the base of the cilia (Figure 3.8a). Punctate staining under the cilia was also evident in a confocal bird's eye projection down on the apical surface (Fig. 3.8b). Using antibodies specific to individual nucleoporins, NUP62 and NUP133 could be detected at the ciliary base of epithelial cells (Figure 3.8 c, d).

To more precisely define the localization of nucleoporins at the base of cilia, we performed immuno-electron microscopy (EM) of rat trachea. Using mAb414 in single-label immunogold EM, gold particles labeled the ciliary transition zone and basal body in addition to the expected localization at NPCs on the nuclear envelope (Figure 3.9b, d). In double-label immunogold EM with mAb414 and antibodies to CEP290/NPHP6, co-staining was observed in clusters (Figure 3.7f) and as single gold particles (Figure 3.7g) at the transition zone. Thus, while mAb414 staining appears to primarily colocalize with the basal body by fluorescence microscopy, mAb414 antigens localize at the transition zone and

basal body by EM, perhaps due to differences in antigen accessibility. Further work is required to define the localization of specific nucleoporins at the ciliary base. Collectively, fluorescence and electron microscopy experiments demonstrate that endogenous nucleoporins localize not only in the NPCs of the nuclear envelope but also in CPCs at the ciliary base.

To determine whether nucleoporins function to regulate import of ciliary proteins, we microinjected two different NPC function-blocking reagents into ciliated cells, mAb414 (Clever et al., 1991) and a truncated version of importin-β1 (Kutay et al., 1997). NIH3T3 cells co-expressing KIF17-mCitrine and Arl13b-mCherry were microinjected with mAb414 or importin-β1(45-462) together with TAMRA dye to mark injected cells (Figure 3.10a). As controls, cells were injected with TAMRA dye alone or not injected. KIF17-mCitrine fluorescence at the tips of cilia was photobleached and the subsequent fluorescence recovery (Figure 3.10b-d) was taken as a measure of ciliary entry of new KIF17-mCitrine molecules as described (Dishinger et al., 2010). Microinjection of mAb414 or importin-β1(45-462) resulted in a significant reduction in KIF17-mCitrine fluorescence recovery when compared to control cells (Figure 3.10d, e). We conclude that functionally inhibiting nucleoporins restricts KIF17-mCitrine entry into the ciliary compartment.

Discussion

I propose a model in which ciliary import displays selective and molecular features characteristic of nuclear import. First, we demonstrate that soluble molecules above a specific size threshold are restricted from passively entering the ciliary compartment, analogous to the manner in which the NPC acts as a sieve to prevent spurious entry of molecules. This CPC permeability barrier thus allows the enrichment of specific proteins destined for the cilium through active transport mechanisms. Furthermore, I show that several nucleoporins localize to and function at the base of the cilium in a similar manner to their functional roles at the NPC. Nucleoporins are found in several cilia proteomes

(http://v3.ciliaproteome.org/cgi-bin/index.php). Thus, we propose that nucleoporins not only form the molecular components that regulate transport across the NPC, but also transport across the CPC. Collectively with our previous work (Dishinger et al., 2010; Hurd et al., 2011), we demonstrate that ciliary import utilizes the three defining functional components that regulate nucleocytoplasmic transport – nuclear transport factors like importins, the Ran GTPase system, and nucleoporins.

Interestingly, not all fluorescent nucleoporins localize to the base of the cilium. The absence of EGFP3-NUP153 at the cilia base may be due to the nuclear-specific functions of this subcomplex, which forms a basket structure that serves as a platform for transcriptional regulation and chromatin stability in the nucleoplasm (Strambio-De-Castillia et al., 2010). NUP153 was demonstrated not be required for transportin-mediated nuclear import in *Xenopus* nuclei (Walther et al., 2001). The absence of POM121-3GFP, GFP-GP210, and NDC1-GFP at the ciliary base may be due to their nuclear-specific roles in anchoring components of the NPC in the nuclear envelope (Fahrenkrog and Aebi, 2003). Indeed, the structural differences between nuclear and ciliary membranes suggest that a different membrane-associated protein complex anchors the CPC to the surrounding ciliary membrane. It is tempting to speculate that the N*ephronopthisis (NPHP)* and Meckel-Gruber Syndrome (MKS) disease-related gene networks may play a role in anchoring nucleoporins at the CPC. Recent work demonstrated that disruption of NPHP and/or MKS genes caused defects in anchoring transition zone structures to the ciliary membrane and abnormal ciliary protein composition (Chih et al., 2011; Craige et al., 2010; Garcia-Gonzalo et al., 2011; Sang et al., 2011; Williams et al., 2011). Clearly, further studies are required to determine whether NPHP, MKS and nucleoporin components are functionally integrated together at the base of the cilium.

As ciliary and nuclear import share several molecular and mechanistic features, how cargoes are distinguished from entering the cilium versus the nucleus is

unclear. Cilia have evolved distinct mechanisms for ciliary trafficking that may be important in defining ciliary versus nuclear transport, such as the Intraflagellar Transport (IFT) complex that drives transport along axonemal microtubules, the BBSome coat complex, and small GTPases of the Arf and Rab families (reviewed in (Nachury et al., 2010; Rosenbaum and Witman, 2002)). Future work is clearly required to uncover the complex molecular network at the base of the cilium and to delineate the mechanisms by which these components establish the primary cilium as a complex signaling center and their implications in ciliopathies.

Materials and methods

Antibodies and Plasmids.

Commercial antibodies include: acetylated α-tubulin (1:10,000; clone 6-11B-1, Sigma), gamma-tubulin (1:500; T6557, Sigma), mAb414 (1:400 for immunofluorescence, 1:50 for immunoEM; ab24609, Abcam), NUP62 (1:250; sc-48373, Santa Cruz), polyglutamylated tubulin (1:1000; GT335, Enzo Life Sciences), and CEP290/NPHP6 (1:50 for immunoEM, IHC-00365, Bethyl Laboratories). Rabbit polyclonal anti-acetylated tubulin antibody (1:1000) was raised against the synthetic peptide: CGQMPSD(AcK)TIGGGDD. NUP133 (1:750) and SDCCAG8/NPHP10 (1:1000) antibodies were gifts from Martin Hetzer (Salk Institute) and Friedhelm Hildebrandt (University of Michigan), respectively. Secondary fluorescence-conjugated antibodies were from Invitrogen and Jackson ImmunoResearch.

The KIF17-mCitrine plasmid has been described (Hammond et al., 2010). The Arl13b-mCherry plasmid was constructed by subcloning human Arl13b cDNA from Arl13b-EGFP (gift of Kenji Kontani, University of Tokyo) into the KpnI and AgeI sites of mCherry-N1. The EGFP-Nucleoporin plasmids (EGFP-NUP214, EGFP-NUP37, EGFP-NUP35, NUP93-EGFP3, NUP62-EGFP3, EGFP3-NUP153) were purchased from EUROSCARF. POM121-3GFP, NDC1-GFP and GFP-GP210 were gifts from Richard Wozniak (University of Alberta), Martin Hetzer (Salk Institute), and Bill Dauer (University of Michigan), respectively. Importin-β1(45-462) was a gift from Ulrike Kutay (ETH Zurich) and recombinant protein was purified as described [36].

Cell Culture.

hTERT-RPE cells were grown in DMEM/F12 supplemented with 10% fetal bovine serum, 1% Pen/Strep and 0.01 mg/ml Hygromycin B, transfected with Trans-IT (Mirus), and serum starved for 48-60 hr to induce ciliogenesis. Odora and NIH3T3 cells were grown in DMEM supplemented with 10% fetal calf serum and

1% Pen/Strep/Gluta-MAX I and DNA constructs were transfected cells using Trans-IT LTI (Mirus) transfection reagent.

Microinjection.

Fluorescently labeled dextrans of different molecular weights – 3 kDa-FITC, 10 kDa-FITC, 40 kDa-FITC, 70 kDa-FITC (Molecular Probes) - were reconstituted in buffer containing 25 mM Hepes pH7.4, 115 mM KOAc, 5 mM NaOAc, 5 mM $MgCl_2$, 0.5 mM EDTA, 1 mM GTP and 1 mM ATP and microinjected into cells at 10 mg/ml. hTERT-RPE cells were microinjected and visualized using the FemtoJet Microinjector System (Eppendorf) mounted on an inverted epifluorescence microscope (Nikon TE2000-E) with 40 x 0.75 N.A. (with 1.5 x Optivar) and 60 x 1.40 (oil) objectives and Photometrics CoolSnap ES2 camera. Dextran solutions were centrifuged at 10,000g for 5 min to remove any aggregates before loading into Femtotips (Eppendorf).

Recombinant α-lactalbumin and BSA were purchased from Sigma and recombinant GFP and protein A were purchased from Prospec. All recombinant proteins (except rGFP) were brought to a concentration of 1mg/ml before labeling with Alexa 488 using a microscale protein labeling kit (Invitrogen). rGFP was at 1 mg/ml before injection. All of the proteins were spun down before injection to remove any aggregates.

Quantification of relative mean pixel intensities of the cilia versus cytoplasm in microinjected cells was determined using ImageJ. The ciliary region indicated by Arl13b-mCherry signal projecting off the cell body was used to generate a ciliary region of interest (ROI). The average fluorescence in the ciliary ROI was background subtracted using a ROI off the cell. The average fluorescence intensity in the cytoplasmic region half the distance between the nuclear envelope and cell periphery was measured and background subtracted the same way. The Diffusion Barrier Index was calculated as the ratio of mean

fluorescence intensity in the cilia versus the cytoplasm. 10-12 cells from separate experiments were measured for each dextran or protein.

Immunostaining and Microscopy.

The trachea was dissected from adult rats and epithelial cells were dissociated with a toothpick, spun onto coverslips, and immediately fixed and immunostained. All experimental procedures were approved by the University of Michigan Committee on the Use and Care of Animals and performed in accordance with the Guide for the Care and Use of Laboratory Animals.

Odora and hTERT-RPE cells were fixed with 4% PFA, permeabilized with 0.1% Triton X-100 or 0.1%SDS in PBS, and blocked with 0.2% fish skin gelatin (FSG, Sigma) in PBS. Samples were incubated in primary antibodies for 1 hr at room temperature and washed three times with 0.2% FSG/PBS. Samples were incubated in fluorescent-conjugated secondary antibodies for 1 hr, washed three times with 0.2% FSG/PBS, and mounted using Prolong Gold (Invitrogen). Immunostaining of NIH3T3 cells were carried out in a similar manner but were washed and incubated with antibodies in a solution of 0.1% Triton X-100, 0.02% SDS, 10 mg/ml BSA in PBS. Immunostaining of rat tracheal cells was carried out in a similar manner except that 0.1% Triton X-100 and 0.05% SDS in PBS was used for permeabilization.

Confocal imaging was performed on Leica SP5X and Olympus Fluoview 500 confocal microscopes with a 60 x 1.40 numerical aperture (N.A.). Epifluoresence imaging was performed on an inverted epifluorescence microscope (Nikon TE2000-E) with 40 x 0.75 N.A. and 60 x 1.40 objectives and Photometrics CoolSnap HQ camera.

Electron Microscopy.

Rat tracheas were fixed with 4% paraformaldehyde/0.25% glutaraldehyde in 0.1M cacodylate buffer at 4^{o}C overnight. For TEM only (Figure 4d), tissue was

post fixed with 1% Osmium tetraoxide. After dehydration in a graded series of ethanol, the samples were embedded in LR White (EMS; Hatfield, PA) in gelatin capsules and cured at 55^{o}C for 72 hr. Thin sections of 80nm were collected on formvar carbon coated 100 Mesh nickel grids. For immunogold staining, grids were rinsed with PBS with 0.1 % Triton X-100 for 10 min, then rinsed with PBS two more times. After blocking with Aurion blocking buffer at RT for 1 hr, the grids were incubated with primary antibody at 25-50x dilution in 0.2%BSA/PBS overnight at room temperature, followed by 6 nm immunogold conjugated goat anti-rabbit IgG (Aurion, Netherlands) or 12 nm gold conjugated goat anti mouse secondary (Jackson Lab) at 25x dilution for 2 hr. After rinsing with PBS, grids were post fixed with 2.5% glutaraldehyde in PBS for 20 min, and some samples were treated with 4% aqueous uranyl acetate to increase contrast. Images were taken with a Phillip CM-100 transmission electron microscope operated at 60kV.

FRAP experiments.

NIH 3T3 cells were plated in glass-bottom dishes (MatTek), co-transfected with KIF17-mCitrine and Arl13b-mCherry and serum starved for 24-48 hours. Expressing cells were microinjected with TAMRA dye alone, TAMRA dye (50 μM) + mAb414 antibody (0.95 mg/ml), or TAMRA dye (50 μM) + Importin-β1(45-462) (133 μM) using the FemtoJet Microinjector System (Eppendorf) mounted onto a Nikon Ti Eclipse inverted microscope. The cells were maintained in a live-cell chamber at 37°C and 5% CO_2. Using the Nikon A-1 Confocal System with Perfect Focus, microinjected cells were identified due to the presence of the TAMRA dye. A pre-bleach picture was taken and then the KIF17-mCitrine fluorescence at the distal tip of cilia was photobleached using 50% laser power for 1 sec. KIF17-mCitrine fluorescence recovery images were taken postbleach at 10-minute intervals for 30 minutes. Fluorescence signals were quantified using Metamorph software, background subtracted, and the average fluorescence values from 8 cells were plotted using Prism software (Graphpad).

Statistical Analysis.

All statistical analysis was performed using Prism software and specific tests are noted in the text. Error bars are ±SEM and significance was assessed as $p<0.05$.

Figures

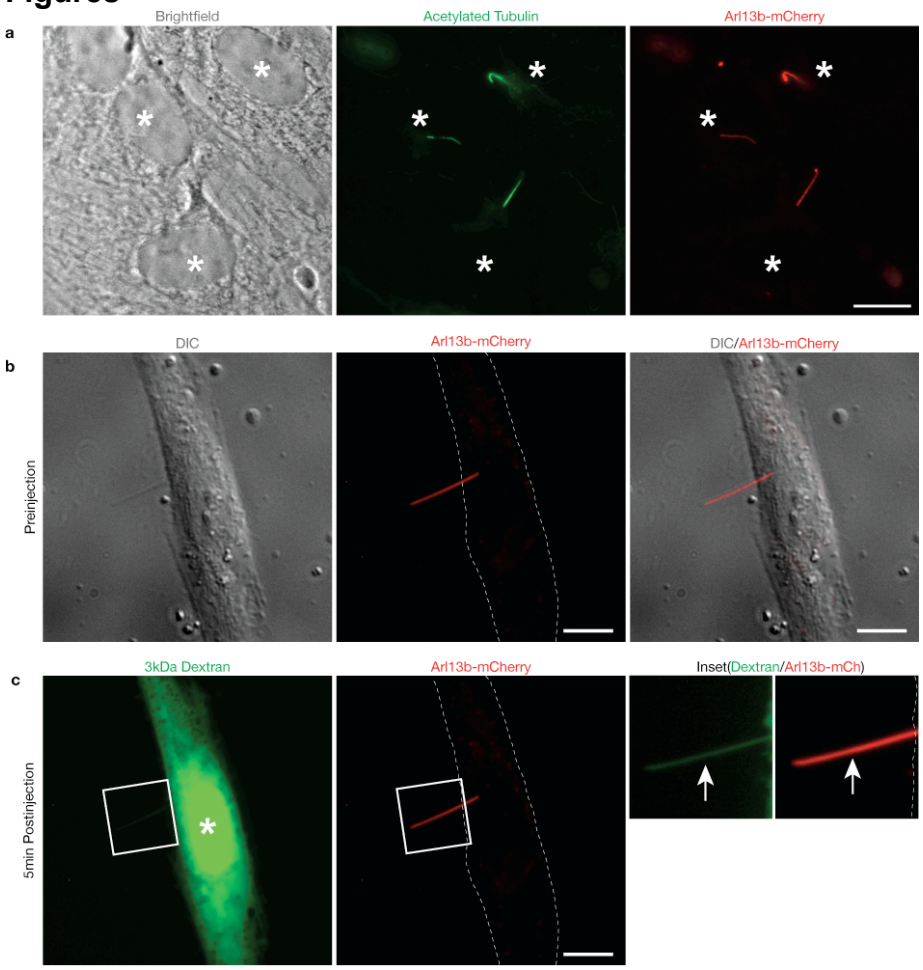

Figure 3.1 Microinjection using Arl13b-mCherry as a live cell marker for primary cilia

(**a**) Localization of Arl13b-mCherry to primary cilia in fixed cells. hTERT-RPE cells expressing Arl13b-mCherry (red) were fixed and immunostained for acetylated tubulin (green) to mark the microtubule axoneme of the primary cilium. White asterisks indicate the nuclei. (**b, c**) Arl13b-mCherry marks the primary cilium in live hTERT-RPE cells used for microinjection. In hTERT-RPE cells, the primary cilium is usually located on the top of the cell, often on top or by the nucleus, which hindered visualization of fluorescent dextrans in the nuclear and ciliary compartments. Thus, cells were chosen for microinjection based on the protrusion of the Arl13b-marked primary cilium off the cell body as shown for the representative cell prior to microinjection in (**b**). Dashed white lines represent cell periphery. After microinjection of fluorescent dextrans into the cell body, the Arl13b-mCherry (red) and fluorescent dextrans (green) were imaged at various time points. Shown in (**c**) are images from the same cell in (**b**) 5 min after microinjection with 3 kDa dextran. White asterisk indicates the nucleus. Far right panels are higher magnifications of the cilium in the white-boxed area. Scale bars, 10 μm.

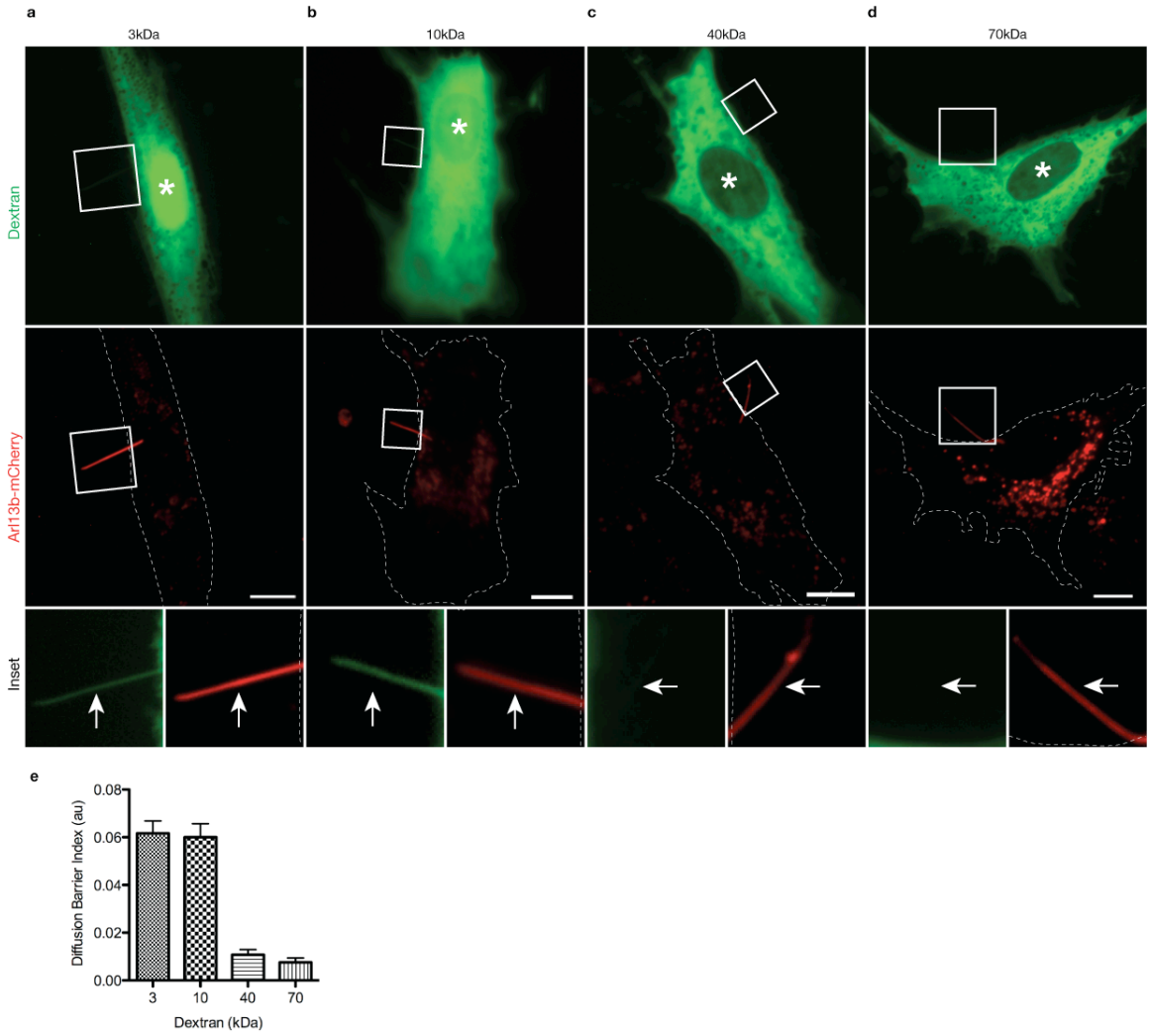

Figure 3.2 The cilia base acts as a size-dependent barrier for entry of cytoplasmic dextran molecules

hTERT-RPE cells expressing Arl13b-mCherry to mark the primary cilium in live cells were microinjected with (**a**) 3 kDa (**b**) 10 kDa (**c**) 40 kDa or (**d**) 70 kDa fluorescent dextrans. Shown are representative images taken 20 min post-injection. White asterisks indicate the nuclei. Dashed white lines represent cell periphery. The bottom row shows higher magnifications of primary cilia in the boxed regions. White arrows point to primary cilia. Scale bars, 10 μm. (**e**) Quantification of ciliary localization of fluorescent dextrans. The data are expressed as a Diffusion Barrier Index, which represents the ratio of the mean fluorescence intensity in the cilium versus the cytoplasm. Error bars represent SEM. *N* = 11 **(a)**, 12 **(b)**, 11 **(c)**, 10 **(d)** cells.

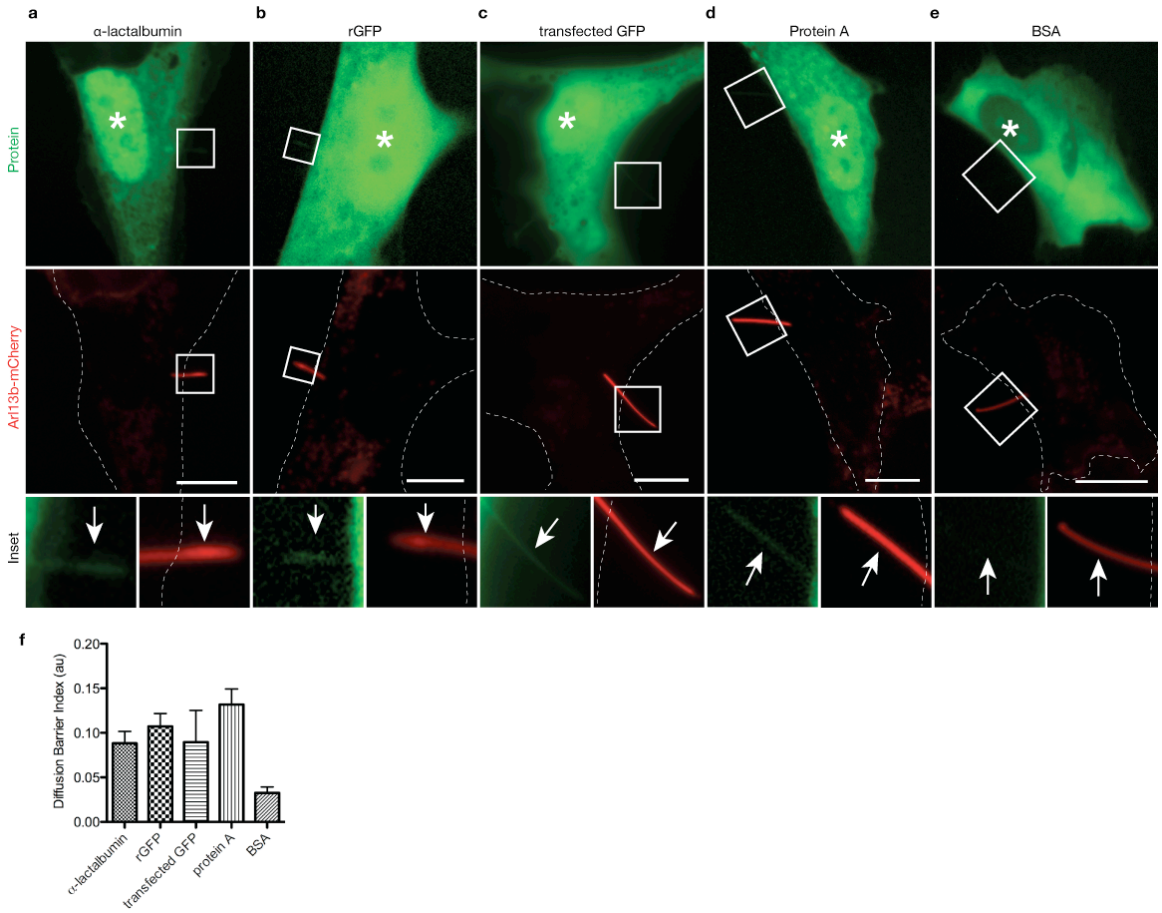

Figure 3.3 The ciliary base acts as a size-dependent barrier for entry of inert cytoplasmic proteins

hTERT-RPE cells expressing Arl13b-mCherry to mark the primary cilium in live cells were either microinjected with Alexa448-labeled purified proteins (**a**) α-lactalbumin (14 kDa), (**b**) recombinant GFP (rGFP, 27 kDa), (**d**) Protein A (41 kDa), (**e**) BSA (67 kDa) or were (**c**) transfected with GFP-expressing plasmid. Shown are representative images taken 5 min post-injection. White asterisks indicate the nuclei. Dashed white lines indicate the cell periphery. The bottom row shows higher magnifications of primary cilia in the boxed regions. White arrows point to primary cilia. Scale bars, 10 μm. (**f**) Quantification of ciliary localization of microinjected fluorescent proteins. The data are expressed as a Diffusion Barrier Index. Error bars represent SEM. *N* = 11 **(a)**, 10 **(b)**, 7 **(c)**, 8 **(d)**, 11 **(e)** cells.

John Dishinger in the Verhey lab conducted the microinjection studies with recombinant proteins presented in Figure 3.3 a,b,d,e. Lynne Blasius in the Verhey lab conducted the live imaging of transfected rGFP presented in Figure 3.3d.

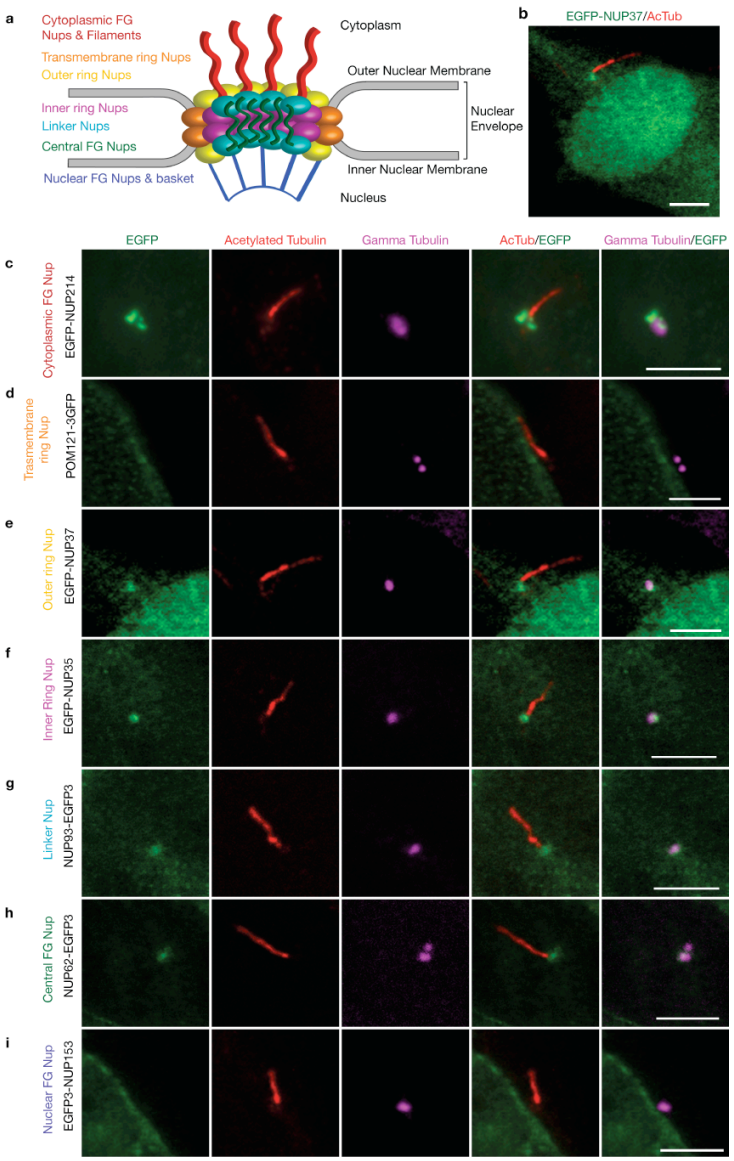

Figure 3.4 Fluorescently-tagged nucleoporins localize to the base of primary cilia

(**a**) Diagram depicting the overall structure and subcomplexes of the NPC, based on the model in (Strambio-De-Castillia et al., 2010). Odora cells expressing (**c**) EGFP-NUP214, (**d**) POM121-3GFP, (**b**, **e**) EGFP-NUP37, (**f**) EGFP-NUP35, (**g**) NUP93-EGFP3, (**h**) NUP62-EGFP3, (**i**) EGFP-NUP153 were fixed and stained with antibodies to acetylated α-tubulin (red) and γ-tubulin (magenta) to mark the primary cilium and basal bodies, respectively. Merged images are shown in the right panels. Shown are representative images of the ciliary region of the cells; whole cell views are shown in Figure 3.5. Scale bars, 5 μm.

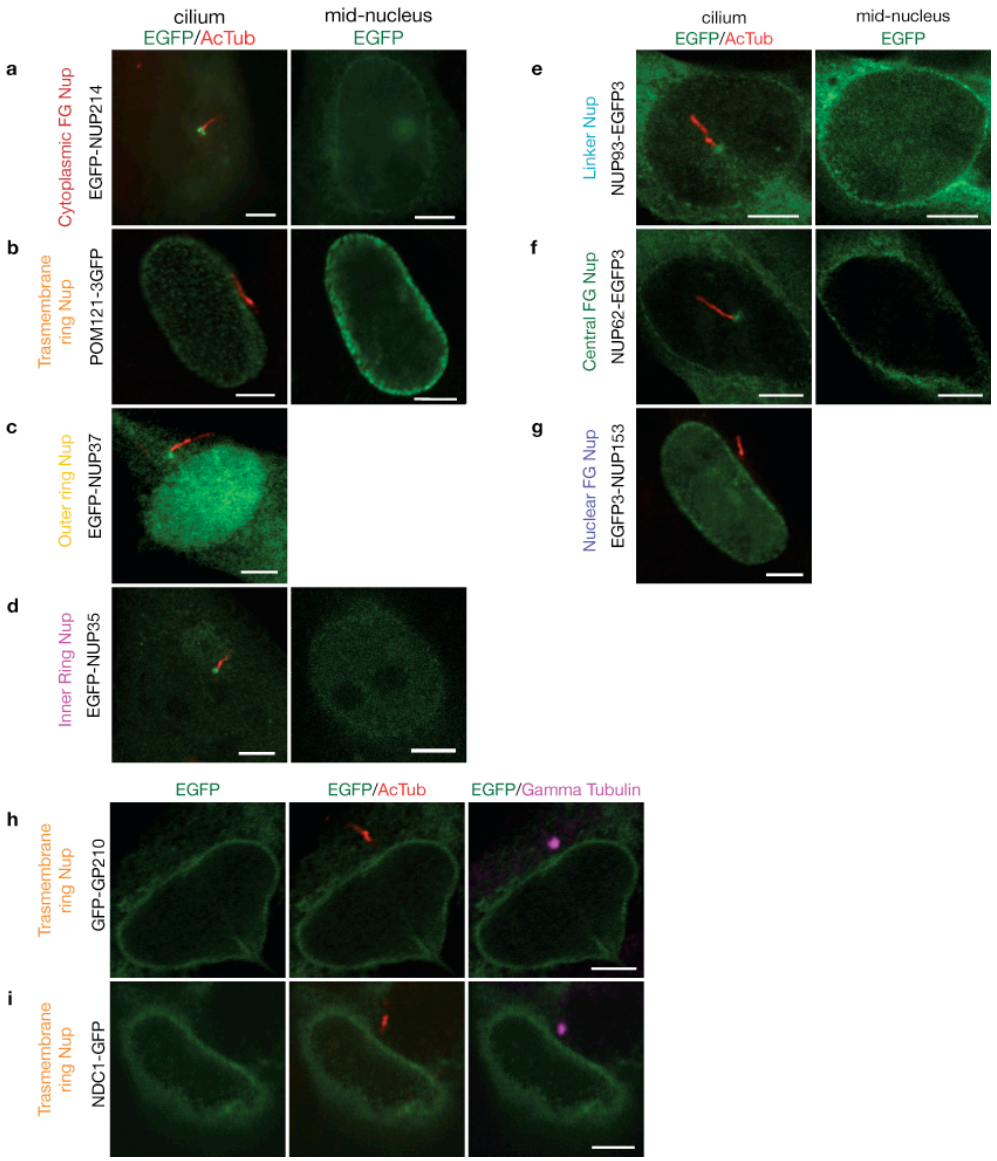

Figure 3.5 Fluorescently-tagged nucleoporins localize to the nuclear envelope and, in some cases, to the base of primary cilia in Odora cells

Odora cells expressing (**a**) EGFP-NUP214, (**b**) POM121-EGFP3, (**c**) EGFP-NUP37, (**d**) EGFP-NUP35, (**e**) NUP93-EGFP3, (**f**) NUP62-EGFP3, and (**g**) EGFP-NUP153, were fixed and stained with antibodies to acetylated α-tubulin (red) and gamma-tubulin (magenta) to mark the primary cilium and basal body. Shown are representative confocal sections taken in the plane of the cilium (left panels) and in the cell center (right panels). Odora cells expressing (**h**) GFP-GP210 and (**i**) NDC1-GFP were fixed and stained with antibodies to acetylated α-tubulin (red) and γ-tubulin (magenta). GFP-GP210 and NDC1-GFP localizes to the nuclear envelope but not the base of primary cilia. Scale bars, 5 μm.

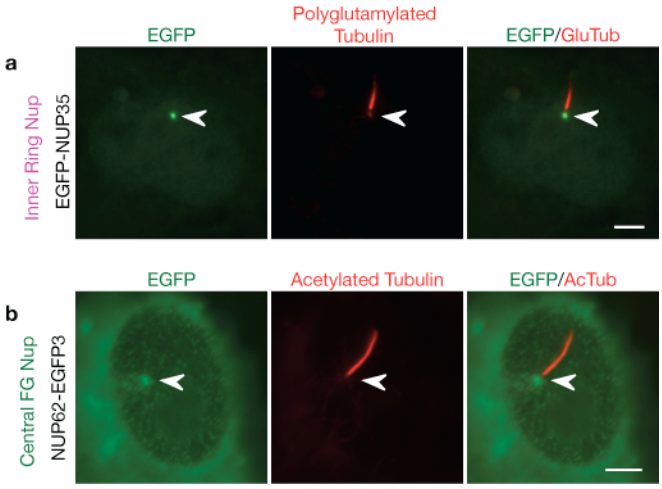

Figure 3.6 Fluorescently-tagged nucleoporins localize to the base of primary cilia in hTERT-RPE cells

hTERT-RPE cells expressing (**a**) EGFP-NUP35 or (**b**) NUP62-EGFP3 were fixed and stained with antibodies to acetylated α-tubulin or polyglutamylated tubulin (red) to mark the primary cilium. Arrowhead indicates the base of cilia. Scale bar, 5 μm.

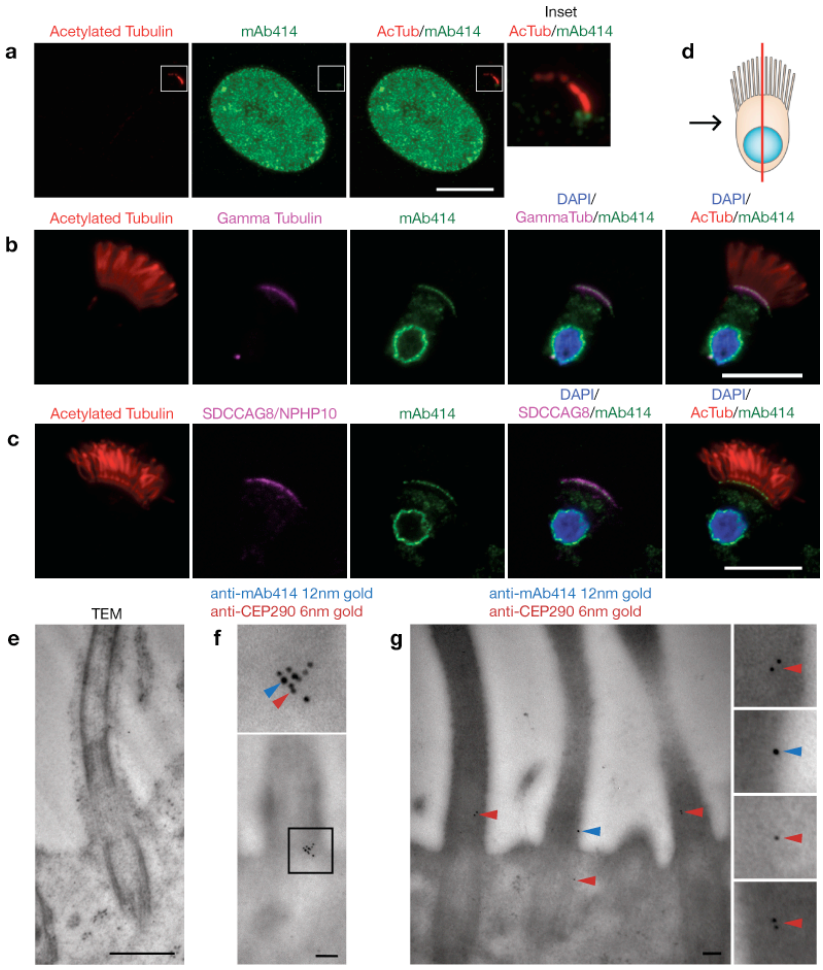

Figure 3.7 Endogenous nucleoporins localize to the base of cilia

(**a**) Representative image of an NIH3T3 cell fixed and stained with antibodies to nucleoporins (mAb414, green) and acetylated α-tubulin (red) to mark the primary cilium. The right panels show higher magnifications of primary cilium in the boxed region. (**b**) Rat trachea cells were fixed and stained with antibodies to nucleoporins (mAb414, green), acetylated α-tubulin (red) and γ-tubulin (magenta). (**c**) Rat trachea cells were fixed and stained with antibodies to nucleoporins (mAb414, green), acetylated α-tubulin (red) and SDCCAG8/NPHP10 (magenta). DAPI (blue) indicates the nucleus. For (**b**) and (**c**), (**d**) depicts a schematic representation of the epithelial cells in which the red line indicates the confocal section and the black arrow represents the point of view. Scale bars, 5 μm. **(e-g)** Rat trachea tissue was fixed and processed for EM. **(e)** Addition of osmium tetraoxide during EM processing resulted in higher contrast. Scale bar, 500nm. **(f, g)** Dual-label immunogold EM of sections of tracheal tissue using mAb414 and antibodies to CEP290/NPHP6. Blue arrowheads, 12nm gold particles (mAb414); red arrowheads, 6nm gold particles (anti-CEP290/NPHP6). Scale bars, 100nm.

Lynne Blasius in the Verhey lab conducted the immunofluorescence experiment in Figure 3.7a. Albert Liu in the Margolis lab conducted the electron microscopy experiments in Figure 3.7 e-g.

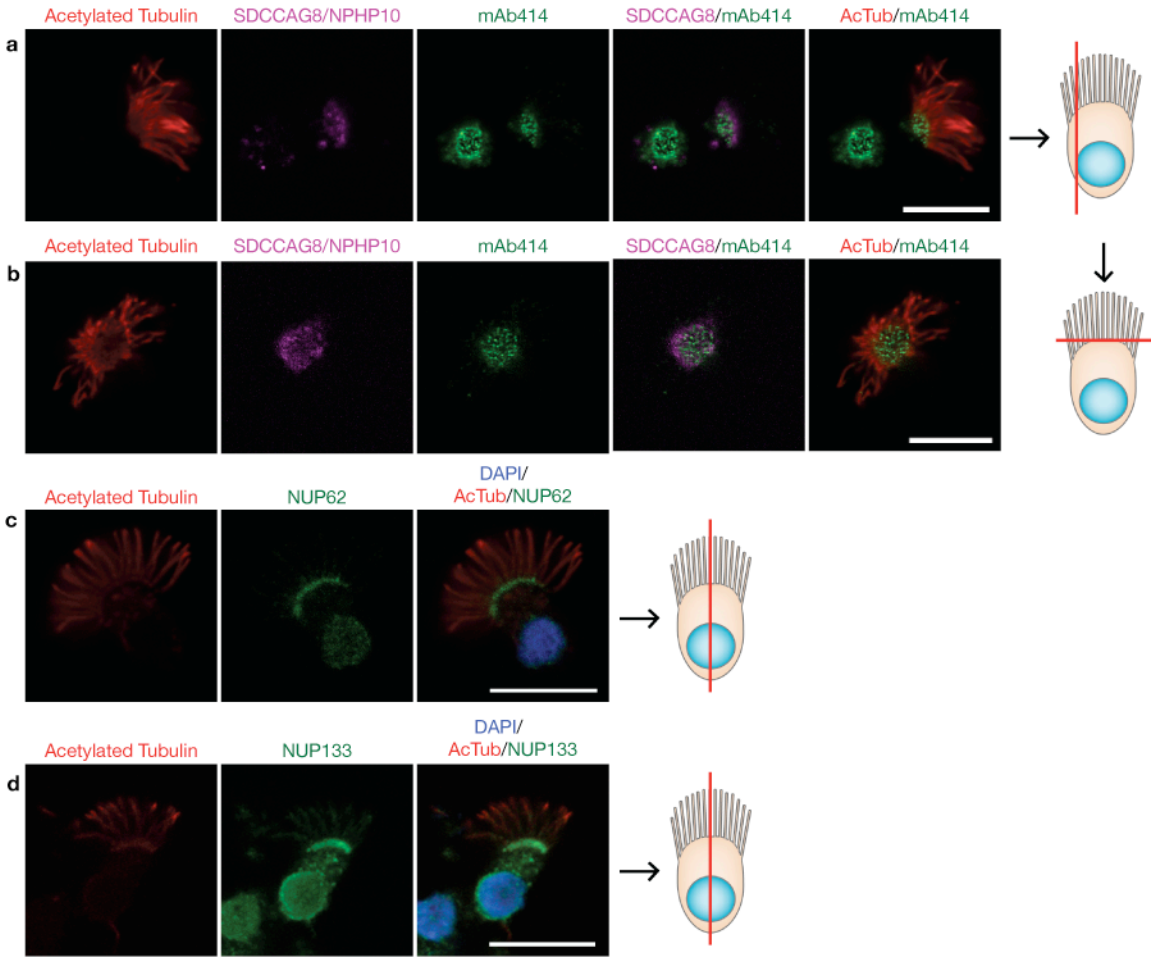

Figure 3.8 Endogenous nucleoporins localize to the base of motile cilia in rat trachea epithelial cells

Rat trachea cells were fixed and stained with antibodies to nucleoporins (green) using **(a,b)** mAb414, **(c)** anti-NUP62 or **(d)** anti-NUP133. The cells were costained with antibodies to acetylated α-tubulin (red) and SDCCAG8/NPHP10 (magenta). DAPI (blue) indicates the nucleus. Far right images are schematic representations of the epithelial cells in which the red line indicates the confocal section and the black arrow represents the point of view. Ciliary localization of nucleoporins can be visualized in confocal sections (**a**) along the side of the cell and (**b**) at base of cilia. Scale bars, 5 μm.

Lynne Blasius in the Verhey lab conducted the immunofluorescence experiments of tracheal cells in Figure 3.8c-d.

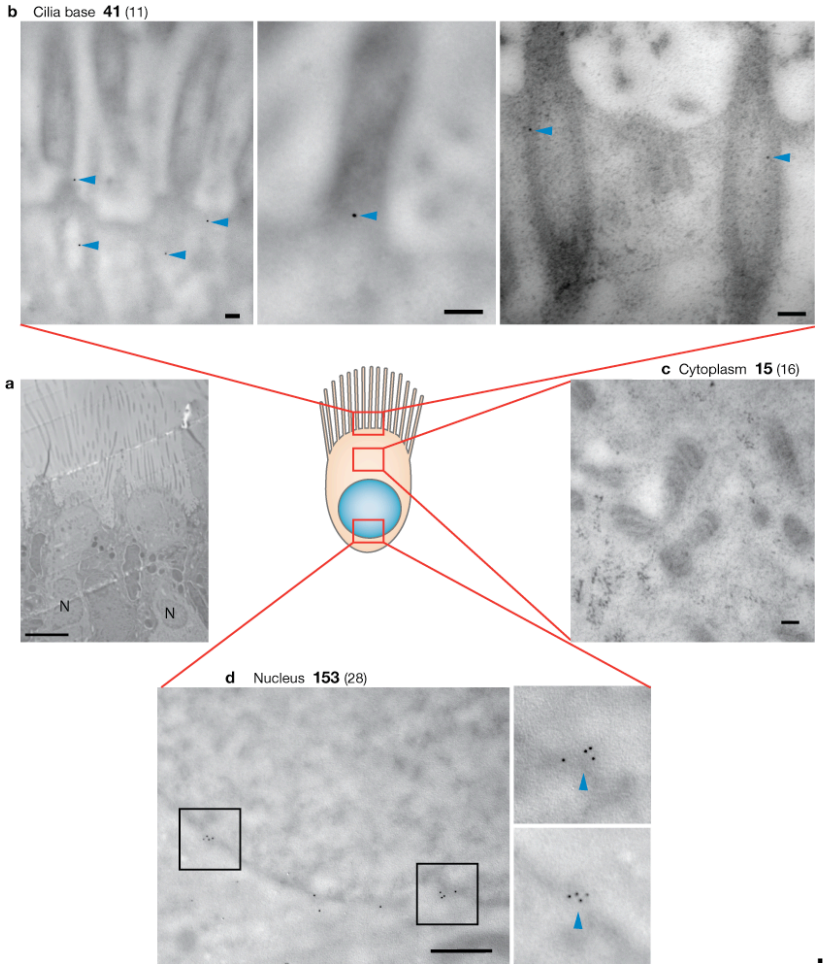

Figure 3.9 Immunogold electron microscopy localization of mAb414 in rat trachea

Rat trachea tissue was fixed and processed for immunogold EM using antibodies to mAb414. **(a)** Representative TEM image of the tissue surface showing epithelial and goblet cells (scale bar, 5um). N indicates nuclei of epithelial cells. To the right is a schematic representation of an epithelial cell. Higher magnification TEM views are shown of (**b**) the cilia base (scale bar, 100 nm), (**c**) cytoplasm (scale bar, 100 nm), and (**d**) nucleus (scale bar, 500 nm). Blue arrowheads indicate gold particles to mAb414. The number of gold particles in the cilia base, cytoplasmic, and nuclear regions was counted for 8 cells stained with mAb414 and immunogold secondary antibodies and for 8 cells from a control staining with only immunogold secondary antibodies (no mAb414). Numbers in bold indicate the number of gold particles for mAb414-stained cells; numbers in parentheses indicate the number of gold particles for control cells. Some samples were treated with 4% aqueous uranyl acetate to increase contrast, as shown in (**b**, right panel) and (**c**).

Albert Liu in the Margolis lab conducted electron microscopy experiments in Figure 3.9.

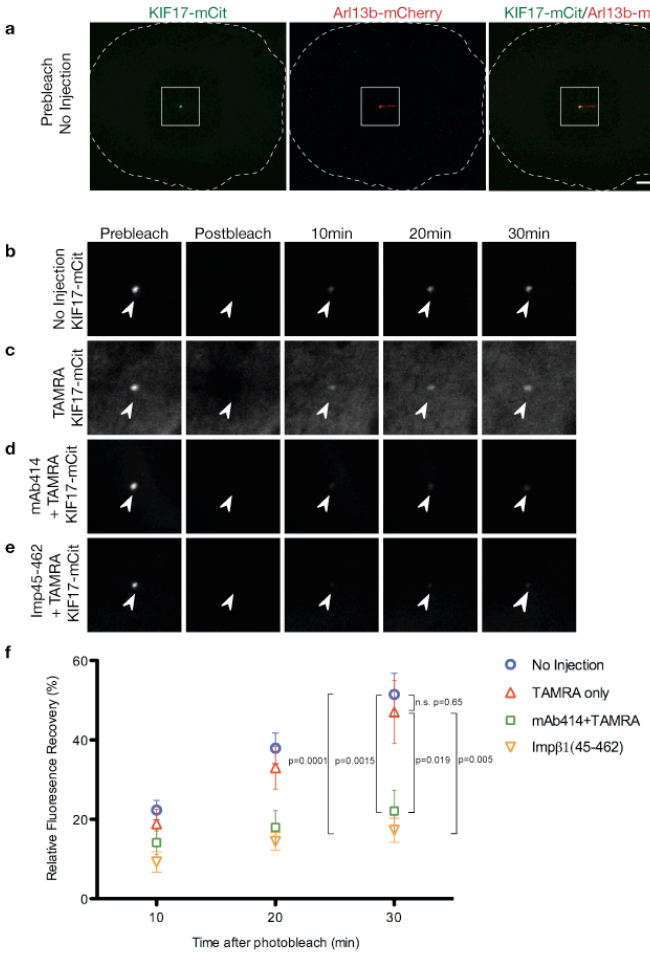

Figure 3.10 Microinjection of nucleoporin function-blocking reagents into cells restricts the ciliary entry of KIF17 motors

Odora cells coexpressing KIF17-mCitrine and Arl13b-mCherry were (**a, b**) uninjected or were injected with (**c**) fluorescent TAMRA dye alone, (**d**) mAb414 antibodies and TAMRA or (**e**) Importin-β1(45-462) and TAMRA. Expressing cells were imaged [(**a**) prebleach] and then the KIF17-mCitrine fluorescence at the distal tip of the cilium was bleached with high laser power. Dashed white line indicates the edge of the cell. Scale bar, 10 μm. Following the bleach, the cells were imaged (postbleach) and the fluorescence recovery of KIF17 was measured over time. **(b-e)** show prebleach, postbleach and recovery images of KIF17-mCitrine in the cilium. Arrowheads point to the distal tip of the cilium. (**f**) Quantification of the fluorescence recovery of KIF17-mCitrine in the distal tips of cilia. The data are represented as mean ±SEM of fluorescence recovery after photobleach. *N*=8 **(a)**, 8 **(b)**, 8 **(c)** and 7 **(d)**. Statistical significance was assessed by student's t-test. n.s. denotes no significant difference.

Chapter 4
Conclusions

Defining the cilium as a privileged domain

The eurkaryotic cell has evolved to form topologically distinct organelles, most of which are fully enclosed membrane compartments (Alberts et al. 2002). The nucleus, mitochondria and endoplasmic reticulum (ER) are examples of organelles defined by lipid bilayers that separate their contents from the cytoplasm to carry out organelle specific functions. In contrast to these organelles, the cilium or flagellum is not fully bound by a lipid bilayer. Instead, the cilium protrudes from the surface of the cell and so the ciliary membrane is continuous with the plasma membrane, leaving an open gap at the base of the cilium. It is proposed that cellular structures such as the basal body and transition zone form a ciliary pore complex, much like the nuclear pore complex, that restricts movement between the ciliary and cytoplasmic compartments (Rosenbaum, 2002). However, it has not been previously demonstrated whether the intraciliary compartment, like other organelles, is physically separated from the cytoplasm, albeit by a different mechanism than a limiting membrane. Thus, I set out in my thesis to determine if the cilium utilizes a barrier mechanism to restrict movement of soluble molecules.

One of the simplest methods by which molecules move is by basic diffusion. Therefore, one of my first questions was whether soluble cellular molecules could gain entry to the cilium by simple diffusion. We hypothesized that if a barrier mechanism exists that controls diffusion into the cilium, then entry into the cilium by diffusion should be a function of size of the diffusible molecule. By microinjecting soluble molecules into the cytoplasm in mammalian cells we

demonstrated that there is a soluble diffusion barrier at the ciliary base (schematic, Figure 4.1). Initial microinjection experiments involved injecting fluorescent dextrans of different molecular weights and we observed that dextrans ≥ 40kDa are restricted. A second set of experiments examined soluble proteins and again found a size-based restriction against passive diffusion into the cilium. We thus concluded that mechanisms are in place to maintain the cilium as a privileged domain accessible only to specific constituents. Our analysis of this data highlighted some key factors that likely regulate protein entry into the cilium. For example, in comparing the entry of dextrans to that of recombinant soluble proteins, we see that the 41kDa Protein A is able to passively enter the cilium although the 40kDa dextran is restricted. A possible explanation for this difference is that dextrans are long, branched polysaccharides, and thus structurally different from the globular structures of natively folded proteins, demonstrating that cilia entry may be a function of protein conformation. A related and additional explanation for differences between the entries of recombinant proteins versus dextrans is that the molecules may differ in charge. The fluorescently labeled dextrans are hydrophilic in nature, and thus differ from the mainly hydrophobic surfaces of recombinant proteins. Therefore, further experiments are needed to fully understand the contributions of size, shape, and charge in regulating diffusive entry into the ciliary compartment.

An important test of the size exclusion mechanism outlined above was tracking the movement of GFP into the cilium of cells. Both we and others initially believed that soluble GFP (27 kDa) could not enter the cilium in mammalian cells. These experiments were hampered by: a) the use of fixed cells in which the ciliary compartment was identified by staining for acetylated tubulin and b) the fact that the cilium is nearly always lying over or under the cell and can thus be obscured by cytoplasmic fluorescence. However, Calvert *et al.* determined that GFP diffuses through the connecting cilium of live *Xenopus* rod photoreceptor cells (Calvert et al., 2010). This data together with recent reports suggesting

discrepancies between live and fixed samples (Francis et al., 2011) motivated us to revisit the question of GFP diffusion in the cilium by microinjection of GFP and visualization in live cells. In these microinjection experiments, one must scan the dish for cells that have a cilium protruding off the cell body into empty dish space so that the fluorescent signal can be visualized without cell body background fluorescence. Indeed, visualization in live cells of recombinant GFP clearly demonstrated that GFP is able to enter into the cilium by diffusion (schematic, Figure 4.1). By using the same screening criteria, we also observed transfected EGFP in the cilium in fixed cells.

In an attempt to examine the size-based restriction of ciliary entry, we created fusion proteins (FP) containing tandem FPs in order to increase protein size in a linear manner. We transfected tandem EGFP (2x-EGFP) and mCitrine (3xmCitrine) proteins and were surprised to find that these constructs were also able to enter into the ciliary compartment of hTERT-RPE cells (data not shown). While the calculated MW of these tandem FPs suggest that they should be restricted from freely entering the cilium, we believe that these proteins are able to enter the cilium given the fact that their radius is identical to that of a single EGFP. A caveat to these experiments is that we cannot rule out the possibility that the expressed tandem FPs were able to enter the ciliary compartment before the barrier was formed. In future experiments, it is more ideal to test the ability of tandem GFP to enter the ciliary compartment by microinjection of cells after cilia formation (e.g. in cells that have been serum starved for about 48 hours). Recently, tandem dimer (54kDa) and trimer (81kDa) GFP were found to localize to the outer segment of Xenopus photoreceptor cells, although to a lesser extent than single GFP (27kDa) (Najafi et al., 2012). An important consideration here is that specialized photoreceptor cells require a large quantity of protein be trafficked to the outer segments to accommodate disc shedding and the demands of photodetection. Thus, it is possible that different cell types form different barriers to accommodate function and specificity.

As alluded to in the above paragraph, a key question concerns when the cilary permeability barrier is formed. More specifically, does the barrier form during ciliogenesis, or it is set up post-ciliogenesis? Tackling this question would require developing new assays that can probe the permeability barrier in a time-dependent manner. One way is to design probes that will fluoresce upon entry into the ciliary compartment. A major advantage to this approach is that cellular background fluorescence is omitted, greatly enhancing our ability to visualize ciliary entry over time. I began developing such an approach using a split superfolder GFP that self-associates with high affinity (Pedelacq et al., 2006). The idea behind this approach is that one part of the split GFP will be anchored within the ciliary compartment and the complementing part of the split GFP will be fused to inert cytoplasmic proteins of different sizes. In the absence of a ciliary barrier, all probes will generate fluorescent cilia regardless of their size. Once the ciliary barrier has formed, only small molecules will be able to diffuse into the ciliary compartment and reconstitute fluorescence. I have encountered two main obstacles in developing this approach. First, the ciliary part of the split GFP was fused to Arl13b, which is not stationary in the ciliary compartment but rather traffics in and out. Second, this approach still requires microinjection of the cytoplasmic probes. Nevertheless, it will be useful in the future for this and similar assays to be further developed in order to determine the timing and functioning of the ciliary barrier in live cells.

Ciliary trafficking of KIF17 motor

Having defined the presence of a permeability barrier, the question arises as to how ciliary proteins are targeted to and enter the ciliary compartment. For example, the kinesin motors involved in anterograde IFT are multi-subunit proteins of total molecular weight about 250 kDa, well above our size permeability cutoff. To investigate active entry of a large soluble ciliary protein, ciliary trafficking of the kinesin-2 motor KIF17 in mammalian cells was examined. By tagging KIF17 with a fluorescent protein, we observed that KIF17-mCitrine

accumulates at the tip of the cilium in various cell lines. The distal tip localization is presumably the result of, first, the entry of KIF17 into the cilium proper at its base, and secondly, KIF17 traveling anterograde along the axoneme via its motor activity to reach the plus end. Why KIF17-mCitrine is observed at distal tips and not along the ciliary axoneme is not clear. One explanation is that although there are individual motors walking along the microtubule axoneme, the fluorescence output of these individual motors is below the limit of detection of the light microscope. Using microscopes with higher signal to noise capabilities, such as total internal reflection fluorescence (TIRF) microscopy, may get around this problem. Furthermore, the presence of endogenous motors along the axoneme further limit the number of exogenous fluorescent motors walking along the axoneme. This raises an interesting question of stoichiometry with regards to ciliary motors that will need to be addressed in the future. One obvious experiment that could be done to answer these questions is to exogenously express KIF17 fusion proteins in KIF17 -/- MEFs and monitor KIF17 localization and movement in both fixed and live samples.

Another goal of my thesis work was to determine which domains are required for ciliary entry of KIF17. We generated various truncated versions of KIF17 and monitored the localization of these truncation mutants in cells. My studies suggest that the motor domain is not necessary for entry into the cilium. Truncated KIF17 constructs without the motor domain, but containing the stalk+tail or tail domain alone, were able to enter the ciliary compartment (schematic, Figure 4.2a). This data suggests that the KIF17 tail domain contains the information that specifies KIF17 localization to the cilium. Interestingly, the KIF17 tail domain demonstrated a variety of localization patterns including along the ciliary axoneme, at the tip, and at both the tip and base. What could be the significance of these varying localizations? One aspect of our data that we have not tested is whether the KIF17 tail domain is able to interact with endogenous motors and/or cargoes that would affect its localization. It is tempting to speculate that the KIF17 tail domain interacts with endogenous KIF17, however,

this seems unlikely since the tail does not have any coiled coil segments for dimerization. Whether the tail domain can dimerize with itself or full-length motors should be tested however. Alternatively, it may be that the tail interacts with endogenous cargoes like IFT particles and is carried along by endogenous motors attached to the same cargo. This would explain the tail's localization along the cilium and accumulation at the distal tip. In addition, it may be that the tail domain interacts with endogenous importin β2 and is imported into the ciliary compartment. KIF17 tail localized at the base of the cilium then might represent tail imported into the cilium, but not yet moved anterograde along the axoneme. Future experiments are needed to directly test these possibilities.

Although our results indicate that the tail domain is necessary and sufficient for ciliary entry of KIF17, it is not known whether the motor activity of KIF17 (i.e. ATP hydrolysis) is required for ciliary entry or only for movement of cargoes along the axoneme. To test this, I propose constructing motor-dead KIF17 mutants and conducting ciliary localization experiments. If motor-dead KIF17 does not localize to the cilium, then it suggests that KIF17 utilizes its motor activity for ciliary entry. In contrast, if motor activity is not required for ciliary entry, we expect to observe ciliary localization of motor-dead KIF17. How would KIF17 lacking motor activity be imported into the cilium? Based on our studies where we observed ciliary localization of truncated KIF17 lacking motor domain, I predict that motor-dead KIF17 can associate with importin β2 and be imported into the ciliary compartment.

Having determined that the tail domain is necessary for the ciliary trafficking of KIF17, we then identified a ciliary localization sequence (CLS) within the KIF17 tail domain that is required for ciliary localization of both KIF17 full length and tail domain (schematic, Figure 4.2b). Interestingly, in contrast to full length KIF17 CLS mutant, I observed a pool of KIF17 CLS mutant tail domain that is highly concentrated at the basal bodies. I hypothesize that KIF17 CLS mutant tail at the basal body represents a pool that is in transit into to ciliary compartment but is

“stuck” and unable to be imported due to mutations to the CLS. This suggests that a signal exists within the tail domain that promotes docking at the basal body prior to ciliary import. Interestingly, we did not observe full length KIF17 CLS mutant at the basal body, suggesting motor structure or activity may affect localization as well. KIF17, similar to other kinesins, exists as an autoinhibited molecule when not bound to cargo. When we consider KIF17 autoinhibition with our data of full length KIF17 CLS mutant, one possible explanation is that a signal that promotes basal body localization is masked in the full-length KIF17 motor when it is in its compact, folded auto-inhibited state. The autoinhibition of full length KIF17 can be relieved by a Glycine to Glutamine substitution at residue 754 (Hammond et al., 2010). By creating a full length KIF17 construct containing both the Gly765 to Glu (G765E) substitution and CLS mutation one can test whether autoinhibition is involved in masking a potential signal. If that is the case, then I expect KIF17 containing G765E and CLS mutations to localize to the basal body.

To further investigate the CLS in the KIF17 tail domain, we created chimeric molecules to assay the sufficiency of the CLS for ciliary entry. While the KIF17 tail domain (aa801-1029) was sufficient to target another kinesin, cytoplasmic KHC, to the cilium, the KIF17 CLS (aa995-1025 or aa1001-1029) was not (schematic, Figure 4.2b). This data indicates that additional signals in the KIF17 tail domain promote ciliary targeting. To that end, we identified the sequence Pro-His-Pro (amino acids 896-898) in the KIF17 tail domain as a potential secondary ciliary targeting signal. Mutations to this PHP signal resulted in loss of ciliary trafficking and surprisingly promoted nuclear localization of mutated proteins. As mutation of PHP promotes rather than abolishes nuclear targeting of KIF17, I expect that the mutant constructs will still interact with importin β2. This can be tested by co-immunoprecipitation assays. How does the PHP signal promote ciliary targeting of KIF17? I hypothesize that the PHP signal is important for associating with specific proteins such as IFT proteins that aid in ciliary entry of KIF17. Studies demonstrated that KIF17 interacts with multiple IFT proteins

including IFT20, IFT57, IFT88, IFT81 and IFT74 (Hao et al., 2011; Insinna et al., 2009). Interestingly, IFT20 is involved in Golgi to ciliary base vesicular trafficking (Follit et al., 2006), thus suggesting that KIF17 may bind IFT components before reaching the cilium proper. In future experiments, one can test through binding assays whether mutation of PHP disrupts association with IFT20, and whether this interaction facilitates ciliary entry. A second explanation for the role of PHP in ciliary targeting is that the mutation of PHP affects the structure of KIF17. It may be that because PHP are three sequential bulky amino acids, it plays an important role in the overall conformation of the motor.

Collectively, our studies suggest a model where KIF17 interacts with importin β2 at the base of the cilium and is shuttled into the ciliary compartment where a high Ran-GTP gradient dissociates the complex, allowing KIF17 to move towards the distal tip of the cilium along the axoneme (schematic, Figure 4.3). At first glance, it seems strange that KIF17 would utilize nuclear import machinery to enter into the cilium. Our lab, alongside the Margolis and Martens labs, has continued to provide evidence supporting a role for Ran and importins in ciliary assembly and entry (Fan et al., 2007; Fan and Margolis, 2011; Fan et al., 2011; Hurd et al., 2011). Nuclear import machinery is found in ciliary proteomic studies (Gherman et al., 2006; Liu et al., 2007). Furthermore, Ran GTPase and importins have been shown to play important roles outside of nuclear trafficking including spindle formation (Gruss et al., 2001; Schatz et al., 2003).

A key question that remains unanswered is how is the exit of KIF17 from the cilium into the cytoplasm regulated? Given that a Ran-GTP gradient provides directionality of KIF17 into the cilium, then one can imagine that the export of KIF17 out of the cilium may utilize a mechanism similar to nuclear export. To explore whether KIF17 export is regulated by nuclear export mechanisms, our lab has begin to examine whether KIF17 has any nuclear export-like sequences. John Dishinger, a postdoctoral fellow in the lab, created mutations of nuclear export-like sequences in full length KIF17. However, when he expressed these in

ciliated cells, he did not observe much difference from wild-type. It would be interesting to observe if there are any effects of these nuclear export-like sequences in KIF17 -/- MEF cells. Other experiments that one could conduct include immunostaining for nuclear export receptors called exportins in ciliated cells.

The Ciliary Pore Complex

Rosenbaum first postulated based on immunoelectron microscopy of IFT particles “docked” on transition fibers that the base of the cilium forms the “flagellar pore complex” (FPC) to regulate passage of material into the cilium (Deane et al., 2001; Rosenbaum and Witman, 2002). Our observations that there are parallels between ciliary and nuclear import prompted us to examine whether nucleoporins, which make up the nuclear pore complexes (NPC) that regulate entry into the nucleus, also localize to the base of the cilium. By staining for endogenous proteins and expressing a GFP-tagged nucleoporin from each subclass, I found that specific nucleoporins do localize to the base of the cilium to form a ciliary pore complex (CPC). Whether other members of each subcomplex localize to the base of the cilium would be important to test, as our data has demonstrated that not all nucleoporins from the different classes localize to the ciliary base. It will be important to determine by immunostaining whether endogenous nucleoporins can be detected in a variety of ciliated cells. We observed endogenous nucleoporins in both NIH3T3 and primary rat trachea cells. Our lab and others are currently screening other cells types such as multi-ciliated olfactory sensory neurons and mono-ciliated cells such as embryonic nodal cells, photoreceptors, and kidney epithelial cells for endogenous nucleoporins.

One important difference between the NPC and CPC is that the three known transmembrane nucleoporins (NDC1, POM121 and GP210) that anchor the NPC in the nuclear membrane do not localize to the base of cilia in Odora cells.

These results raise the important question of how nucleoporins are recruited to and anchored at the base of the cilium. If a different transmembrane protein complex has evolved to anchor nucleoporins in the plasma membrane, then identification of these proteins is an important goal. A potential anchor for nucleoporins at the base of cilia is the NPHP/MKS complex of proteins that localizes to the cilia base and whose mutations are known to cause human ciliopathies. There are seven proteins in the NPHP/MKS complex that have predicted transmembrane domains including TCTN2, TCTN3, TMEM17, TMEM67, TMEM231, and TMEM237 (Garcia-Gonzalo and Reiter, 2012). First, one can determine whether nucleoporins interact with these transition zone proteins through immunoprecipitation and binding assays. If positive interactions are found, then one can ask whether the transmembrane proteins of this complex are required for nucleoporin localization at the cilia base using genetic knockdown experiments in ciliated cells. Thus, if the NPHP/MKS proteins serve as cilia-specific anchors for nucleoporins, then one would expect that loss of NPHP/MKS proteins would have measurable and direct effects on nucleoporin localization to the cilia base but will have no effect on localization of nucleoporins to the nuclear envelope. These experiments will be important not only for defining the ciliary functions of NPHP proteins but also provide a molecular basis for nucleoporin localization to two distinct cellular complexes.

Our study raises key questions about the overall structure of the CPC at the base of the cilium. The NPC has typically a 8-fold rotational symmetry with 8 spokes arranged radially around a central transport channel for the passage of molecules (Alber et al., 2007; Yang et al., 1998). In contrast, the ciliary base is characterized by 9-fold symmetry of microtubule filaments, Y-links and transition fibers. However, it is interesting to note that there have been reports of NPCs existing with 9-fold and 10-fold symmetry (Franke, 1966; Hinshaw and Milligan, 2003), suggesting that the NPC does not exclusively exist in 8-fold symmetry. It is not clear whether the difference between the 8-fold symmetry of the NPC and the 9-fold symmetry of the cilium is important as we do not have any information

about how the nucleoporin subunits are arranged at the base of the cilium to form an actual pore. It is possible that there are actually 9 pores at the base of the cilium with each pore positioned between the Y-links and transition fibers. An alternative possibility, based on the fact that the base of the cilium forms a donut-shaped “pore” with the axonemal/basal body structure projecting through the middle, is that the CPC exists with the outer ring and linker nucleoporins positioned just inside the ciliary membrane and the core nucleoporins touching the axoneme/basal body. The diameter across the base of the cilium is about 300nm, which is almost twice as wide as the diameter of the NPC (Hoelz et al., 2011; Nachury et al., 2010). Thus, it will be important to use high-resolution microscopy techniques such as super resolution and/or transmission electron microscopy to define the spatial localization and orientation of the CPC at the base of the cilium.

Despite structural differences, there are a few similarities between the cilium and nucleus that are worth considering. For example, Y-link structures are key features of the transition zone at the base of the cilium. Immunogold electron microscopy positioned nephronophthisis-associated NPHP6/CEP290 at the Y-links in *Chlamydomonas* flagella. In further studies, double mutants of NPHP and MKS proteins in *C. elegans* result in defective Y-links and transition fibers (Craige et al., 2010; Williams et al., 2011). However the molecular composition of the ciliary Y-links still remains a mystery. Interestingly, the NPC also contains Y-shaped structures (Lutzmann et al., 2002; Siniossoglou et al., 2000). The NPC’s 40nm long Y structure is made up of the outer ring Nup84 subcomplex (Seh1, Nup85, Nup120, Sec13, Nup145c, Nup84 and Nup133) in yeast (Lutzmann et al., 2002; Siniossoglou et al., 2000) and the Nup107-160 subcomplex (including two additional members Nup37 and Nup43) in vertebrates (Walther et al., 2003). In my studies, initially I had difficulty expressing EGFP-Nup37 in cells. However, after talking to Martin Hetzer who suggested waiting 3-4 days after transfection to allow for incorporation into the NPC, I was finally able to observe EGFP-Nup37 localized to the base of the cilium in Odora cells. Whether other members of this

complex also localize to the cilia base is definitely worth investigating. I have tried to express EGFP-tagged versions of Nup43, SEH1, Nup107 and Nup133, but had difficulties observing even nuclear NPC-localized nucleoporins. In future experiments, one can create stable expressing cell lines to determine whether other membranes of outer ring nucleoporins localize to base of the cilium.

Mechanisms of ciliary trafficking

In my studies, I demonstrated that nucleoporins regulate trafficking of KIF17 into cilia. In future experiments, one can test whether nucleoporins function to regulate the entry of other soluble proteins and membrane proteins into the cilium. Given that cilia are sensory organelles, particular attention has been focused on how membrane proteins such as GPCRs and small G proteins gain entry into the cilium. Varying mechanisms have been proposed to regulate the entry of membrane proteins. There are a growing number of proteins involved in regulating the ciliary trafficking of membrane proteins including the BBSome complex and GTPases Rab8 and Arf4 (Deretic et al., 2005; Follit et al., 2006; Jin et al., 2010; Mazelova et al., 2009; Moritz et al., 2001; Nachury et al., 2007; Westlake et al., 2011; Yoshimura et al., 2007). Furthermore, ciliary targeting sequences have been identified in several membrane proteins (Berbari et al., 2008a; Deretic et al., 2005; Follit et al., 2010; Geng et al., 2006; Tam et al., 2000; Tao et al., 2009). An emerging characteristic amongst ciliary transmembrane and membrane associated proteins is post-translational lipidation by myristoylation and palmitoylation (Cevik et al., 2010; Follit et al., 2010; Godsel and Engman, 1999; Hurd et al., 2010; Tam et al., 2000; Tao et al., 2009).

To investigate if lipid modifications influences ciliary targeting and entry, I expressed GFP fused to motifs that serve as substrates for various lipid modifications that are inserted into the inner leaflet of the plasma membrane. I compared the ability of myristoylation and palmitoylation (MyrPalm), dual palmitoylation (PalmPalm), and geranylgeranyl (GerGer) lipid moieties to target

GFP to the ciliary membrane in mammalian cells (depicted in Fig. 4.4e-g). MyrPalm-GFP and PalmPalm-GFP colocalized with acetylated tubulin in fixed MDCK cells (Fig. 4.4a-b) Given the discrepancies between live and fixed cells, the lipid-anchors were also expressed in NIH 3T3 cells with a live ciliary marker and ciliary localization was verified (Figure 4.4h-j). That dual acylation is sufficient for partitioning into the ciliary membrane is an important extension to previous work demonstrating that myristoylation and/or palmitoylation modifications are necessary for ciliary targeting of several transmembrane and membrane-associated proteins (Cevik et al., 2010; Follit et al., 2010; Godsel and Engman, 1999; Hurd et al., 2010; Tam et al., 2000; Tao et al., 2009). In contrast, GFP-GerGer did not localize to the ciliary membrane in MDCK cells, suggesting that prenyl modifications prevent partitioning into the ciliary membrane (Fig.4.4c). The abilities of these lipid anchors to partition into the ciliary membrane may be related to their association with specific membranes. MyrPalm-GFP and PalmPalm-GFP partition into detergent-resistant membranes whereas GFP-GerGer associates with detergent-soluble membranes and is largely excluded from detergent-resistant membranes (Zacharias et al., 2002). Thus, acylation may provide a signal to partition into specific lipid microdomains that constitute the ciliary membrane.

To examine the dynamics of lipid-anchored GFP movement between the ciliary and plasma membranes, I conducted FRAP analysis of PalmPam-EGFP in NIH 3T3 cells. Using a high laser power, I bleached the ciliary PalmPalm-EGFP and measured recovery of newly imported fluorescent molecules. Interestingly, the recovery of PalmPalm-EGFP into the cilia was rapid (within minutes, Figure 4.5a, c, d). This suggests that the movement of PalmPalm-EGFP is dynamic between the ciliary and plasma membranes and that lipid-anchored proteins are capable of swift entry into the cilium (schematic, Figure 4.6a). This may be significant, as membrane associated G-proteins are known to localize to the cilium and most likely require the ability to undergo dynamic movements to facilitate rapid cellular signaling responses. The rapid movement of PalmPalm-EGFP contrasts with

previous FRAP studies showing that ciliary transmembrane proteins are not motile between the ciliary and plasma membranes but are able to diffuse rapidly within the ciliary membrane (Chih et al., 2011; Hu et al., 2010; Hurd et al., 2010; Jenkins et al., 2006; Larkins et al., 2011).

Although FRAP is currently one of the most common methods to measure the movement of ciliary membrane proteins, my data suggest a caveat to these experiments that is important to consider when interpreting FRAP data. Overexpressed fluorescently-tagged ciliary membrane proteins, such as SSTR3-EGFP (transmembrane) or Arl13b-mCherry (lipid anchored), localize within the ciliary membrane and may lack a sufficient plasma membrane pool available to move into the bleached region. Thus, the lack of recovery that was interpreted as being due to the presence of a membrane diffusion barrier (Hu et al., 2010; Larkins et al., 2011) may simply reflect the lack of a plasma membrane pool of fluorescent molecules that can contribute to fluorescence recovery. A second point that should be considered in interpreting FRAP recovery data is that the bleached molecules are still present in the ciliary membrane and may prevent the movement of new molecules into the compartment at steady-state (schematic, Figure 4.6b).

The development of tools other than FRAP will allow further insight into how transmembrane and membrane-associated proteins are compartmentalized into the ciliary membrane. Several studies have recently used alternative novel tools to investigate the movement of transmembrane transducer Smoothened into the cilium of cultured cells (Milenkovic et al., 2009; Wang et al., 2009). These studies utilized antibodies and/or chemical modification of extracellular domains to monitor movement into the cilium (Milenkovic et al., 2009; Wang et al., 2009). Whether these tools can be applied to other membrane proteins would be interesting to test.

Cilia Diversity

It is becoming clear that not all cilia are created equal. Although the core cilium structure is mainly conserved, there are key differences between cell types and species. For example, specific cell types like olfactory sensory neurons, photoreceptor cells and *C. elegans* sensory neurons contain an elongated distal segment composed of singlet microtubules. The significance of the distal segments is not clear, but one could speculate that long distal segments accommodate the unique ciliary structures that provide cell-specific function. Another example of structural difference is that *C. elegans* sensory neurons lack the basal body structure (Reiter et al., 2012). It is believed that the basal body docks at the dendritic tip to nucleate the axoneme and then degenerates post-ciliogenesis but leaves behind transition zone fibers and Y-link structures. It is intriguing that the lack of a basal body still allows for proper cilia and neuronal function in *C. elegans*.

In addition to structural differences, the permeability barrier at the base of the cilium may also vary across cell types and species. Evidence for this comes from the Martens lab, where Jeremy McIntyre probed whether a diffusion barrier exists in olfactory sensory neurons. They observed that fluorescent dyes like fluorescein could not even traverse into the cilia from the dendritic knob (McIntyre and Martens, unpublished results), suggesting that entry into the olfactory cilia is even more highly regulated than the cultured hTERT-RPE cells that I tested. It is possible that multi-ciliated cells form a diffusion barrier with tighter limitations than mono-ciliated cells, or that different cells maintain a specific diffusion barrier to meet the demands of their ciliary function.

Another difference worth discussing is that the localization of both soluble and membrane proteins to cilia varies between species and cell types. For example, in *C. elegans*, GFP-tagged OSM-3 localizes along the ciliary axoneme, while in cultured cells, FP-KIF17 is found at the distal tip (Dishinger et al., 2010; Signor et al., 1999b). One could make a stable cell line of FP-KIF17 to determine whether

it can be visualized along the cilium. Additionally, membrane associated RP2 localizes to the basal body and the cilium of mammalian cells but is not observed in the cilia of *C. elegans* sensory neurons (Hurd et al., 2010; Reiter et al., 2012; Williams et al., 2010). Instead, RP2 in *C. elegans* sensory neurons form a ring-like localization at the dendritic tip below the ciliary base where it is thought to facilitate tubulin quality control for axoneme incorporation (Williams et al., 2010). From these studies, it is clear that the localization of a protein in one cell type or species may not be conserved, and that it is important that we do not make generalizations of ciliary protein localization without sufficient evidence.

Despite cilia being evolutionarily conserved organelles, there are ciliary proteins that are not shared across species and cell types. For example, CEP290/NPHP6 is present in *Chlamydomonas*, mouse olfactory sensory neuron and cultured mammalian cells, but not in *C. elegans* (Garcia-Gonzalo et al., 2011; Kim et al., 2008; McEwen et al., 2007; Sang et al., 2011). CEP290 plays a role in regulating transport of proteins into the cilium. However, it is possible that other proteins can compensate for the loss of CEP290 function in *C. elegans*. Furthermore, even the localization of CEP290 varies from the basal body, transition zone, to centriolar satellites (Garcia-Gonzalo et al., 2011; Kim et al., 2008; McEwen et al., 2007; Sang et al., 2011). It is not clear whether the difference observed is because its localization is dynamic or due to cell specific differences. Further studies will continue to elucidate the diversity of cilia in different cell types and species.

Summary

In summary, the work presented in this thesis has demonstrated that the cilium is a privileged domain. I report for the first time that a size-dependent barrier mechanism excludes cytoplasmic molecules. Additionally, together with John Dishinger, we were able to define the mechanism for KIF17 ciliary trafficking by demonstrating that KIF17 contains a CLS signal in its tail domain that is

regulated by the nuclear receptor importin-β2. We determined that the tail domain is both necessary and sufficient to confer ciliary localization. Additional experiments are necessary to elucidate the mechanism of a potential secondary CLS in the tail domain of KIF17. Furthermore, I demonstrated that several nucleoporins localize to the base of the cilium and that inhibition of nucleoporin resulted in reduced KIF17 trafficking to cilia. This work has demonstrated that the basic cellular machinery regulating nuclear import is utilized by cells for controlling ciliary targeting. This body of work lays the foundation for further investigations focused on understanding the molecular, structural and physical mechanisms that regulate entry and exit into the ciliary compartment.

Methods

Antibodies and Plasmids.

Commercial antibodies include acetylated α-tubulin (clone 6-11 B-1, Sigma), and secondary fluorescence-conjugated antibodies from Invitrogen and Jackson ImmunoResearch.

The lipid anchored GFP constructs were constructed by annealing oligonucleotides encoding the 13 N-terminal residues from Lyn kinase (MyrPalm), the 20 N-terminal residues from GAP43 (PalmPalm), and the 9 C-terminal residues from the guanine triphosphatase Rho (GerGer) into the KpnI and AgeI sites of pEGFP-N1 (Clontech). Arl13b-mCherry was constructed by subcloning human Arl13b cDNA from Arl13b-EGFP into the KpnI and AgeI sites of mCherry-N1.

Cell Culture

Madin Darby canine kidney (MDCK) and NIH 3T3 cells were grown in DMEM supplemented with 10% fetal bovine serum and 1% Pen/Strep/Gluta-MAX I. Stable MDCK cells lines were generated by transfection of DNA constructs into cells using Trans-IT LTI (Mirus) transfection reagent, followed by selection with 600ug/ml G418 (Invitrogen) for 1-2 weeks. MDCK cells were grown 7 days post-confluence on Transwell filter supports (0.4 mm pore size, Corning) for immunofluorescence.

FRAP

FRAP assays were conducted on a Nikon A1 confocal system, a Nikon Eclipse Ti microscope equipped with a live-cell temperature controlled chamber (Tokai Hit) at 37 °C with 5% CO_2 supply. Imaging is captured using a 60x/1.2 N.A. water immersion objective equipped with an objective heater and a Perfect Focus System. Imaging of EGFP and mCherry channels were captured sequentially to limit signal bleed through between channels. Laser power was set at 2% for a

488 nm line (Spectra-Physics air-cooled argon ion laser, 40 mW run at 50% power) and 30% for a 543 nm line (Melles Griot HeNe laser, 5 mW).

Figures

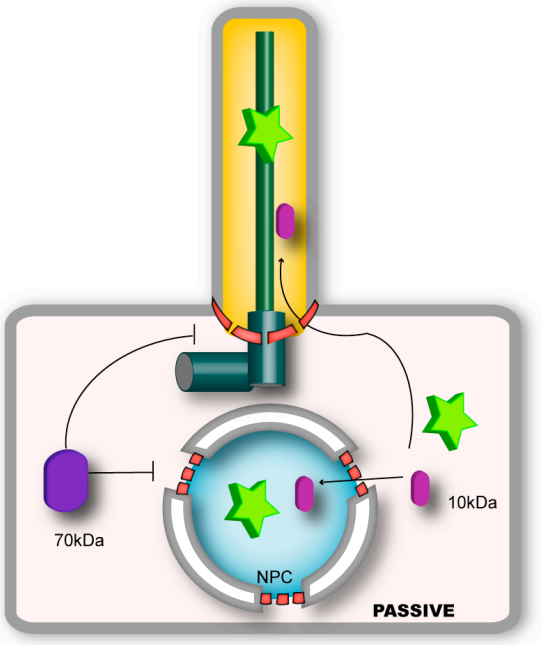

Figure 4.1 Model of size-dependent diffusion barrier at the cilia base

Schematic showing that there is a size-dependent diffusion barrier at the base of the cilium, analogous to the barrier formed by the nuclear pore complex (NPC) in the nuclear envelope. 10 kDa molecules and GFP can enter both the cilium and nucleus, but 70 kDa molecules are restricted from both compartments.

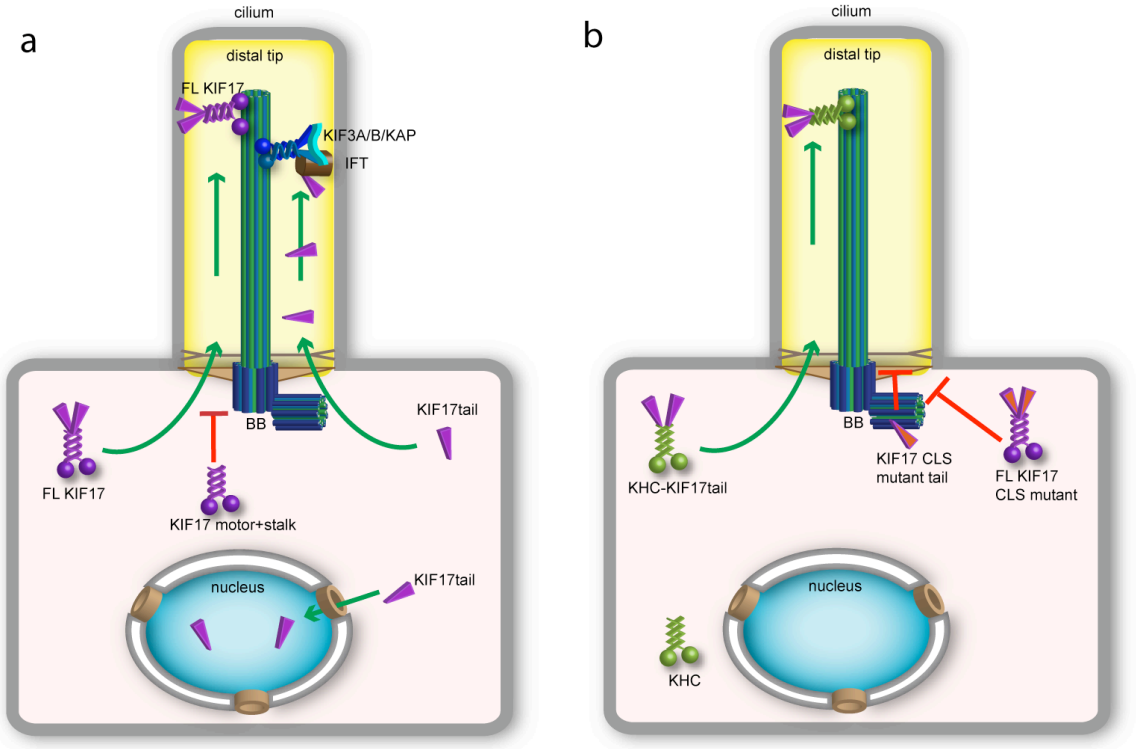

Figure 4.2 Model of cellular and ciliary localization of KIF17-mCitrine constructs

(a) Full length KIF17-mCitrine localizes to the cytoplasm and distal tip of the cilium. Truncated KIF17 motor+stalk does not localize to the cilium. Truncated tail domain localizes to the cilium (base, along and at the tip), in addition to the nucleus. (b) Full length KIF17 CLS mutant-mCitrine is restricted from the cilium. Truncated KIF17 CLS mutant tail is displaced to the basal body (BB). KIF17 tail fused to a non-ciliary motor KHC (KHC-KIF17tail) localizes to the distal tip of the cilium.

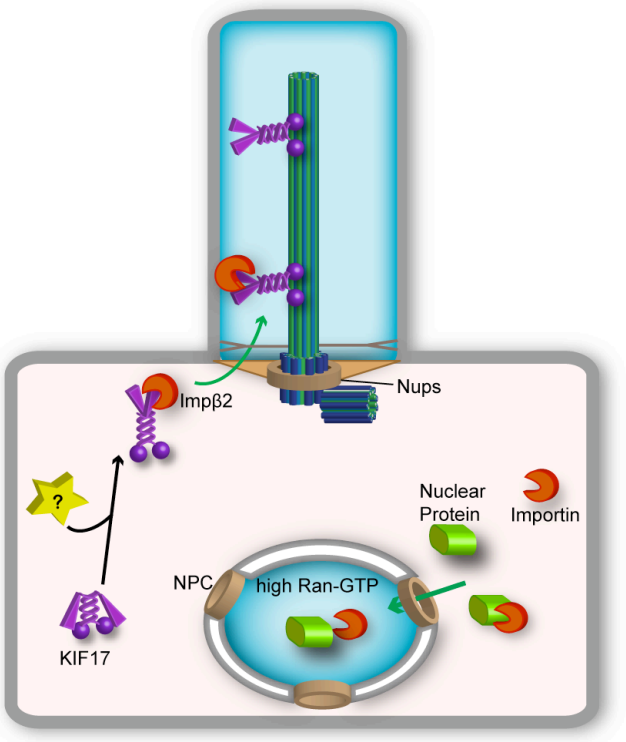

Figure 4.3 Model for ciliary entry of KIF17

In the cytoplasm, KIF17 interacts with Importin-β2 in a CLS-dependent manner. The KIF17-Importin-β2 complex shuttles across the base of the cilium. A high Ran-GTP concentration in the cilium dissociates the complex, allowing KIF17 to proceed along the axoneme. Blue shading indicates high levels of Ran-GTP. Specific nucleoporins (brown ring) localize to the base of the cilium. Prior to ciliary entry, an unidentified cargo (star) may bind to KIF17 in the cytoplasm, changing its conformation to release it from its autoinhibited state.
For nuclear trafficking, a nuclear-destined protein interacts with importin receptor in a NLS-dependent manner in the cytoplasm. The complex shuttles through the nuclear pore complex (NPC) and a high RanGTP concentration dissociates the complex.

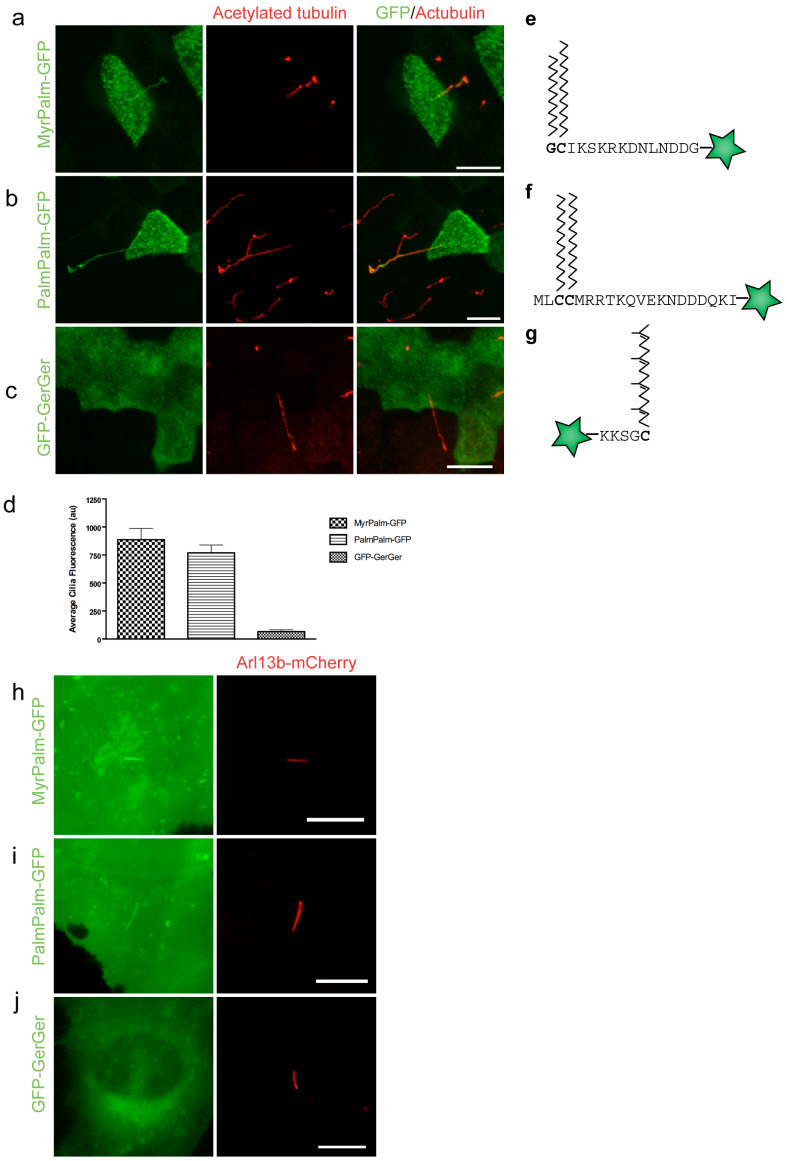

Figure 4.4 Lipid anchors regulate partitioning of GFP into the ciliary membrane

(a-g) MDCK cell lines stably expressing (a) MyrPalm-GFP (myristoylated and palmitoylated), (b) PalmPalm-GFP (tandemly palmitoylated), or (**c**) GFP-GerGer (geranylgeranylated) were fixed and stained with antibodies to acetylated α-tubulin (red) to mark the primary cilium. Scale bar, 10 μm. (e, f, g) schematic depiction of each GFP fusion construct with the amino acid sequences of the lipid modification sites attached to GFP (green star). (d) Quantification of mean GFP fluorescence in the cilia of MDCK cells expressing MyrPalm-GFP, PalmPalm-GFP, or GFP-GerGer. *N*= 13-16 cells per construct. Values are mean ± SEM. (h-j) NIH3T3 cells transiently co-expressing Arl13b-mCherry as a live cell ciliary marker and (h) MyrPalm-GFP, (i) PalmPalm-GFP or (j) GFP-GerGer. Cells were imaged under live conditions. Scale bar, 10 μm.

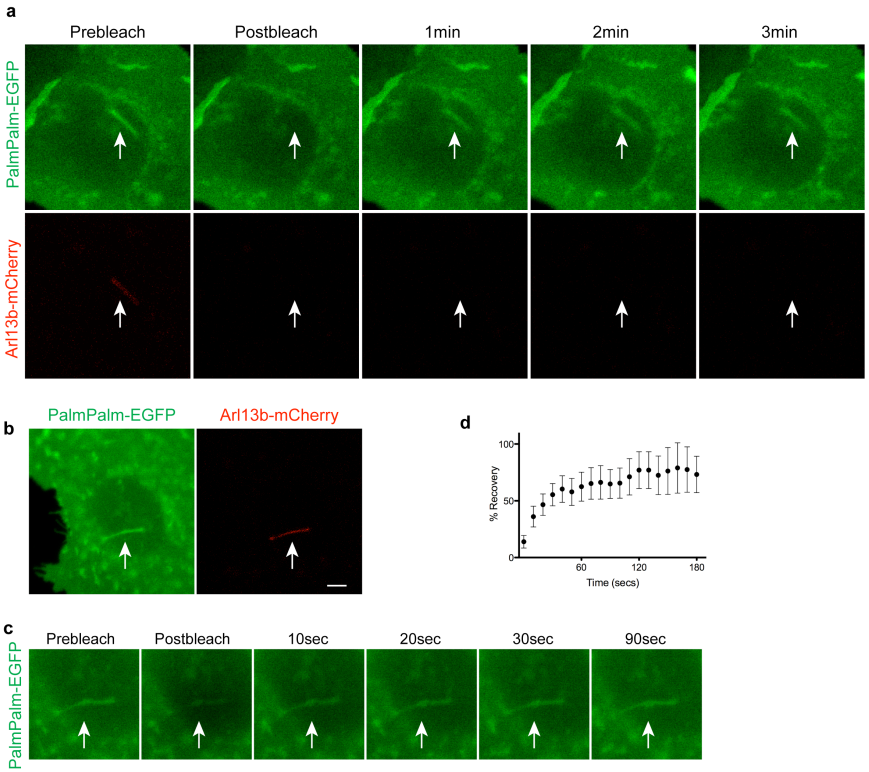

Figure 4.5 PalmPalm-GFP rapidly exchanges between ciliary and plasma membranes

(a) Ciliary-localized PalmPalm-EGFP and Arl13b-mCherry transiently expressed in an NIH 3T3 cell were photobleached with high laser power and fluorescence recovery was measured every 1 minute for 3 minutes. PalmPalm-EGFP fluorescence in the ciliary compartment (white arrow) recovered within the first time point whereas Arl13b-mCherry fluorescence did not recover. (b-d) An NIH 3T3 cell co-expressing PalmPalm-EGFP and Arl13b-mCherry. Scale bar, 5 μm. (c) Ciliary-localized PalmPalm-EGFP was photobleached with high laser power and fluorescence recovery was measured every 10 seconds for 3 minutes. (d) Quantification of the fluorescence recovery of PalmPalm-EGFP in cilia. The data are represented as mean±SEM fluorescence in the ciliary compartment as compared to pre-bleach levels. *N* = 5 cells.

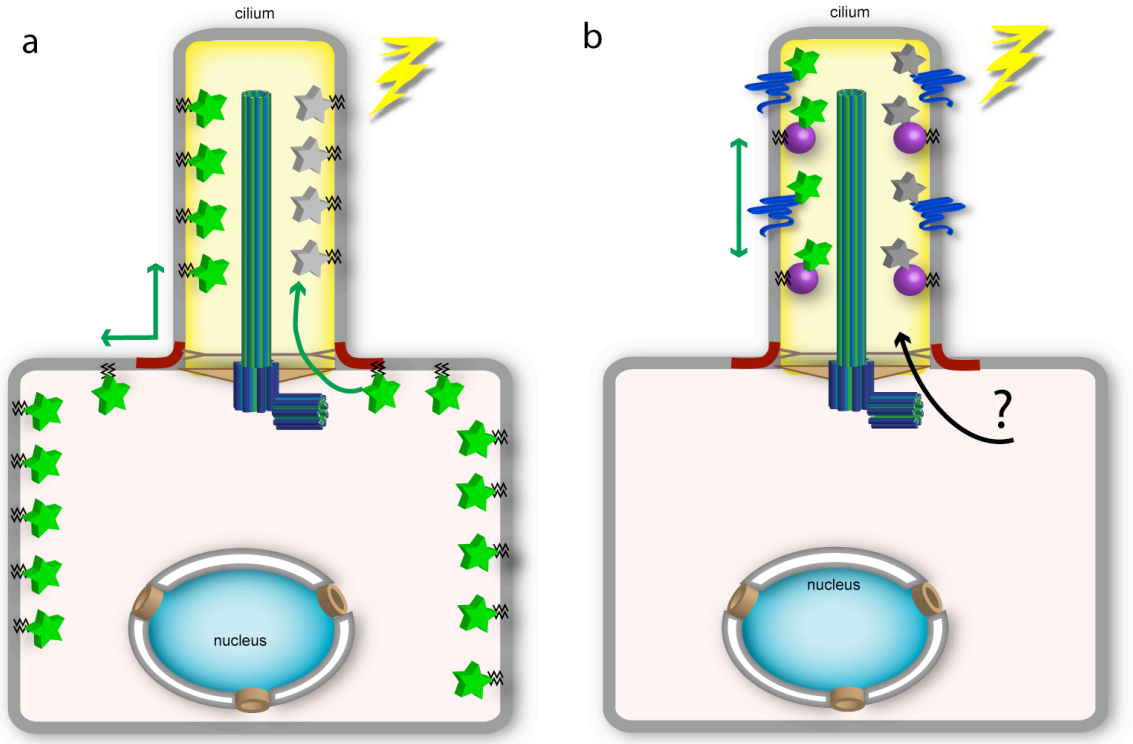

Figure 4.6 Model of FRAP experiments of lipid-GFPs and ciliary membrane proteins

(a) Schematic of a cell expressing lipid-anchored GFP that partitions in the inner leaflet of the plasma and ciliary membranes. FRAP results show that lipid-GFPs move into the ciliary membrane after bleaching (lightning) ciliary lipid-GFPs with high laser power (depicted on the right side of the cell). GFP is represented as a green star. Bleached GFP is represented as a grey star. (b) Schematic of a cell expressing ciliary transmembrane and peripheral membrane proteins that are compartmentalized in the ciliary membrane. Previous FRAP studies have shown membrane proteins move within the ciliary membrane when a portion of the ciliary pool is bleached (Chih et al., 2011; Hu et al., 2010; Hurd et al., 2010; Jenkins et al., 2006; Larkins et al.). FRAP studies have also demonstrated that when the entire ciliary pool is bleached, there is limited recovery (Chih et al., 2011; Hu et al., 2010; Larkins et al., 2011). Red lines indicates proposed membrane diffusion barrier at the base of the cilium.

References

Adam, E.J., and S.A. Adam. 1994. Identification of cytosolic factors required for nuclear location sequence-mediated binding to the nuclear envelope. *The Journal of cell biology*. 125:547-555.

Adam, S.A., and L. Gerace. 1991. Cytosolic proteins that specifically bind nuclear location signals are receptors for nuclear import. *Cell*. 66:837-847.

Alber, F., S. Dokudovskaya, L.M. Veenhoff, W. Zhang, J. Kipper, D. Devos, A. Suprapto, O. Karni-Schmidt, R. Williams, B.T. Chait, A. Sali, and M.P. Rout. 2007. The molecular architecture of the nuclear pore complex. *Nature*. 450:695-701.

Anderson, R.G. 1972. The three-dimensional structure of the basal body from the rhesus monkey oviduct. *The Journal of cell biology*. 54:246-265.

Badano, J.L., N. Mitsuma, P.L. Beales, and N. Katsanis. 2006. The ciliopathies: an emerging class of human genetic disorders. *Annu Rev Genomics Hum Genet*. 7:125-148.

Baker, S.A., K. Freeman, K. Luby-Phelps, G.J. Pazour, and J.C. Besharse. 2003. IFT20 links kinesin II with a mammalian intraflagellar transport complex that is conserved in motile flagella and sensory cilia. *The Journal of biological chemistry*. 278:34211-34218.

Barr, M.M., and P.W. Sternberg. 1999. A polycystic kidney-disease gene homologue required for male mating behaviour in C. elegans. *Nature*. 401:386-389.

Berbari, N.F., A.D. Johnson, J.S. Lewis, C.C. Askwith, and K. Mykytyn. 2008a. Identification of ciliary localization sequences within the third intracellular loop of G protein-coupled receptors. *Mol Biol Cell*. 19:1540-1547.

Berbari, N.F., J.S. Lewis, G.A. Bishop, C.C. Askwith, and K. Mykytyn. 2008b. Bardet-Biedl syndrome proteins are required for the localization of G protein-coupled receptors to primary cilia. *Proc Natl Acad Sci U S A*. 105:4242-4246.

Bischoff, F.R., C. Klebe, J. Kretschmer, A. Wittinghofer, and H. Ponstingl. 1994. RanGAP1 induces GTPase activity of nuclear Ras-related Ran. *Proceedings of the National Academy of Sciences of the United States of America*. 91:2587-2591.

Bischoff, F.R., H. Krebber, E. Smirnova, W. Dong, and H. Ponstingl. 1995. Co-activation of RanGTPase and inhibition of GTP dissociation by Ran-GTP binding protein RanBP1. *The EMBO journal*. 14:705-715.

Bischoff, F.R., and H. Ponstingl. 1991. Mitotic regulator protein RCC1 is complexed with a nuclear ras-related polypeptide. *Proceedings of the*

National Academy of Sciences of the United States of America. 88:10830-10834.
Bishop, G.A., N.F. Berbari, J. Lewis, and K. Mykytyn. 2007. Type III adenylyl cyclase localizes to primary cilia throughout the adult mouse brain. *J Comp Neurol*. 505:562-571.
Bonifaci, N., J. Moroianu, A. Radu, and G. Blobel. 1997. Karyopherin beta2 mediates nuclear import of a mRNA binding protein. *Proceedings of the National Academy of Sciences of the United States of America*. 94:5055-5060.
Brohawn, S.G., J.R. Partridge, J.R. Whittle, and T.U. Schwartz. 2009. The nuclear pore complex has entered the atomic age. *Structure*. 17:1156-1168.
Calvert, P.D., W.E. Schiesser, and E.N. Pugh, Jr. 2010. Diffusion of a soluble protein, photoactivatable GFP, through a sensory cilium. *J Gen Physiol*. 135:173-196.
Cevik, S., Y. Hori, O.I. Kaplan, K. Kida, T. Toivenon, C. Foley-Fisher, D. Cottell, T. Katada, K. Kontani, and O.E. Blacque. 2010. Joubert syndrome Arl13b functions at ciliary membranes and stabilizes protein transport in Caenorhabditis elegans. *J Cell Biol*. 188:953-969.
Cheung, H.O., X. Zhang, A. Ribeiro, R. Mo, S. Makino, V. Puviindran, K.K. Law, J. Briscoe, and C.C. Hui. 2009. The kinesin protein Kif7 is a critical regulator of Gli transcription factors in mammalian hedgehog signaling. *Sci Signal*. 2:ra29.
Chi, N.C., E.J. Adam, and S.A. Adam. 1995. Sequence and characterization of cytoplasmic nuclear protein import factor p97. *The Journal of cell biology*. 130:265-274.
Chih, B., P. Liu, Y. Chinn, C. Chalouni, L.G. Komuves, P.E. Hass, W. Sandoval, and A.S. Peterson. 2011. A ciliopathy complex at the transition zone protects the cilia as a privileged membrane domain. *Nature cell biology*. 14:61-72.
Clever, J., M. Yamada, and H. Kasamatsu. 1991. Import of simian virus 40 virions through nuclear pore complexes. *Proceedings of the National Academy of Sciences of the United States of America*. 88:7333-7337.
Cole, D.G. 2005. Intraflagellar transport: keeping the motors coordinated. *Current biology : CB*. 15:R798-801.
Cole, D.G., D.R. Diener, A.L. Himelblau, P.L. Beech, J.C. Fuster, and J.L. Rosenbaum. 1998. Chlamydomonas kinesin-II-dependent intraflagellar transport (IFT): IFT particles contain proteins required for ciliary assembly in Caenorhabditis elegans sensory neurons. *The Journal of cell biology*. 141:993-1008.
Corbit, K.C., P. Aanstad, V. Singla, A.R. Norman, D.Y. Stainier, and J.F. Reiter. 2005. Vertebrate Smoothened functions at the primary cilium. *Nature*. 437:1018-1021.
Coy, D.L., W.O. Hancock, M. Wagenbach, and J. Howard. 1999. Kinesin's tail domain is an inhibitory regulator of the motor domain. *Nature cell biology*. 1:288-292.

Craige, B., C.C. Tsao, D.R. Diener, Y. Hou, K.F. Lechtreck, J.L. Rosenbaum, and G.B. Witman. 2010. CEP290 tethers flagellar transition zone microtubules to the membrane and regulates flagellar protein content. *J Cell Biol*. 190:927-940.

Cuschieri, A., and L.H. Bannister. 1975a. The development of the olfactory mucosa in the mouse: electron microscopy. *J Anat*. 119:471-498.

Cuschieri, A., and L.H. Bannister. 1975b. The development of the olfactory mucosa in the mouse: light microscopy. *J Anat*. 119:277-286.

D'Angelo, M.A., and M.W. Hetzer. 2008. Structure, dynamics and function of nuclear pore complexes. *Trends in cell biology*. 18:456-466.

Davis, L.I., and G. Blobel. 1986. Identification and characterization of a nuclear pore complex protein. *Cell*. 45:699-709.

Deane, J.A., D.G. Cole, E.S. Seeley, D.R. Diener, and J.L. Rosenbaum. 2001. Localization of intraflagellar transport protein IFT52 identifies basal body transitional fibers as the docking site for IFT particles. *Current biology : CB*. 11:1586-1590.

Denning, D.P., S.S. Patel, V. Uversky, A.L. Fink, and M. Rexach. 2003. Disorder in the nuclear pore complex: the FG repeat regions of nucleoporins are natively unfolded. *Proceedings of the National Academy of Sciences of the United States of America*. 100:2450-2455.

Deretic, D., A.H. Williams, N. Ransom, V. Morel, P.A. Hargrave, and A. Arendt. 2005. Rhodopsin C terminus, the site of mutations causing retinal disease, regulates trafficking by binding to ADP-ribosylation factor 4 (ARF4). *Proc Natl Acad Sci U S A*. 102:3301-3306.

Dingwall, C., S.V. Sharnick, and R.A. Laskey. 1982. A polypeptide domain that specifies migration of nucleoplasmin into the nucleus. *Cell*. 30:449-458.

Dishinger, J.F., H.L. Kee, P.M. Jenkins, S. Fan, T.W. Hurd, J.W. Hammond, Y.N. Truong, B. Margolis, J.R. Martens, and K.J. Verhey. 2010. Ciliary entry of the kinesin-2 motor KIF17 is regulated by importin-beta2 and RanGTP. *Nat Cell Biol*. 12:703-710.

Domire, J.S., J.A. Green, K.G. Lee, A.D. Johnson, C.C. Askwith, and K. Mykytyn. 2011. Dopamine receptor 1 localizes to neuronal cilia in a dynamic process that requires the Bardet-Biedl syndrome proteins. *Cell Mol Life Sci*. 68:2951-2960.

Dultz, E., and J. Ellenberg. 2010. Live imaging of single nuclear pores reveals unique assembly kinetics and mechanism in interphase. *The Journal of cell biology*. 191:15-22.

El Zein, L., H. Omran, and P. Bouvagnet. 2003. Lateralization defects and ciliary dyskinesia: lessons from algae. *Trends Genet*. 19:162-167.

Endoh-Yamagami, S., M. Evangelista, D. Wilson, X. Wen, J.W. Theunissen, K. Phamluong, M. Davis, S.J. Scales, M.J. Solloway, F.J. de Sauvage, and A.S. Peterson. 2009. The mammalian Cos2 homolog Kif7 plays an essential role in modulating Hh signal transduction during development. *Current biology : CB*. 19:1320-1326.

Fahrenkrog, B., and U. Aebi. 2003. The nuclear pore complex: nucleocytoplasmic transport and beyond. *Nature reviews. Molecular cell biology*. 4:757-766.
Fan, S., V. Fogg, Q. Wang, X.W. Chen, C.J. Liu, and B. Margolis. 2007. A novel Crumbs3 isoform regulates cell division and ciliogenesis via importin beta interactions. *J Cell Biol*. 178:387-398.
Fan, S., and B. Margolis. 2011. The Ran importin system in cilia trafficking. *Organogenesis*. 7.
Fan, S., E.L. Whiteman, T.W. Hurd, J.C. McIntyre, J.F. Dishinger, C.J. Liu, J.R. Martens, K.J. Verhey, U. Sajjan, and B. Margolis. 2011. Induction of Ran GTP drives ciliogenesis. *Molecular biology of the cell*. 22:4539-4548.
Follit, J.A., L. Li, Y. Vucica, and G.J. Pazour. 2010. The cytoplasmic tail of fibrocystin contains a ciliary targeting sequence. *J Cell Biol*. 188:21-28.
Follit, J.A., R.A. Tuft, K.E. Fogarty, and G.J. Pazour. 2006. The intraflagellar transport protein IFT20 is associated with the Golgi complex and is required for cilia assembly. *Mol Biol Cell*. 17:3781-3792.
Francis, S.S., J. Sfakianos, B. Lo, and I. Mellman. 2011. A hierarchy of signals regulates entry of membrane proteins into the ciliary membrane domain in epithelial cells. *The Journal of cell biology*. 193:219-233.
Franke, W.W. 1966. Isolated nuclear membranes. *The Journal of cell biology*. 31:619-623.
Fridell, R.A., R. Truant, L. Thorne, R.E. Benson, and B.R. Cullen. 1997. Nuclear import of hnRNP A1 is mediated by a novel cellular cofactor related to karyopherin-beta. *J Cell Sci*. 110 (Pt 11):1325-1331.
Gaertig, J., and D. Wloga. 2008. Ciliary tubulin and its post-translational modifications. *Current topics in developmental biology*. 85:83-113.
Garcia-Gonzalo, F.R., K.C. Corbit, M.S. Sirerol-Piquer, G. Ramaswami, E.A. Otto, T.R. Noriega, A.D. Seol, J.F. Robinson, C.L. Bennett, D.J. Josifova, J.M. Garcia-Verdugo, N. Katsanis, F. Hildebrandt, and J.F. Reiter. 2011. A transition zone complex regulates mammalian ciliogenesis and ciliary membrane composition. *Nature genetics*. 43:776-784.
Garcia-Gonzalo, F.R., and J.F. Reiter. 2012. Scoring a backstage pass: mechanisms of ciliogenesis and ciliary access. *The Journal of cell biology*. 197:697-709.
Geng, L., D. Okuhara, Z. Yu, X. Tian, Y. Cai, S. Shibazaki, and S. Somlo. 2006. Polycystin-2 traffics to cilia independently of polycystin-1 by using an N-terminal RVxP motif. *J Cell Sci*. 119:1383-1395.
Gherman, A., E.E. Davis, and N. Katsanis. 2006. The ciliary proteome database: an integrated community resource for the genetic and functional dissection of cilia. *Nat Genet*. 38:961-962.
Gilula, N.B., and P. Satir. 1972. The ciliary necklace. A ciliary membrane specialization. *J Cell Biol*. 53:494-509.
Godsel, L.M., and D.M. Engman. 1999. Flagellar protein localization mediated by a calcium-myristoyl/palmitoyl switch mechanism. *EMBO J*. 18:2057-2065.
Goetz, S.C., and K.V. Anderson. 2010. The primary cilium: a signalling centre during vertebrate development. *Nat Rev Genet*. 11:331-344.

Gorlich, D., and U. Kutay. 1999. Transport between the cell nucleus and the cytoplasm. *Annu Rev Cell Dev Biol*. 15:607-660.
Gorlich, D., S. Prehn, R.A. Laskey, and E. Hartmann. 1994. Isolation of a protein that is essential for the first step of nuclear protein import. *Cell*. 79:767-778.
Gorlich, D., F. Vogel, A.D. Mills, E. Hartmann, and R.A. Laskey. 1995. Distinct functions for the two importin subunits in nuclear protein import. *Nature*. 377:246-248.
Greiner, J.V., T.A. Weidman, H.D. Bodley, and C.A. Greiner. 1981. Ciliogenesis in photoreceptor cells of the retina. *Experimental eye research*. 33:433-446.
Gruss, O.J., R.E. Carazo-Salas, C.A. Schatz, G. Guarguaglini, J. Kast, M. Wilm, N. Le Bot, I. Vernos, E. Karsenti, and I.W. Mattaj. 2001. Ran induces spindle assembly by reversing the inhibitory effect of importin alpha on TPX2 activity. *Cell*. 104:83-93.
Hallberg, E., R.W. Wozniak, and G. Blobel. 1993. An integral membrane protein of the pore membrane domain of the nuclear envelope contains a nucleoporin-like region. *The Journal of cell biology*. 122:513-521.
Hammond, J.W., T.L. Blasius, V. Soppina, D. Cai, and K.J. Verhey. 2010. Autoinhibition of the kinesin-2 motor KIF17 via dual intramolecular mechanisms. *The Journal of cell biology*. 189:1013-1025.
Hammond, J.W., D. Cai, T.L. Blasius, Z. Li, Y. Jiang, G.T. Jih, E. Meyhofer, and K.J. Verhey. 2009. Mammalian Kinesin-3 motors are dimeric in vivo and move by processive motility upon release of autoinhibition. *PLoS Biol*. 7:e72.
Hao, L., M. Thein, I. Brust-Mascher, G. Civelekoglu-Scholey, Y. Lu, S. Acar, B. Prevo, S. Shaham, and J.M. Scholey. 2011. Intraflagellar transport delivers tubulin isotypes to sensory cilium middle and distal segments. *Nature cell biology*. 13:790-798.
Haycraft, C.J., B. Banizs, Y. Aydin-Son, Q. Zhang, E.J. Michaud, and B.K. Yoder. 2005. Gli2 and Gli3 localize to cilia and require the intraflagellar transport protein polaris for processing and function. *PLoS genetics*. 1:e53.
Hildebrandt, F., M. Attanasio, and E. Otto. 2009. Nephronophthisis: disease mechanisms of a ciliopathy. *Journal of the American Society of Nephrology : JASN*. 20:23-35.
Hinshaw, J.E., and R.A. Milligan. 2003. Nuclear pore complexes exceeding eightfold rotational symmetry. *J Struct Biol*. 141:259-268.
Hirokawa, N., S. Niwa, and Y. Tanaka. 2010. Molecular motors in neurons: transport mechanisms and roles in brain function, development, and disease. *Neuron*. 68:610-638.
Hirokawa, N., Y. Noda, Y. Tanaka, and S. Niwa. 2009. Kinesin superfamily motor proteins and intracellular transport. *Nature reviews. Molecular cell biology*. 10:682-696.
Hirokawa, N., K.K. Pfister, H. Yorifuji, M.C. Wagner, S.T. Brady, and G.S. Bloom. 1989. Submolecular domains of bovine brain kinesin identified by electron microscopy and monoclonal antibody decoration. *Cell*. 56:867-878.

Hoelz, A., E.W. Debler, and G. Blobel. 2011. The structure of the nuclear pore complex. *Annual review of biochemistry*. 80:613-643.
Hou, Y., H. Qin, J.A. Follit, G.J. Pazour, J.L. Rosenbaum, and G.B. Witman. 2007. Functional analysis of an individual IFT protein: IFT46 is required for transport of outer dynein arms into flagella. *The Journal of cell biology*. 176:653-665.
Hu, Q., L. Milenkovic, H. Jin, M.P. Scott, M.V. Nachury, E.T. Spiliotis, and W.J. Nelson. 2010. A septin diffusion barrier at the base of the primary cilium maintains ciliary membrane protein distribution. *Science*. 329:436-439.
Huangfu, D., A. Liu, A.S. Rakeman, N.S. Murcia, L. Niswander, and K.V. Anderson. 2003. Hedgehog signalling in the mouse requires intraflagellar transport proteins. *Nature*. 426:83-87.
Hurd, T., W. Zhou, P. Jenkins, C.J. Liu, A. Swaroop, H. Khanna, J. Martens, F. Hildebrandt, and B. Margolis. 2010. The retinitis pigmentosa protein RP2 interacts with polycystin 2 and regulates cilia-mediated vertebrate development. *Hum Mol Genet*. 19:4330-4344.
Hurd, T.W., S. Fan, and B.L. Margolis. 2011. Localization of retinitis pigmentosa 2 to cilia is regulated by Importin beta2. *J Cell Sci*. 124:718-726.
Ibanez-Tallon, I., N. Heintz, and H. Omran. 2003. To beat or not to beat: roles of cilia in development and disease. *Human molecular genetics*. 12 Spec No 1:R27-35.
Ikegami, K., S. Sato, K. Nakamura, L.E. Ostrowski, and M. Setou. 2010. Tubulin polyglutamylation is essential for airway ciliary function through the regulation of beating asymmetry. *Proceedings of the National Academy of Sciences of the United States of America*. 107:10490-10495.
Insinna, C., and J.C. Besharse. 2008. Intraflagellar transport and the sensory outer segment of vertebrate photoreceptors. *Dev Dyn*. 237:1982-1992.
Insinna, C., M. Humby, T. Sedmak, U. Wolfrum, and J.C. Besharse. 2009. Different roles for KIF17 and kinesin II in photoreceptor development and maintenance. *Dev Dyn*. 238:2211-2222.
Iomini, C., V. Babaev-Khaimov, M. Sassaroli, and G. Piperno. 2001. Protein particles in Chlamydomonas flagella undergo a transport cycle consisting of four phases. *The Journal of cell biology*. 153:13-24.
Isgro, T.A., and K. Schulten. 2007. Association of nuclear pore FG-repeat domains to NTF2 import and export complexes. *J Mol Biol*. 366:330-345.
Jenkins, P.M., T.W. Hurd, L. Zhang, D.P. McEwen, R.L. Brown, B. Margolis, K.J. Verhey, and J.R. Martens. 2006. Ciliary targeting of olfactory CNG channels requires the CNGB1b subunit and the kinesin-2 motor protein, KIF17. *Curr Biol*. 16:1211-1216.
Jenkins, P.M., D.P. McEwen, and J.R. Martens. 2009. Olfactory cilia: linking sensory cilia function and human disease. *Chem Senses*. 34:451-464.
Jin, H., S.R. White, T. Shida, S. Schulz, M. Aguiar, S.P. Gygi, J.F. Bazan, and M.V. Nachury. 2010. The conserved Bardet-Biedl syndrome proteins assemble a coat that traffics membrane proteins to cilia. *Cell*. 141:1208-1219.

Johnson, K.A., and J.L. Rosenbaum. 1992. Polarity of flagellar assembly in Chlamydomonas. *The Journal of cell biology*. 119:1605-1611.
Kalderon, D., W.D. Richardson, A.F. Markham, and A.E. Smith. 1984. Sequence requirements for nuclear location of simian virus 40 large-T antigen. *Nature*. 311:33-38.
Kikkawa, M., E.P. Sablin, Y. Okada, H. Yajima, R.J. Fletterick, and N. Hirokawa. 2001. Switch-based mechanism of kinesin motors. *Nature*. 411:439-445.
Kim, J., S.R. Krishnaswami, and J.G. Gleeson. 2008. CEP290 interacts with the centriolar satellite component PCM-1 and is required for Rab8 localization to the primary cilium. *Human molecular genetics*. 17:3796-3805.
Knabe, W., and H.J. Kuhn. 1997. Ciliogenesis in photoreceptor cells of the tree shrew retina. *Anat Embryol (Berl)*. 196:123-131.
Kozminski, K.G., P.L. Beech, and J.L. Rosenbaum. 1995. The Chlamydomonas kinesin-like protein FLA10 is involved in motility associated with the flagellar membrane. *The Journal of cell biology*. 131:1517-1527.
Kozminski, K.G., K.A. Johnson, P. Forscher, and J.L. Rosenbaum. 1993. A motility in the eukaryotic flagellum unrelated to flagellar beating. *Proceedings of the National Academy of Sciences of the United States of America*. 90:5519-5523.
Kraemer, D., R.W. Wozniak, G. Blobel, and A. Radu. 1994. The human CAN protein, a putative oncogene product associated with myeloid leukemogenesis, is a nuclear pore complex protein that faces the cytoplasm. *Proceedings of the National Academy of Sciences of the United States of America*. 91:1519-1523.
Krull, S., J. Thyberg, B. Bjorkroth, H.R. Rackwitz, and V.C. Cordes. 2004. Nucleoporins as components of the nuclear pore complex core structure and Tpr as the architectural element of the nuclear basket. *Molecular biology of the cell*. 15:4261-4277.
Kubo, T., H.A. Yanagisawa, T. Yagi, M. Hirono, and R. Kamiya. 2010. Tubulin polyglutamylation regulates axonemal motility by modulating activities of inner-arm dyneins. *Current biology : CB*. 20:441-445.
Kutay, U., E. Izaurralde, F.R. Bischoff, I.W. Mattaj, and D. Gorlich. 1997. Dominant-negative mutants of importin-beta block multiple pathways of import and export through the nuclear pore complex. *The EMBO journal*. 16:1153-1163.
Lanford, R.E., and J.S. Butel. 1984. Construction and characterization of an SV40 mutant defective in nuclear transport of T antigen. *Cell*. 37:801-813.
Lang, I., M. Scholz, and R. Peters. 1986. Molecular mobility and nucleocytoplasmic flux in hepatoma cells. *J Cell Biol*. 102:1183-1190.
Larkins, C.E., G.D. Aviles, M.P. East, R.A. Kahn, and T. Caspary. 2011. Arl13b regulates ciliogenesis and the dynamic localization of Shh signaling proteins. *Molecular biology of the cell*. 22:4694-4703.
Liem, K.F., Jr., M. He, P.J. Ocbina, and K.V. Anderson. 2009. Mouse Kif7/Costal2 is a cilia-associated protein that regulates Sonic hedgehog signaling. *Proceedings of the National Academy of Sciences of the United States of America*. 106:13377-13382.

Lin, F., T. Hiesberger, K. Cordes, A.M. Sinclair, L.S. Goldstein, S. Somlo, and P. Igarashi. 2003. Kidney-specific inactivation of the KIF3A subunit of kinesin-II inhibits renal ciliogenesis and produces polycystic kidney disease. *Proceedings of the National Academy of Sciences of the United States of America*. 100:5286-5291.

Liu, Q., G. Tan, N. Levenkova, T. Li, E.N. Pugh, Jr., J.J. Rux, D.W. Speicher, and E.A. Pierce. 2007. The proteome of the mouse photoreceptor sensory cilium complex. *Mol Cell Proteomics*. 6:1299-1317.

Lutzmann, M., R. Kunze, A. Buerer, U. Aebi, and E. Hurt. 2002. Modular self-assembly of a Y-shaped multiprotein complex from seven nucleoporins. *The EMBO journal*. 21:387-397.

Marszalek, J.R., P. Ruiz-Lozano, E. Roberts, K.R. Chien, and L.S. Goldstein. 1999. Situs inversus and embryonic ciliary morphogenesis defects in mouse mutants lacking the KIF3A subunit of kinesin-II. *Proceedings of the National Academy of Sciences of the United States of America*. 96:5043-5048.

Mazelova, J., L. Astuto-Gribble, H. Inoue, B.M. Tam, E. Schonteich, R. Prekeris, O.L. Moritz, P.A. Randazzo, and D. Deretic. 2009. Ciliary targeting motif VxPx directs assembly of a trafficking module through Arf4. *The EMBO journal*. 28:183-192.

McEwen, D.P., P.M. Jenkins, and J.R. Martens. 2008. Olfactory cilia: our direct neuronal connection to the external world. *Curr Top Dev Biol*. 85:333-370.

McEwen, D.P., R.K. Koenekoop, H. Khanna, P.M. Jenkins, I. Lopez, A. Swaroop, and J.R. Martens. 2007. Hypomorphic CEP290/NPHP6 mutations result in anosmia caused by the selective loss of G proteins in cilia of olfactory sensory neurons. *Proc Natl Acad Sci U S A*. 104:15917-15922.

Menco, B.P. 1984. Ciliated and microvillous structures of rat olfactory and nasal respiratory epithelia. A study using ultra-rapid cryo-fixation followed by freeze-substitution or freeze-etching. *Cell and tissue research*. 235:225-241.

Miki, H., Y. Okada, and N. Hirokawa. 2005. Analysis of the kinesin superfamily: insights into structure and function. *Trends in cell biology*. 15:467-476.

Milenkovic, L., M.P. Scott, and R. Rohatgi. 2009. Lateral transport of Smoothened from the plasma membrane to the membrane of the cilium. *The Journal of cell biology*. 187:365-374.

Mohr, D., S. Frey, T. Fischer, T. Guttler, and D. Gorlich. 2009. Characterisation of the passive permeability barrier of nuclear pore complexes. *EMBO J*. 28:2541-2553.

Moritz, O.L., B.M. Tam, L.L. Hurd, J. Peranen, D. Deretic, and D.S. Papermaster. 2001. Mutant rab8 Impairs docking and fusion of rhodopsin-bearing post-Golgi membranes and causes cell death of transgenic Xenopus rods. *Molecular biology of the cell*. 12:2341-2351.

Morris, R.L., C.N. English, J.E. Lou, F.J. Dufort, J. Nordberg, M. Terasaki, and B. Hinkle. 2004. Redistribution of the kinesin-II subunit KAP from cilia to nuclei during the mitotic and ciliogenic cycles in sea urchin embryos. *Dev Biol*. 274:56-69.

Morsci, N.S., and M.M. Barr. 2011. Kinesin-3 KLP-6 regulates intraflagellar transport in male-specific cilia of Caenorhabditis elegans. *Current biology : CB*. 21:1239-1244.

Mukhopadhyay, S., Y. Lu, H. Qin, A. Lanjuin, S. Shaham, and P. Sengupta. 2007. Distinct IFT mechanisms contribute to the generation of ciliary structural diversity in C. elegans. *EMBO J*. 26:2966-2980.

Murcia, N.S., W.G. Richards, B.K. Yoder, M.L. Mucenski, J.R. Dunlap, and R.P. Woychik. 2000. The Oak Ridge Polycystic Kidney (orpk) disease gene is required for left-right axis determination. *Development*. 127:2347-2355.

Murrell, J.R., and D.D. Hunter. 1999. An olfactory sensory neuron line, odora, properly targets olfactory proteins and responds to odorants. *The Journal of neuroscience : the official journal of the Society for Neuroscience*. 19:8260-8270.

Nachury, M.V., A.V. Loktev, Q. Zhang, C.J. Westlake, J. Peranen, A. Merdes, D.C. Slusarski, R.H. Scheller, J.F. Bazan, V.C. Sheffield, and P.K. Jackson. 2007. A core complex of BBS proteins cooperates with the GTPase Rab8 to promote ciliary membrane biogenesis. *Cell*. 129:1201-1213.

Nachury, M.V., E.S. Seeley, and H. Jin. 2010. Trafficking to the ciliary membrane: how to get across the periciliary diffusion barrier? *Annu Rev Cell Dev Biol*. 26:59-87.

Najafi, M., N.A. Maza, and P.D. Calvert. 2012. Steric volume exclusion sets soluble protein concentrations in photoreceptor sensory cilia. *Proceedings of the National Academy of Sciences of the United States of America*. 109:203-208.

Nigg, E.A., and J.W. Raff. 2009. Centrioles, centrosomes, and cilia in health and disease. *Cell*. 139:663-678.

Nitta, R., M. Kikkawa, Y. Okada, and N. Hirokawa. 2004. KIF1A alternately uses two loops to bind microtubules. *Science*. 305:678-683.

Nonaka, S., Y. Tanaka, Y. Okada, S. Takeda, A. Harada, Y. Kanai, M. Kido, and N. Hirokawa. 1998. Randomization of left-right asymmetry due to loss of nodal cilia generating leftward flow of extraembryonic fluid in mice lacking KIF3B motor protein. *Cell*. 95:829-837.

Omran, H. 2010. NPHP proteins: gatekeepers of the ciliary compartment. *J Cell Biol*. 190:715-717.

Orozco, J.T., K.P. Wedaman, D. Signor, H. Brown, L. Rose, and J.M. Scholey. 1999. Movement of motor and cargo along cilia. *Nature*. 398:674.

Otto, E.A., T.W. Hurd, R. Airik, M. Chaki, W. Zhou, C. Stoetzel, S.B. Patil, S. Levy, A.K. Ghosh, C.A. Murga-Zamalloa, J. van Reeuwijk, S.J. Letteboer, L. Sang, R.H. Giles, Q. Liu, K.L. Coene, A. Estrada-Cuzcano, R.W. Collin, H.M. McLaughlin, S. Held, J.M. Kasanuki, G. Ramaswami, J. Conte, I. Lopez, J. Washburn, J. Macdonald, J. Hu, Y. Yamashita, E.R. Maher, L.M. Guay-Woodford, H.P. Neumann, N. Obermuller, R.K. Koenekoop, C. Bergmann, X. Bei, R.A. Lewis, N. Katsanis, V. Lopes, D.S. Williams, R.H. Lyons, C.V. Dang, D.A. Brito, M.B. Dias, X. Zhang, J.D. Cavalcoli, G. Nurnberg, P. Nurnberg, E.A. Pierce, P.K. Jackson, C. Antignac, S.

Saunier, R. Roepman, H. Dollfus, H. Khanna, and F. Hildebrandt. 2010. Candidate exome capture identifies mutation of SDCCAG8 as the cause of a retinal-renal ciliopathy. *Nature genetics*. 42:840-850.
Ou, G., O.E. Blacque, J.J. Snow, M.R. Leroux, and J.M. Scholey. 2005. Functional coordination of intraflagellar transport motors. *Nature*. 436:583-587.
Paine, P.L., L.C. Moore, and S.B. Horowitz. 1975. Nuclear envelope permeability. *Nature*. 254:109-114.
Pan, J., and W.J. Snell. 2005. Chlamydomonas shortens its flagella by activating axonemal disassembly, stimulating IFT particle trafficking, and blocking anterograde cargo loading. *Developmental cell*. 9:431-438.
Pan, J., Q. Wang, and W.J. Snell. 2004. An aurora kinase is essential for flagellar disassembly in Chlamydomonas. *Developmental cell*. 6:445-451.
Pan, X., G. Ou, G. Civelekoglu-Scholey, O.E. Blacque, N.F. Endres, L. Tao, A. Mogilner, M.R. Leroux, R.D. Vale, and J.M. Scholey. 2006. Mechanism of transport of IFT particles in C. elegans cilia by the concerted action of kinesin-II and OSM-3 motors. *The Journal of cell biology*. 174:1035-1045.
Pathak, N., C.A. Austin, and I.A. Drummond. 2011. Tubulin tyrosine ligase-like genes ttll3 and ttll6 maintain zebrafish cilia structure and motility. *The Journal of biological chemistry*. 286:11685-11695.
Pazour, G.J., B.L. Dickert, Y. Vucica, E.S. Seeley, J.L. Rosenbaum, G.B. Witman, and D.G. Cole. 2000. Chlamydomonas IFT88 and its mouse homologue, polycystic kidney disease gene tg737, are required for assembly of cilia and flagella. *The Journal of cell biology*. 151:709-718.
Pazour, G.J., J.T. San Agustin, J.A. Follit, J.L. Rosenbaum, and G.B. Witman. 2002. Polycystin-2 localizes to kidney cilia and the ciliary level is elevated in orpk mice with polycystic kidney disease. *Current biology : CB*. 12:R378-380.
Pazour, G.J., C.G. Wilkerson, and G.B. Witman. 1998. A dynein light chain is essential for the retrograde particle movement of intraflagellar transport (IFT). *The Journal of cell biology*. 141:979-992.
Pedelacq, J.D., S. Cabantous, T. Tran, T.C. Terwilliger, and G.S. Waldo. 2006. Engineering and characterization of a superfolder green fluorescent protein. *Nat Biotechnol*. 24:79-88.
Peters, R., I. Lang, M. Scholz, B. Schulz, and F. Kayne. 1986. Fluorescence microphotolysis to measure nucleocytoplasmic transport in vivo and in vitro. *Biochem Soc Trans*. 14:821-822.
Piperno, G., E. Siuda, S. Henderson, M. Segil, H. Vaananen, and M. Sassaroli. 1998. Distinct mutants of retrograde intraflagellar transport (IFT) share similar morphological and molecular defects. *The Journal of cell biology*. 143:1591-1601.
Pugacheva, E.N., S.A. Jablonski, T.R. Hartman, E.P. Henske, and E.A. Golemis. 2007. HEF1-dependent Aurora A activation induces disassembly of the primary cilium. *Cell*. 129:1351-1363.
Qin, H., D.R. Diener, S. Geimer, D.G. Cole, and J.L. Rosenbaum. 2004. Intraflagellar transport (IFT) cargo: IFT transports flagellar precursors to

the tip and turnover products to the cell body. *The Journal of cell biology*. 164:255-266.
Rabut, G., V. Doye, and J. Ellenberg. 2004. Mapping the dynamic organization of the nuclear pore complex inside single living cells. *Nature cell biology*. 6:1114-1121.
Rapoport, T.A. 2007. Protein translocation across the eukaryotic endoplasmic reticulum and bacterial plasma membranes. *Nature*. 450:663-669.
Reese, T.S. 1965. Olfactory Cilia in the Frog. *The Journal of cell biology*. 25:209-230.
Reiter, J.F., O.E. Blacque, and M.R. Leroux. 2012. The base of the cilium: roles for transition fibres and the transition zone in ciliary formation, maintenance and compartmentalization. *EMBO Rep*. 13:608-618.
Robbins, J., S.M. Dilworth, R.A. Laskey, and C. Dingwall. 1991. Two interdependent basic domains in nucleoplasmin nuclear targeting sequence: identification of a class of bipartite nuclear targeting sequence. *Cell*. 64:615-623.
Rohatgi, R., L. Milenkovic, R.B. Corcoran, and M.P. Scott. 2009. Hedgehog signal transduction by Smoothened: pharmacologic evidence for a 2-step activation process. *Proceedings of the National Academy of Sciences of the United States of America*. 106:3196-3201.
Rohatgi, R., L. Milenkovic, and M.P. Scott. 2007. Patched1 regulates hedgehog signaling at the primary cilium. *Science*. 317:372-376.
Rosenbaum, J. 2002. Intraflagellar transport. *Curr Biol*. 12:R125.
Rosenbaum, J.L., and G.B. Witman. 2002. Intraflagellar transport. *Nat Rev Mol Cell Biol*. 3:813-825.
Ross, A.J., H. May-Simera, E.R. Eichers, M. Kai, J. Hill, D.J. Jagger, C.C. Leitch, J.P. Chapple, P.M. Munro, S. Fisher, P.L. Tan, H.M. Phillips, M.R. Leroux, D.J. Henderson, J.N. Murdoch, A.J. Copp, M.M. Eliot, J.R. Lupski, D.T. Kemp, H. Dollfus, M. Tada, N. Katsanis, A. Forge, and P.L. Beales. 2005. Disruption of Bardet-Biedl syndrome ciliary proteins perturbs planar cell polarity in vertebrates. *Nature genetics*. 37:1135-1140.
Sang, L., J.J. Miller, K.C. Corbit, R.H. Giles, M.J. Brauer, E.A. Otto, L.M. Baye, X. Wen, S.J. Scales, M. Kwong, E.G. Huntzicker, M.K. Sfakianos, W. Sandoval, J.F. Bazan, P. Kulkarni, F.R. Garcia-Gonzalo, A.D. Seol, J.F. O'Toole, S. Held, H.M. Reutter, W.S. Lane, M.A. Rafiq, A. Noor, M. Ansar, A.R. Devi, V.C. Sheffield, D.C. Slusarski, J.B. Vincent, D.A. Doherty, F. Hildebrandt, J.F. Reiter, and P.K. Jackson. 2011. Mapping the NPHP-JBTS-MKS protein network reveals ciliopathy disease genes and pathways. *Cell*. 145:513-528.
Schatz, C.A., R. Santarella, A. Hoenger, E. Karsenti, I.W. Mattaj, O.J. Gruss, and R.E. Carazo-Salas. 2003. Importin alpha-regulated nucleation of microtubules by TPX2. *The EMBO journal*. 22:2060-2070.
Schneider, L., C.A. Clement, S.C. Teilmann, G.J. Pazour, E.K. Hoffmann, P. Satir, and S.T. Christensen. 2005. PDGFRalphaalpha signaling is regulated through the primary cilium in fibroblasts. *Current biology : CB*. 15:1861-1866.

Scholey, J.M. 2008. Intraflagellar transport motors in cilia: moving along the cell's antenna. *The Journal of cell biology*. 180:23-29.
Schrader, N., P. Stelter, D. Flemming, R. Kunze, E. Hurt, and I.R. Vetter. 2008. Structural basis of the nic96 subcomplex organization in the nuclear pore channel. *Mol Cell*. 29:46-55.
Setou, M., T. Nakagawa, D.H. Seog, and N. Hirokawa. 2000. Kinesin superfamily motor protein KIF17 and mLin-10 in NMDA receptor-containing vesicle transport. *Science*. 288:1796-1802.
Signor, D., K.P. Wedaman, J.T. Orozco, N.D. Dwyer, C.I. Bargmann, L.S. Rose, and J.M. Scholey. 1999a. Role of a class DHC1b dynein in retrograde transport of IFT motors and IFT raft particles along cilia, but not dendrites, in chemosensory neurons of living Caenorhabditis elegans. *The Journal of cell biology*. 147:519-530.
Signor, D., K.P. Wedaman, L.S. Rose, and J.M. Scholey. 1999b. Two heteromeric kinesin complexes in chemosensory neurons and sensory cilia of Caenorhabditis elegans. *Molecular biology of the cell*. 10:345-360.
Siniossoglou, S., M. Lutzmann, H. Santos-Rosa, K. Leonard, S. Mueller, U. Aebi, and E. Hurt. 2000. Structure and assembly of the Nup84p complex. *The Journal of cell biology*. 149:41-54.
Snow, J.J., G. Ou, A.L. Gunnarson, M.R. Walker, H.M. Zhou, I. Brust-Mascher, and J.M. Scholey. 2004. Two anterograde intraflagellar transport motors cooperate to build sensory cilia on C. elegans neurons. *Nature cell biology*. 6:1109-1113.
Starr, C.M., M. D'Onofrio, M.K. Park, and J.A. Hanover. 1990. Primary sequence and heterologous expression of nuclear pore glycoprotein p62. *The Journal of cell biology*. 110:1861-1871.
Stewart, M. 2007. Molecular mechanism of the nuclear protein import cycle. *Nat Rev Mol Cell Biol*. 8:195-208.
Strambio-De-Castillia, C., M. Niepel, and M.P. Rout. 2010. The nuclear pore complex: bridging nuclear transport and gene regulation. *Nature reviews. Molecular cell biology*. 11:490-501.
Strawn, L.A., T. Shen, N. Shulga, D.S. Goldfarb, and S.R. Wente. 2004. Minimal nuclear pore complexes define FG repeat domains essential for transport. *Nature cell biology*. 6:197-206.
Suryavanshi, S., B. Edde, L.A. Fox, S. Guerrero, R. Hard, T. Hennessey, A. Kabi, D. Malison, D. Pennock, W.S. Sale, D. Wloga, and J. Gaertig. 2010. Tubulin glutamylation regulates ciliary motility by altering inner dynein arm activity. *Current biology : CB*. 20:435-440.
Takao, D., and S. Kamimura. 2010. Single-cell electroporation of fluorescent probes into sea urchin sperm cells and subsequent FRAP analysis. *Zoolog Sci*. 27:279-284.
Takeda, S., Y. Yonekawa, Y. Tanaka, Y. Okada, S. Nonaka, and N. Hirokawa. 1999. Left-right asymmetry and kinesin superfamily protein KIF3A: new insights in determination of laterality and mesoderm induction by kif3A-/- mice analysis. *The Journal of cell biology*. 145:825-836.

Tam, B.M., O.L. Moritz, L.B. Hurd, and D.S. Papermaster. 2000. Identification of an outer segment targeting signal in the COOH terminus of rhodopsin using transgenic Xenopus laevis. *J Cell Biol*. 151:1369-1380.
Tao, B., S. Bu, Z. Yang, B. Siroky, J.C. Kappes, A. Kispert, and L.M. Guay-Woodford. 2009. Cystin localizes to primary cilia via membrane microdomains and a targeting motif. *J Am Soc Nephrol*. 20:2570-2580.
Taulman, P.D., C.J. Haycraft, D.F. Balkovetz, and B.K. Yoder. 2001. Polaris, a protein involved in left-right axis patterning, localizes to basal bodies and cilia. *Molecular biology of the cell*. 12:589-599.
Tobin, J.L., and P.L. Beales. 2009. The nonmotile ciliopathies. *Genet Med*. 11:386-402.
Verhey, K.J., and J.W. Hammond. 2009. Traffic control: regulation of kinesin motors. *Nature reviews. Molecular cell biology*. 10:765-777.
Walther, T.C., A. Alves, H. Pickersgill, I. Loiodice, M. Hetzer, V. Galy, B.B. Hulsmann, T. Kocher, M. Wilm, T. Allen, I.W. Mattaj, and V. Doye. 2003. The conserved Nup107-160 complex is critical for nuclear pore complex assembly. *Cell*. 113:195-206.
Walther, T.C., M. Fornerod, H. Pickersgill, M. Goldberg, T.D. Allen, and I.W. Mattaj. 2001. The nucleoporin Nup153 is required for nuclear pore basket formation, nuclear pore complex anchoring and import of a subset of nuclear proteins. *The EMBO journal*. 20:5703-5714.
Wang, Y., Z. Zhou, C.T. Walsh, and A.P. McMahon. 2009. Selective translocation of intracellular Smoothened to the primary cilium in response to Hedgehog pathway modulation. *Proceedings of the National Academy of Sciences of the United States of America*. 106:2623-2628.
Watson, M.L. 1955. The nuclear envelope; its structure and relation to cytoplasmic membranes. *J Biophys Biochem Cytol*. 1:257-270.
Westlake, C.J., L.M. Baye, M.V. Nachury, K.J. Wright, K.E. Ervin, L. Phu, C. Chalouni, J.S. Beck, D.S. Kirkpatrick, D.C. Slusarski, V.C. Sheffield, R.H. Scheller, and P.K. Jackson. 2011. Primary cilia membrane assembly is initiated by Rab11 and transport protein particle II (TRAPPII) complex-dependent trafficking of Rabin8 to the centrosome. *Proceedings of the National Academy of Sciences of the United States of America*. 108:2759-2764.
Williams, C.L., C. Li, K. Kida, P.N. Inglis, S. Mohan, L. Semenec, N.J. Bialas, R.M. Stupay, N. Chen, O.E. Blacque, B.K. Yoder, and M.R. Leroux. 2011. MKS and NPHP modules cooperate to establish basal body/transition zone membrane associations and ciliary gate function during ciliogenesis. *The Journal of cell biology*. 192:1023-1041.
Williams, C.L., S.V. Masyukova, and B.K. Yoder. 2010. Normal ciliogenesis requires synergy between the cystic kidney disease genes MKS-3 and NPHP-4. *J Am Soc Nephrol*. 21:782-793.
Wloga, D., K. Rogowski, N. Sharma, J. Van Dijk, C. Janke, B. Edde, M.H. Bre, N. Levilliers, V. Redeker, J. Duan, M.A. Gorovsky, M. Jerka-Dziadosz, and J. Gaertig. 2008. Glutamylation on alpha-tubulin is not essential but affects

the assembly and functions of a subset of microtubules in Tetrahymena thermophila. *Eukaryot Cell*. 7:1362-1372.

Wloga, D., D.M. Webster, K. Rogowski, M.H. Bre, N. Levilliers, M. Jerka-Dziadosz, C. Janke, S.T. Dougan, and J. Gaertig. 2009. TTLL3 Is a tubulin glycine ligase that regulates the assembly of cilia. *Developmental cell*. 16:867-876.

Wong, S.Y., and J.F. Reiter. 2008. The primary cilium at the crossroads of mammalian hedgehog signaling. *Current topics in developmental biology*. 85:225-260.

Yamazaki, H., T. Nakata, Y. Okada, and N. Hirokawa. 1995. KIF3A/B: a heterodimeric kinesin superfamily protein that works as a microtubule plus end-directed motor for membrane organelle transport. *The Journal of cell biology*. 130:1387-1399.

Yamazaki, H., T. Nakata, Y. Okada, and N. Hirokawa. 1996. Cloning and characterization of KAP3: a novel kinesin superfamily-associated protein of KIF3A/3B. *Proceedings of the National Academy of Sciences of the United States of America*. 93:8443-8448.

Yang, Q., M.P. Rout, and C.W. Akey. 1998. Three-dimensional architecture of the isolated yeast nuclear pore complex: functional and evolutionary implications. *Mol Cell*. 1:223-234.

Yoder, B.K., X. Hou, and L.M. Guay-Woodford. 2002. The polycystic kidney disease proteins, polycystin-1, polycystin-2, polaris, and cystin, are co-localized in renal cilia. *J Am Soc Nephrol*. 13:2508-2516.

Yoshimura, S., J. Egerer, E. Fuchs, A.K. Haas, and F.A. Barr. 2007. Functional dissection of Rab GTPases involved in primary cilium formation. *The Journal of cell biology*. 178:363-369.

Zacharias, D.A., J.D. Violin, A.C. Newton, and R.Y. Tsien. 2002. Partitioning of lipid-modified monomeric GFPs into membrane microdomains of live cells. *Science*. 296:913-916.

Zhao, C., Y. Omori, K. Brodowska, P. Kovach, and J. Malicki. 2012. Kinesin-2 family in vertebrate ciliogenesis. *Proceedings of the National Academy of Sciences of the United States of America*. 109:2388-2393.